Pure Appl. Geophys.

https://doi.org/10.1007/s00024-024-03515-y

Pure and Applied Geophysics

A Review of Tsunamis Generated by Volcanoes (TGV) Source Mechanism, Modelling, Monitoring and Warning Systems

François Schindelé,[1] Laura Kong,[2] Emily M. Lane,[3] Raphaël Paris,[4] Maurizio Ripepe,[5] Vasily Titov,[6] and Rick Bailey[7]

Abstract—Tsunamis generated by volcanic eruptions have risen to prominence since the December 2018 tsunami generated by the flank collapse of Anak Krakatau during a moderate eruption and then the global tsunami generated by the explosive eruption of the Hunga volcano in the Tongan Archipelago in January 2022. Both events cause fatalities and highlight the lack in tsunami warning systems to detect and warn for tsunamis induced by volcanic mechanisms. Following the Hunga Tonga—Hunga Ha'apai eruption and tsunami, an ad hoc working group on Tsunamis Generated by Volcanoes was formed by the Intergovernmental Oceanographic Commission of UNESCO. Volcanic tsunamis differ from seismic tsunamis in that there are a wide range of source mechanisms that can generate the tsunamis waves and this makes understanding, modelling and monitoring volcanic tsunamis much more difficult than seismic tsunamis. This paper provides a review of both the mechanisms behind volcanic tsunamis and the variety of modelling techniques that can be used to simulate their effects for tsunami hazard assessment and forecasting. It gives an example of a volcanic tsunami risk assessment undertaken for Stromboli, outlines the requirement of volcanic monitoring to warn for tsunami hazard and provides examples of volcanic tsunami warning systems in Italy, the Hawaiian Island (USA), Tonga and Indonesia. The paper finishes by highlighting the need for implementing monitoring and warning systems for volcanic tsunamis for locations with submarine volcanoes or near-shore volcanoes which could potentially generate tsunamis.

Keywords: Volcanic tsunami, tsunami source mechanisms, modelling, hazard assessment, monitoring, warning system.

1. Introduction

Six percent of all tsunamis over the last four centuries have been generated by volcanoes (NCEI database, US NOAA, 2023). Most volcanic tsunamis have their greatest impact in the region near the volcano, and they can cause many casualties. In some rare cases (e.g. Krakatau, 1883; Hunga, 2022), volcanic tsunamis can have global impacts. Recent events such as the Anak Krakatau 2018 and Hunga 2022 tsunamis are a reminder that such volcanic tsunamis can occur at any time. Worldwide there are over a hundred currently active volcanoes, many located under or near water.

The Anak Krakatau tsunami (2018) inundated western Java and southern Sumatra in Indonesia and caused 432 fatalities. While the tsunami generated by the Hunga eruption only caused six fatalities (four in Tonga and two in Peru), it caused measurable waves worldwide. The event also highlighted deficiencies in our tsunami warning systems with regards to tsunamis generated by sources other than earthquakes.

Following the Hunga eruption and tsunami, an ad hoc working group on Tsunamis Generated by Volcanoes (TGV) was formed by the Tsunamis and Other Hazards related to Sea Level Warning and Mitigation Systems Working Group (TOWS-WG) of the Intergovernmental Oceanographic Commisssion (IOC) of UNESCO. This ad hoc group took stock of different volcanic tsunami mechanisms, assessed the simulation methods and codes best used to model these events for hazard assessments and real-time tsunami forecasting studies and undertook a survey of current volcanic tsunami monitoring and warning practices globally.

[1] CEA, DAM, DIF, 91297 Arpajon, France. E-mail: francois.schindele@gmail.com
[2] UNESCO/IOC, NOAA International Tsunami Information Centre, Honolulu, HI, USA.
[3] National Institute of Water and Atmospheric Research, 10 Kyle Street, Riccarton, Christchurch 8011, New Zealand.
[4] Université Clermont Auvergne, CNRS, IRD, OPGC, Laboratoire Magmas et Volcans, 63000 Clermont-Ferrand, France.
[5] Dipartimento di Scienze della Terra, Universitá di Firenze, Florence, Italy.
[6] NOAA/Pacific Marine Environmental Laboratory, 7600 Sand Point Way Northeast, Seattle, WA 981105, USA.
[7] UNESCO/IOC Tsunami Resilience Section, Paris, France.

Published online: 14 June 2024

This paper has been developed from the results of that work. Its overarching aim is to provide an overview of the state of the art of current practices in volcanic tsunami modelling, monitoring and warning. The paper is structured as follows:

Section 2 presents the different generation mechanisms of volcanic tsunamis and gives an overview of historical examples of volcanic tsunamis. Section 3 presents numerical modelling methods used to perform research analysis to interpret data, volcanic tsunami hazard assessments and real-time volcanic tsunami forecasting, with a particular focus on initializing volcanic tsunami generation. Section 4 describes the Stromboli Volcanic Tsunami hazard assessment. Section 5 describes several volcano monitoring requirements for tsunami warning while in Sect. 6, we describe the tsunami warning systems currently in place at Stromboli, Hawaii, Hunga Tonga, Anak Krakatau, and proposed for the Caribbean. Conclusions are given in Sect. 7.

2. *Tsunamis Generated by Volcano Activity and Instability*

The term volcanic tsunami refers to a tsunami that is generated by either the eruptive processes, rapid ground deformation, or flank instability of a volcano (Day, 2015; Paris, 2015). Following this definition, volcanic tsunamis represent around 6% of known tsunamis that have occurred in the last four centuries (NCEI database, US NOAA, 2023). Different types of volcanic tsunamis based on their specific generation mechanism have been categorized through analysis of historical events and theoretical and practical studies on tsunami generation (Fig. 1). These generation mechanisms are sub-aerial or submarine landslides, pyroclastic density currents flowing into a water body, caldera collapse, underwater eruption, column collapse of a submarine volcano, atmospheric forcing from an explosive eruption and volcano-tectonic earthquakes (e.g., thrust or trapdoor faults). Here we provide background information on the physical phenomena associated with each generation mechanism, and give examples from historical and recent events. While we explain each mechanism separately, in many cases, the volcanic tsunami may be generated by several different mechanisms over the course of an eruption.

Figure 1
Different types of volcanic tsunami generation mechanisms (updated from Paris et al., 2014a) ▶

2.1. *Subaerial Landslide*

Volcano flanks are well known for their instability. These results from various factors, both endogenous (structural discontinuities, hydrothermal alteration, and magmatic intrusions inside the edifice, rapid growth by accumulation of tephra and lava flows) and exogenous (earthquake, tectonic uplift, climatic event, sea level variations). The instabilities that can occur range from rock falls, cliff collapses and small landslides (with volumes typically in the order of 10^5–10^6 m^3) through to large debris avalanches (10^8–10^9 m^3).

When a subaerial landslide enters the water it generates an impulsive wave, which then propagates away from the source. The water in front of the landslide is pushed forward, and the water above is pushed upward. While the landslide is travelling faster than the shallow water waves speed (i.e., the landslide Froude number is greater that one), the impulse (forced) wave travels at the speed of the landslide front. When the landslide Froude number decreases below one (either due to the decelerating landslide or the increasing water depth) it is released as a free wave. In the near field, this leading wave is usually the largest wave, because it received most of the energy transferred from the landslide at impact. The height of this wave is positively correlated to landslide Froude number, relative thickness, mass flux and volume (e.g., Fritz et al., 2004; Lee & Huang, 2020; Viroulet et al., 2013; Yavari-Ramshe & Ataie-Ashtiani, 2016). In terms of tsunami generation, there are no specific differences between

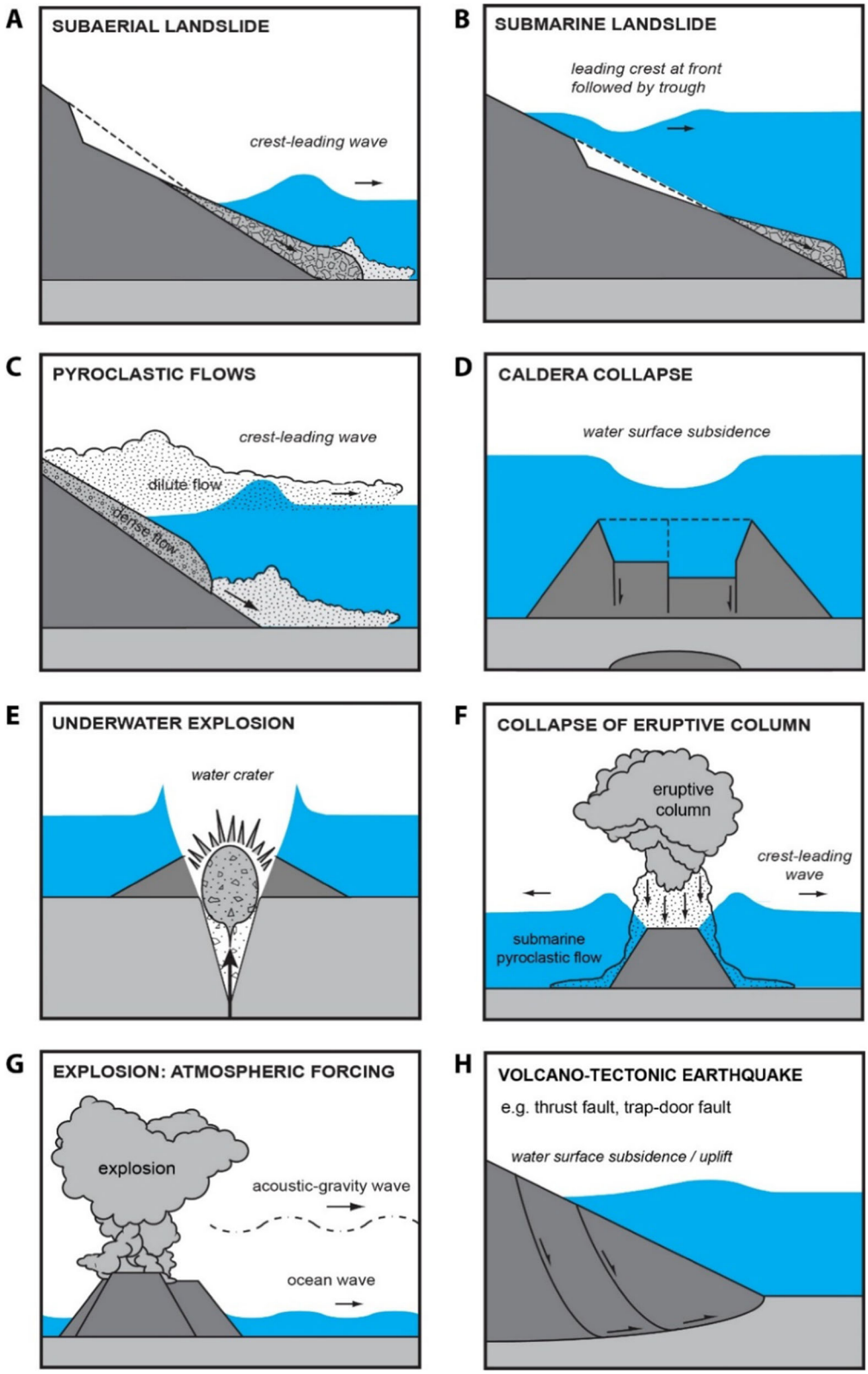
A
SUBAERIAL LANDSLIDE
crest-leading wave
B
SUBMARINE LANDSLIDE
leading crest at front
followed by trough
C
PYROCLASTIC FLOWS
crest-leading wave
dilute flow
dense flow
D
CALDERA COLLAPSE
water surface subsidence
E
UNDERWATER EXPLOSION
water crater
F
COLLAPSE OF ERUPTIVE COLUMN
eruptive
column
crest-leading
wave
submarine
pyroclastic flow
G
EXPLOSION: ATMOSPHERIC FORCING
explosion
acoustic-gravity wave
ocean wave
H
VOLCANO-TECTONIC EARTHQUAKE
e.g. thrust fault, trap-door fault
water surface subsidence / uplift

landslides that occur on the flanks of volcanoes and other landslides, included those occurring on old volcanic coasts as in French Polynesia (Hébert et al., 2002). Each event haves its own structural setting, lithology, and rheology. Landslides on the flanks of a volcano may occur separately from an eruption (e.g., triggered by heavy rains or seismic activity), but the largest landslides are related to increased volcanic activity or major eruptions (e.g., debris avalanche). Some volcanic landslides involve both subaerial and submarine components (e.g., Stromboli, 2002; Anak Krakatau, 2018, Table 1).

2.2. *Submarine Landslide*

Many volcanoes are entirely (e.g., volcanic seamounts) or partly (e.g., volcanic islands) submerged and so may be the site of submarine or sublacustrine landslides (henceforth referred to as submarine landslides). Similarly to subaerial landslides, submarine landslides range in volume from small-scale events (10^5–10^6 m^3, e.g., collapses of coastal lava deltas, landslides in submarine canyons) to massive collapses of the submarine flanks of ocean islands (up to tens of km^3). The number of tsunamis generated by submarine landslides of volcanic flanks is probably underestimated due to a lack of observations. There are only a few unequivocal historical examples (e.g., Ritter Island 1888, Table 1).

The main parameters determining the tsunamigenic potential of submarine landslides are the volume of the sliding mass, its initial acceleration, and its maximum velocity (Grilli & Watts, 2005; Harbitz et al., 2006; Ward, 2001; Yavari-Ramshe & Ataie-Ashtiani, 2016). Tsunamis generated by submarine landslides typically display three successive waves: a first crest ahead of the landslide front, as a consequence of the energy transferred from the slide, followed by a large trough propagating at the speed of the landslide front, and a final crest generated by the deceleration of the landslide which travels in the opposite direction to the landslide (Sue et al., 2011) If the submarine landslide occurs on the flanks of an inhabited island, this final wave often represents the main cause of inundation.

2.3. *Pyroclastic Flow*

Pyroclastic flows are flowing mixtures of gas and particles that can be generated by various aspects of volcanic eruptions including dome collapse and plume (eruptive column) collapse. They are complex turbulent flows that can vary in temperature, composition and density and may include layers of different densities. There have been several recent and historical examples of pyroclastic flows generating tsunamis (Table 1). Due to the complexity of the phenomenon, the conditions required to generate a tsunami and the interactions between the flow and the water are still poorly understood. Direct observations of events are difficult and dangerous to obtain and the physical and numerical models developed to date are fairly simple (Battershill et al., 2021; Bougouin et al., 2020, 2021, 2024; Lipiejko et al., 2022, 2023; Watts & Waythomas, 2003).

The dense basal component of the pyroclastic flow is the main source of tsunami generation similar to a subaerial landslide. Other phenomena associated with pyroclastic flows, such as steam explosions, flow pressure and shear, and pressure impulse could theoretically also generate small waves (Watts & Waythomas, 2003). Important parameters that affect the generation of tsunamis by pyroclastic flows include the flow volume and mass flux, the flow density and permeability (ash-rich flows being more tsunamigenic because of their low permeability), the angle of incidence, and the transport distance from the eruptive vent (Bougouin et al., 2020, 2021, 2024; Lipiejko et al., 2022, 2023; Watts & Waythomas, 2003). High-velocity pyroclastic flows with a bulk density near or even below that of water may generate waves, whatever their temperature (Bougouin et al., 2020; Freundt, 2003).

Table 1

Historical examples of volcanic tsunamis

Volcano	Location	Year	Size of the source	Max tsunami runup (dist. from source)	References
Landslides			Landslide volume		
Anak Krakatau	Sunda Strait, Indonesia	2018	210–300 × 10^6 m^3	85 m (4 km)	Muhari et al. (2019), Walter et al. (2019), Borrero et al. (2020), Perttu et al. (2020), Putra et al. (2020), Hunt et al. (2021), Zengaffinen et al. (2020) and Ren et al. (2020)
Stromboli	Aeolian Islands, Italy	2002	17 × 10^6 m^3 and 5 × 10^6 m^3	11 m (1.5 km)	Bonaccorso et al. (2003) and Maramai et al. (2005)
Kilauea	Hawaï, USA	1994	~ 10^5 m^3	15 m (50 m)	Mattox and Mangan (1997)
Iliwerung	Lembata, Indonesia	1979	50 × 10^6 m^3	9 m (18 km)	Lassa (2009) and Yudhicara et al. (2015)
Ritter Island	Papua New Guinea	1888	5 km^3	15 m (9 km)	Johnson (1987), Ward and Day (2003) and Karstens et al. (2019)
Unzen- 340 × 10^6 m^3	57 m (7 km)		Mayuyama Tsuji and Hino (1993) and Inoue (2000)	Kyushu, Japan	1792
Oshima-Oshima	Japan Sea, Japan	1741	2.4 km^3	13 m (50 km)	Satake and Kato (2001) and Satake (2007)
Pyroclastic flows			Flow volume (flux)		
Stromboli	Aeolian Islands, Italy	2019	10^5–10^6 m^3	0.3 m (2 km)	Italian Civil Protection
Soufriere Hills	Montserrat, Antilles	2003	200 × 10^6 m^3 (13 × 10^4 m^3/s)	4 m (4 km)	Pelinovsky et al. (2004) and Herd et al. (2005)
Soufriere Hills	Montserrat, Antilles	1997	20 × 10^6 m^3	3 m (10 km)	Lander et al. (2002) and Pelinovsky et al. (2004)
Rabaul	Papua New Guinea	1994	Nd	8 m (4 km)	Blong and McKee (1995) and Nishimura et al. (2005)
Krakatau	Sunda Strait, Indonesia	1883	Nd (10^7 m^3/s?)	40 m (67 km)	Simkin and Fiske (1983), Carey et al. (2000), Maeno and Imamura (2011) and Paris et al. (2014b)
Underwater explosions			Explosion energy		
Karymskoye Lake	Kamchatka, Russia	1996	5 × 10^{14} J	19 m (840 m)	Belousov et al. (2000), Torsvik et al. (2010), Ulvrova et al. (2014) and Falvard et al. (2018)
Myojin-Sho	Izu, Japan	1952	10^{15}–10^{16} J	1.5 m (130 km)	Dietz and Sheehy (1954), Nakano et al. (1954) and Lipiejko et al. (2021)
Anak Krakatau	Sunda Strait, Indonesia	1928	Nd	4 m (3.5 km)	Stehn (1929)
Atmospheric forcing by explosion			Explosion energy		
HTHH	Tonga Islands	2022	3.2 × 10^{16} to 1.5 × 10^{16} J	3.4 m (10,300 km)	Astafyeva et al. (2022), Carvajal et al. (2022), Kubota et al. (2022) and Omira et al. (2022)
Krakatau	Sunda Strait, Indonesia	1883	10^{16}–10^{17} J	1.6 m (8600 km)	Harkrider and Press (1967) and Pelinovsky et al. (2005)
Volcano-tectonic earthquakes			Earthquake magnitude		

Table 1 *continued*

Volcano	Location	Year	Size of the source	Max tsunami runup (dist. from source)	References
Sumisu (Smith) caldera	Izu-Bonin Islands, Japan	2015	M_w = 5.7	1 m (180 km)	Sandanbata et al. (2022)
Kilauea	Hawaii, USA	1975	M_s = 7.2	14.6 m ($\sim$ 20 km)	Ando (1979), Ma et al. (1999) and Day et al. (2005)

2.4. Caldera Collapse

Large explosive eruptions may result in the collapse of the central part of the edifice, forming a caldera. When the eruption occurs underwater, the caldera collapse causes the water surface to subside which generates a tsunami. The extent of the water subsidence depends on the volume and geometry of the collapse, and, above all, on its duration (Gray & Monaghan, 2003; Maeno et al., 2006; Ulvrova et al., 2016). The collapse must occur rapidly enough, compared to the local shallow water wave speed, to generate significant water subsidence. Large collapses lasting a few minutes are theoretically tsunamigenic, but probably unrealistic. Based on recent examples, the duration of a caldera collapse during an explosive eruption typically lasts more than 30 min (Stix & Kobayashi, 2008). There are different types of geometry and collapse mechanisms (Roche et al., 2000; Stix & Kobayashi, 2008). Consequently, there is no unequivocal examples of tsunamis generated by a caldera collapse. Other phenomena, such as underwater explosions, eruptive column collapse, and pyroclastic flows may generate tsunamis during an explosive caldera-forming eruption, which makes it difficult to determine the source of the tsunami(s). This is illustrated by the near-field tsunami that impacted the Tonga Islands during the 2022 eruption of Hunga volcano:significant caldera collapse occurred during this event (around 800 m vertical depth change, Seabrook et al., 2023), but it is not certain how big a role this played in the near-field tsunami.

2.5. Underwater Explosion

The theory of water waves generated by underwater explosions is well documented and has been applied to nuclear, chemical, and volcanic explosions (Duffy, 1992; Egorov, 2007; Le Méhauté, 1971; Le Méhauté & Wang, 1996; Mirchina & Pelinovsky, 1988). During an underwater explosion, while different jet flows are ejected, an underwater cavity develops, depending on water depth and energy of explosion. The subsequent expansion, rise and gravitational collapse of this cavity creates two successive bores followed by a number of smaller undulations which propagate radially from the source.

The tsunamigenic potential of an underwater eruption is determined by the strength of the eruption and the depth of the water it occurs in Shen et al., (2021b). Generally, volcanic eruptions in water shallower than 500 m are considered potentially tsunamigenic, but in fact only a few eruptions are large enough to do so. Compared to other sources of underwater explosions, the dynamics of phreatomagmatic eruptions are complex. The physics of magma-water interactions are controlled by many parameters: water depth, geometry of the vent and magma-water interface, transfer of thermal energy, processes of intermingling and mixing between magma and water, metastability of superheated water, and quantity of gas in the ascending magma (Kokelaar, 1986; Valentine & White 2012; Wohletz, 1986). Field observations of underwater eruptions and laboratory experiments show two different types of surface expression of underwater eruptions, dome-regime, and finger-regime fountains, depending on explosion intensity and water depth (Shen et al., 2021a).

There is a critical water depth at which an explosion with a given intensity generates the largest waves (Shen et al., 2021b). Underwater eruptions typically generate dispersive waves with short periods (compared to seismic tsunamis) that propagate radially, thus reducing their far-field impact (Table 1: Myojin-Sho 1952).Violent explosions in shallow waters or lakes, still have the potential to produce high-runup local tsunamis (Table 1: Karymskoye Lake 1996).

2.6. *Collapse of Eruptive Column*

An eruption column or eruption plume is a vertical cloud of volcanic tephra (mostly ash) suspended in gases emitted during an explosive eruption. The column may extend several kilometers in the atmosphere, up to 40–50 km in the stratosphere for the largest explosive eruptions (e.g. Hunga 2022). Continuous or closely spaced, discrete eruptions form sustained columns, whereas discrete eruptions produce transient columns. The collapse of an eruptive column is controlled by the evolution of buoyancy in the column. The column starts to collapse when the initial upward momentum provided by the eruption is not sufficient to counteract gravity or to carry the tephra up to the point of buoyancy inversion (Carazzo et al., 2015; Woods, 1988). This critical condition depends on magma gas content, temperature, and magma discharge rate. The intensity of the collapse varies from one eruption to another, and, for stable plumes, may evolve as a function of the buoyancy ratio (Carazzo et al., 2015). When collapse occurs, the tephra falls under gravity, forming a pyroclastic flow on the flanks of the volcano.

If the eruption occurs on a small volcanic island or a shallow-water volcano, the eruptive column may collapse directly in the water. Pyroclastic flows resulting from the collapse are then subaqueous and the collapse itself becomes the main source of tsunami. Although there is considerable literature on eruptive column collapse in volcanology, it is not commonly addressed as a source of volcanic tsunami. However, this neglected mechanism may have played a role in the generation of near-field tsunami during explosive eruptions such as Krakatau 1883 (Carey et al., 2000; Paris et al., 2014b) and Hunga 2022 (Seabrook et al., 2023).

2.7. *Atmospheric Forcing Following an Explosive Eruption*

The atmospheric waves that are produced during a major volcanic explosion can generate tsunami. This rare phenomenon was first documented for the 1883 eruption of Krakatau (Harkrider & Press, 1967) and extremely well recorded for the 2022 eruption of Hunga volcano in the Tonga Islands (Wright et al., 2022). Tsunamis generated by this type of atmospheric forcing are the only volcanic tsunamis that may have a global reach.

The largest explosive eruptions generate a broad range of waves in the atmosphere, including acoustic-gravity waves that may reach the ionosphere (Astafyeva et al., 2022). Among these atmospheric waves, compressional surface-guided Lamb waves travelling at the speed of sound can produce long-period waves in the ocean (Kubota et al., 2022; Omira et al., 2022). The leading tsunami wave is forced by the Lamb wave and travels at the same speed (i.e., faster than the usual tsunami speed, the shallow water wave speed, $c = \sqrt{gH}$) (Carvajal et al., 2022). Behind this is a wave train that travels at the shallow water wave speed in the ocean (Kubota et al., 2022; Omira et al., 2022; Williams et al., 2021). This phenomenon is known as the Proudman resonance (Proudman, 1929). The closer the speed of the atmospheric forcing is to the shallow water wave speed, the larger the response of the surface elevation. Theoretically, when the atmospheric forcing is travelling at the same speed as the tsunami waves, the sea surface disturbance grows linearly (Williams et al., 2021). When the Lamb waves pass over the deepest ocean trenches (with depths around 10 km) the tsunami wave speed is similar to the Lamb wave speed and most efficiently generating this type of tsunami wave through the Proudman resonance. Once the atmospheric forcing moves on from the trench it

again is moving considerably faster than the shallow water wave speed. These tsunami waves are left behind and no longer being reinforced by the atmospheric wave, but they continue to propagate at the shallow water wave speed. This mechanism explains tsunami waves from the Hunga 2022 eruption that arrived later than the direct meteotsunami arrivals but before the expected first arrival of the conventional tsunami waves, such as in Costa Rica (Chacón-Barrantes et al., 2023). The atmospheric waves can circle the earth multiple times over several days and so the associated tsunami generated by the air–water wave phase coupling lasts longer than the usual earthquake-induced tsunami (Wang et al., 2023).

2.8. Volcano-Tectonic Earthquake

Although earthquakes are often mentioned as a source of tsunami preceding or during a volcanic eruption, historical examples are poorly documented because the distinction between tectonic earthquakes, volcanic earthquakes, or other source mechanisms (e.g., landslide) is often unclear. Among the kinds of earthquakes related to volcanic and magmatic processes, only volcano-tectonic (high-frequency) earthquakes can involve ground deformation large enough to generate tsunami. Volcano-tectonic earthquakes result from the accumulation of stress induced by magma ascent. They are characterized by seismic swarms at shallow depth (< 10 km), with magnitudes typically lower than Ms = 6. Tsunamis generated by these earthquakes are likely to be very small (Paris, 2015).

Two special cases should be mentioned. First, earthquakes with magnitude $M > 6$ can occur on large thrust faults at the base of the oceanic shield volcanoes (e.g., Hawaii) and produce local tsunamis, as demonstrated by the 1975 Kalapana earthquake at Kilauea volcano (Table 1), Hawaii (Ando, 1979; Day et al., 2005; Ma et al., 1999). Second, earthquakes with magnitude $M_w < 6$ resulting from trapdoor faulting of submarine caldera floor can generated small-amplitude tsunamis, as frequently observed around the Sumisu caldera (Table 1), Japan (Sandanbata et al., 2022), and also possibly Curtis Island on the Kermadec Ridge (Gusman et al., 2020; Sandanbata et al., 2023). Shallow submarine trapdoor faulting is an efficient tsunami generation mechanism because it produces large fault slips compared with ordinary tectonic earthquakes, even for relatively low earthquake magnitude (Sandanbata et al., 2022).

2.9. Multiple Mechanisms

Volcanic tsunamis are not confined to a single generation mechanisms, often multiple mechanism may occur within a single eruption to create a combined tsunami (Table 2). This makes it difficult to characterize the source of a tsunami observed during an eruption. All the source mechanisms described above have different characteristics in terms of location, duration, volume, mass flux, and energy, which have consequences on the waves generated. Landslides are the most frequent sources of volcanic tsunamis. From all points of view, volcanic islands (arcs) are the most exposed to volcanic tsunamis.

3. Numerical Modelling of Volcanic Tsunamis

Numerical models provide tools to simulate and understand possible volcanic tsunamis and evaluate their impacts. The main applications of the volcanic tsunami modelling are: (I) Research analysis to interpret data and improve scientific understanding of volcanic tsunami phenomena; (II) Tsunami hazard assessment to evaluate long-term risk from volcanic tsunamis and (III) Real-time tsunami forecasting for tsunami warning and threat mitigation purposes. The appropriate numerical method to use and the specifics of the application of the model should be guided the goal you seek to achieve.

Volcanic tsunami modelling undertaken for research analysis place the fewest requirements on the numerical methods to used. Because volcanic tsunami generation involves interplay of complex

Table 2

Types of potentially tsunamigenic volcanoes and associated source mechanisms of tsunamis (updated from Paris et al., 2014a)

		Volcano type			
		Coastal / island stratovolcano	Submarine stratovolcano	Shallow-water caldera	Oceanic shield volcano
Tsunami source	Subaerial landslide	■		■	■
	Submarine landslide		■	■	■
	Underwater explosion		■	■	
	Caldera collapse		■	■	
	Column collapse		■	■	
	Pyroclastic flow	■	■	■	
	Volcano-tectonic earthquake				■
	Atmospheric forcing	■	■	■	
Examples		Stromboli, Italy	HTHH, Tonga	Taal, Philippines	Kilauea, Hawaii
		Soufriere Hills, Montserrat	Kick'em Jenny, Grenada	Rabaul, Papua New Guinea	Fournaise, Reunion Island
		Unzen, Japan	Kolumbo, Greece	Krakatau, Indonesia	Fogo, Cape Verde

processes, sophisticated models that require considerable computational resources are often needed. These processes may involve multiple densities of fluids, phase-shifts, and very fast, often supersonic flows. The most appropriate models are often based on various discretization and closures of the Navier–Stokes Equations or their higher order approximations. These sophisticated models can be used to develop approximations for more practical modelling applications with greater computational constraints.

Tsunami hazard analyses studies often require modelling multi-scenario ensembles for probabilistic or sensitivity analysis. These computations often require high resolution discretization to capture appropriate topographic features. These high computational requirements (in terms of numbers of scenarios and resolution) limit the complexity of the numerical techniques that can be used. Generally, it is too computationally expensive to solve the Navier–Stokes Equations directly. Approximations must be made that balance computationally achievable numerical analysis and accuracy.

Real-time forecast applications place the highest demands on numerical efficiency because accurate forecasts are needed in limited time. This requires highly efficient implementations of models with optimal approximations of the Navier–Stokes Equations.

The tsunami waves generated by volcanoes are generally shorter than those generated by earthquakes (see Sect. 2). Shorter waves attenuate faster, even if the initial amplitudes are much larger. Therefore, most volcanic tsunamis only impact local coastlines (the exception being atmospheric forcing following an explosion, e.g., Krakatau 1883, Hunga 2022). Local impacts have very little lead time, making real-time modelling especially challenging. Often pre-computed scenarios are the only feasible option.

Hybrid modelling, where precomputed scenarios are used to train a machine learning model which can then rapidly estimate tsunami hazard, could bridge the gap between the computation resource needed for volcanic tsunami modelling and the short timeframes required for warning purposes.

While all model applications require testing and validation, this is especially important for tsunami hazard assessment and real-time forecasting. The simplifications used in such studies should be validated before the model products can be trusted. The tsunami scientific community has developed the process of model validations over the years (Synolakis et al., 2008), which has included benchmarking workshops for specific tsunami applications (see for example Lynett et al., 2017). Real-time applications must go through additional tests for operational suitability and implementation, which put additional demands on model performance and robustness (Titov et al., 2016). As many volcanic tsunami generation mechanisms are similar to landslide-generated tsunamis, the extensive literature developed on that subject should be considered (see Løvholt et al., 2015 and references therein).

Modelling tsunamis generally is divided into three phases: generation, propagation, and inundation. Most of the differences between seismic and volcanic tsunamis occur in the generation phase. Thus, this section mainly focusses on different methods for modelling the generation mechanisms outlined in Sect. 2. We also briefly consider aspects of volcanic tsunami propagation, especially for atmospheric forcing following an explosive eruption, where the propagation and forcing are linked.

3.1. Tsunami Generation and Initialization Modelling

Section 2 outlines the various processes by which volcanoes can generate tsunamis. Many of these mechanisms are complex and not fully understood. Often multiple mechanisms occur at different times over the course of the eruption and the tsunami evolution. This causes additional challenges of incorporating different forcing throughout the simulation. In the next two sections we outline instantaneous and finite time initialization techniques for a range of these mechanisms.

3.1.1 Instantaneous Initialization

If the generation mechanism occurs quickly compared to the shallow water wave speed, it may be appropriate to use an instantaneous initialization of the tsunami by specifying an initially deformed water surface (and potentially an initial velocity field although this is not so common). The assumption behind this initialization is that:

$$t_{init} < L/\sqrt{gH} \tag{1}$$

where t_{init} is the initialization time, L is the characteristic spatial scale of the forcing, g is acceleration due to gravity and H is the characteristic water depth in the generation zone. This can also be thought of as analogous to a Froude number comparing the forcing rate to the shallow water wave speed, $L/t_{init}\sqrt{gH}$. When this value is large, it is reasonable to assume instantaneous initialization.

A common volcanic tsunami initialization is a simple cavity. This is often used for explosive submarine eruptions to represent the area remaining after the eruption has blown the surrounding water away. Le Méhauté (1971) and Le Méhauté and Wang (1996) combined results from theoretical calculations and experiments on underwater explosions to develop relationships between the size and depth of the explosion and the size of the cavity it would generate. Le Méhauté (1971) proposed three different initializations, the first a simple removal of a parabolic cavity of water with a net volume loss and the other two cavities with no net volume loss, a shifted parabola with a discontinuous rim, and a fourth-degree polynomial with a more rounded continuous rim (Fig. 2b, c).

Explosions are classified as shallow-, intermediate- and deep-water explosions based on the depth the explosion occurs at and the energy released. The parameters of the cavity are defined according to those classifications. For volcanoes rather than

explosions, further assumptions are needed to estimate the effective explosive energy released from volcanic parameters. These might include the crater diameter and the ejecta volume (Sato & Taniguchi, 1997). This methodology has been used to initialize volcanic tsunamis for Kolumbo, Greece (Ulvrova et al., 2016) the Campi Flegrei caldera, Italy (Paris et al., 2019), Lake Taal, Philippines (Pakoksung et al., 2021), Lake Taupō, New Zealand, (Hayward et al., 2022) and Hunga, Tonga (Lynett et al., 2022).

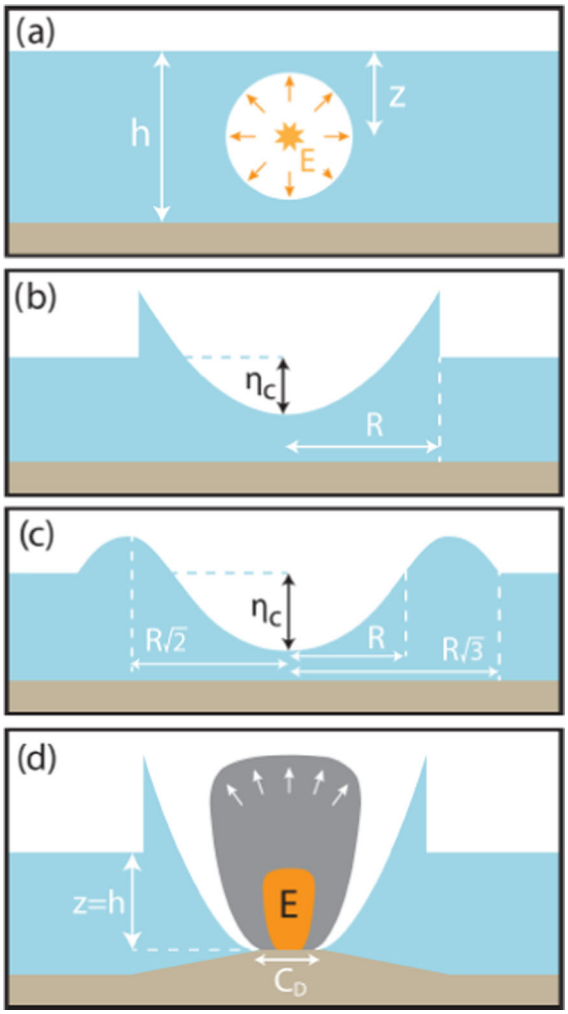

Figure 2
Illustrations of the subaqueous explosion problem. **a** An explosion of yield E at depth z in water of depth h. Various initial surface elevation profile have been proposed including **b** a shifted parabola with a discontinuous rim and **c** a fourth-degree polynomial with a more rounded continuous rim. **d** Schematic of a volcanic scenario in which such an explosion would occur at maximum depth where z = h, and crater diameter C_D (from Hayward et al., 2022)

Tsunamis generated by volcano-tectonic earthquakes are like standard seismic tsunamis and so can also be initialized by instantaneous ground deformation. Ground deformation from earthquakes generally occurs over tens of seconds at most, so Eq. (1) holds for a wide range of initialization parameters (e.g., in 1000 m deep water, a 1km wide forcing would need to occur within 10 s). As for seismic tsunamis, the ground deformation from the earthquake is generally applied instantaneously to the water surface at the start of the simulation. Care must be taken with volcano-tectonic tsunamis as, sometimes larger tsunamis than expected based on the magnitude of the earthquake can result from volcanic earthquakes. This may be caused by trapdoor faulting (Sandanbata et al., 2022) or hydro-fracturing of heated water in shallow sediments, which could cause greater ground deformation than the earthquake alone (Gusman et al., 2020).

Caldera collapse is also sometimes modelled as an instantaneous ground deformation, with the initialization of the water surface either directly replicating the shape of the collapsed caldera or some filtered version (Ulvrova et al., 2016). This is reasonable if the caldera collapse occurs rapidly (as defined by Eq. (1)), but most collapses are thought to occur over tens of minutes or more, which makes the finite time initialization described below more appropriate.

Other volcanic tsunami scenarios have also been modelled using instantaneous changes to the sea surface. The 2018 tsunami generated by the collapse of a large part of Anak Krakatau during an eruption has been modelled as a Gaussian mass of water of approximately the same size as the original volcano (Firdaus et al., 2022; Heidarzadeh et al., 2020). While this is a relatively crude initialization, it can produce waves of a similar magnitude to the event if the magnitude of initialization is correct. However, instantaneous initialization is not appropriate for simulating tsunamis generated by gravitational flows (including pyroclastic flows) because it cannot reproduce the effect of important parameters such as the mass discharge rate, the duration of the flow, and its deformation (Bougouin et al., 2021; Yavari-Ramshe & Ataie-Ashtiani, 2016).

Another tsunami initialization technique involves setting the starting water surface and possibly also

velocity field using information taken from either a more complicated numerical model (e.g., Chang & Wang, 2015), an analytical model (e.g., Duffy, 1992; Egorov, 2007), or an empirical model (e.g. TOPICS). The TOPICS model was primarily developed for initializing landslide tsunamis (Watts et al., 2003) and PDCs (Waythomas & Watts, 2003). It uses empirical formulas based on the characteristics of the landslide and previous physical and numerical modelling to define the water surface and velocity fields. TOPICS has formulations for initializing tsunamis generated by submarine and subaerial landslides, as well as PDCs (see http://www.appliedfluids.com/geowave.html for further details).

Aspects of a volcanic eruption close to the eruption zone can be modelled with hydrocodes using Navier Stokes approximations such as the Volume of Fluid representation. These models often have a simplified representation of the bathymetry and volcano or model a 2D vertical slice assuming rotational symmetry, or some approximation into 3D (Mader & Gittings, 2006; Gisler et al., 2006; Lane et al., 2016; Morrissey et al., 2010; Range et al. 2022). After the main forcing has occurred, the water levels and velocity field can then be transferred to a simpler and numerically faster (generally 2D) model (often with better bathymetry) for the propagation phase. It is important to ensure that at the time of the initialization the volcanic eruption is no longer significantly influencing the tsunami waves. This initialization method has been used for flank collapse and other landslide-tsunami (Abadie et al., 2012; Gauer et al., 2005) and could be used for PDC using results such as from (Battershill et al., 2021). We are

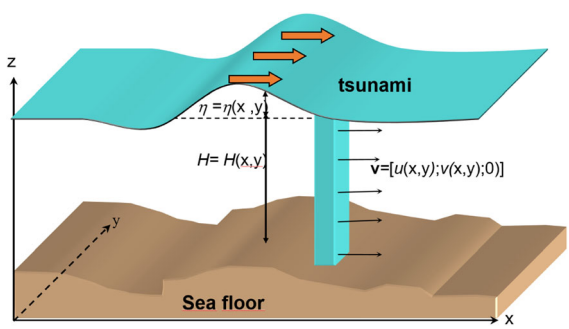

Figure 3
Illustration of the tsunami propagation modeling parameters (Eq. (2))

not assuming in this case that the generation mechanism is instantaneous so Eq. (1) does not need to hold. Rather we are initializing from a snapshot in time after the generation has occurred, but before the tsunami has travelled too far. This technique works best for modelling tsunamis outside of their generation zone because they often assume simplified geometry within it. If very near-field results are needed, a two-layer or multi-layer model might be more appropriate (see Finite time initializations).

3.1.2 *Finite Time Initialization*

If Eq. (1) does not hold, a finite time initialization might be more appropriate. In this case, the forcing occurs over a specified duration, rather than instantaneously.

Ground deformation One example of this is forcing with a specified ground deformation. Depth-integrated equations generally solve for changes in the sea surface elevation over time, assuming that the bathymetry stays constant with time. But temporal changes to the bathymetry can easily be added as a forcing term in the following manner

$$\frac{\partial \eta}{\partial t} = F(\eta, u, v, H) - \frac{\partial H}{\partial t} \tag{2}$$

where $F(\eta, u, v, H)$ is the equation being used (e.g., Saint Venant Shallow Water Equations, Boussinesq Equations etc.), η is the water surface, H the water depth and (u, v) the vertically averaged horizontal velocity (see Fig. 3). This method relies on being able to describe how H evolves over time. For finite time caldera collapse, it could be assumed that the bathymetry varies linearly between the pre- and post-event over a specified time duration (Maeno et al., 2006). Alternatively, for a piston collapse type caldera collapse, this could be specified as a region of collapse (say a circle in the simplest case), a collapse rate and duration. More complicated time histories could also be used, but given the scarcity of knowledge about caldera collapse, there may not be observations to confirm or refute more complicated models.

Specifying bottom forcing has also been used to initialize eruptive column collapse, flank collapse, or PDC entry into the sea (De Lange et al., 2001).

Generally, this relies on assumptions about the speed and thickness of the flank collapse or PDC. Usually, a simplified version of the motion is used, assuming that as long as the general size and timescale of the seafloor motion is approximately captured then the wave motion will be the right order of magnitude. By modelling these changes happening over time, it allows the sea surface to adjust to the changes at its natural speed.

In all these sea floor deformation scenarios, the bathymetry must be updated to maintain consistency with the forcing.

Two-layer and multi-layer models Often for flank collapse and PDC scenarios, the details of how the mass failure occurs (acceleration, flow paths, etc.) are not known a priori. These might need to be modelled together with the overlying ocean. One way of achieving this is to use a two-layer or multi-layer model. The landslide and the ocean are modelled as separate, depth-integrated layers that can influence each other (Maeno & Imamura, 2011; Savage & Hutter, 1989; Voellmy, 1955). This method is appropriate to model the very near-field effects of flank collapse or PDC-generated tsunamis where other initialization techniques such as TOPICS, or initializing from a simplified 3D model, might not be appropriate, as they do not consider the near-field bathymetry. These models generally assume that the flank collapse or PDC is represented by a denser layer of viscous fluid overlain by sea water. In some cases, the less dense component of the PDC has also been considered (Watt & Waythomas, 2003). Different rheologies that better represent mass flows can be specified depending on the sophistication of the equations being used (e.g., Kelfoun, 2011). In the case of flank collapse a more viscous underlying fluid is likely to be more realistic, but for PDCs, experimental modelling suggests that their behavior is well captured by a dense fluid with a viscosity similar to water (Bougouin et al., 2021).

Ongoing forcing Atmospheric forcing can generate a tsunami when an explosive volcano eruption produces a travelling pressure anomaly (such as a Lamb wave) that can travel long distances in the atmosphere at high speeds. The mechanism is generally known as Proudman forcing. It caused the global tsunamis generated by the 1883 Krakatau eruption (Harkrider & Press, 1967) and the 2022 Hunga eruption (Omira et al., 2022). The pressure anomaly forces the ocean surface over large distances due to the pressure gradient. This must be modelled using ongoing forcing throughout the propagation phase. The generation phase cannot be separated from the propagation phase. The pressure anomaly forcing is incorporated into the equations as $-\frac{1}{\rho g}\nabla P$, as is done in storm surge and meteotsunami models. The Proudman expression (Proudman, 1929) for ocean surface amplification due to moving pressure describes the tsunami amplification during this process as:

$$\eta = \frac{c^2 \eta_s}{c^2 - U^2} \tag{3}$$

where η is the sea surface displacement, $c = \sqrt{gD}$ is tsunami wave celerity at depth D, U is the speed of the atmospheric disturbance and $\eta_s = P/\rho g$, where P is the pressure disturbance, ρ the seawater density and g acceleration due to gravity.

This amplification is most effective when the speed of the atmospheric forcing is the same as the shallow water wave speed (Proudman resonance) at which point:

$$\eta(x,t) \approx -\frac{x}{2\rho g} P_x \tag{4}$$

This initial linear growth tapers off as nonlinear effects come into play (Williams et al., 2021).

Because Lamb waves generally move faster ($\sim$ 310 to 320 m/s) than shallow water waves ($\sqrt{gH}$) over most of the world oceans, it is only over the deepest parts of the ocean (Oceanic trenches with depths around 10 km) where the most effective energy coupling occurs, and highest amplitude tsunami waves are generated. The first arrivals of pressure-forced tsunamis occur simultaneously with the Lamb wave arrival. Generally, these have relatively small sea surface heights determined by the off-shore value of Eq. (3). These first waves can be followed by gravity driven tsunami waves that were

generated by the Proudman resonance (Eq. (4)) when the Lamb wave passes over deep ocean trenches. Depending on the relative location of the ocean trench and the arrival location these later wave may have much higher amplitudes than the initial arrival and come much later but still often before the expected conventional tsunami arrival time (Carvajal et al., 2022).

While this modelling just requires the straightforward (addition of the forcing term described above, is very different from the "traditional" tsunami modelling, where the source is pre-defined (often pre-computed) and source modelling is separate from propagation. The process of Lamb wave atmospheric pressure waves being generated during a volcano eruption is not yet fully understood. Nevertheless, the Lamb wave pressure disturbance propagation in the atmosphere is well-described by a simple shallow-water wave model (Themens et al., 2022). This was well verified for the 2022 Hunga volcano tsunami (Wright et al., 2022). The Lamb wave propagation can be prescribed even more simply with a constant propagation speed ($\sim$ 310 m/s) and pressure disturbance with its amplitude scaled to observations (Lynett et al., 2022).

Thus, modelling of a Lamb wave-generated tsunami for a particular event is possible using techniques similar to the meteotsunami simulations, especially if the forcing is simply scaled by the measurements of the pressure wave amplitudes.

The scaling laws for tsunamis generated by atmospheric forcing following an explosion are more difficult to generalize, since the generation of gravity waves by propagating pressure forcing depends on so many parameters. Tsunamis from sources with instantaneous, and even finite time initialization, usually scale relatively well with the magnitude of the source. That is, however, not true for Lamb wave forcing, which is complicated by the Proudman resonance effects. The tsunami arrival time and tsunami amplitudes (at least of the biggest wave) depends on the location of the source, the depth of the ocean between the source and the location of interest, and the parameters of the Lamb wave in very complex ways. Even interpretation of the direct tsunami amplitude is not straightforward. Therefore, modelling of the forcing remains as the main (and so far, the only) tool for tsunami prediction for such events. Finding simplified interpretation tools for the tsunami warning operations for such event requires sensitivity analyses studies using multi-scenario ensemble runs. This work is only just being started by the scientific community.

3.2. *Propagation, Inundation, and Other Volcanic Tsunami Modelling Considerations*

While the main differences between volcanic and seismic tsunami modelling are at the initialization stage, here we give a quick overview of tsunami propagation, inundation, and other considerations.

In general, volcanic tsunami propagation is to the same as the more common seismically generated tsunamis, therefore, most tsunami propagation models are suitable for modelling volcanic tsunami propagation. However, because of the shorter wavelengths that occur for volcanic tsunamis, dispersive effects may need to be considered during the propagation phase (see Glimsdal et al., 2013 for further details). This should be taken into account when applying traditional depth-averaged tsunami models for volcanic tsunami propagation simulations. Most tsunami modelling codes are tested for seismic tsunamis, which tend to have longer wave lengths and wave periods, especially tsunamis generated by large subduction zone earthquakes. The Shallow Water Equations do not resolve dispersive effects and so higher order approximations of the depth-averaged models (e.g., Boussinesq Equations and other dispersive approximations (Popinet, 2015; Watts et al., 2003)) or multi-layer models (Hayward et al., 2022; Ma et al., 2012) are needed where dispersive effects are important.

Inundation dynamics for volcanic tsunamis is also essentially the same as for any tsunami inundation. Volcanic tsunamis are generally a local phenomenon with higher initial amplitudes and impact areas that are much closer to the source than seismic tsunamis.

As a result, the local inundation from volcanic tsunamis can be far more intense. Standard tsunami inundation models are generally suitable to simulate volcanic tsunami inundation. However, testing and additional validations would provide further certainty that the higher amplitude and flow velocities of volcanic tsunamis are properly modelled.

The tsunami inundation phase is often modeled separately from initialization and propagation, especially in the case of very high resolution inundation modelling (e.g., 1–10 m). Many models allow for nested grids with increased resolution nearshore. Through this, the separate inundation modelling has become a standard technique. While this may simplify the inundation modelling, care must be taken for very near-field simulations where the source and inundation areas are close by. For these situations, a single high-resolution grid or adaptive grid might be more appropriate.

Other issues to consider in inundation modelling are the wetting and drying scheme and the friction. An accurate wetting and drying scheme should be used that does not cause instabilities. The on-land friction formulations also need special care, as inundation and shallow water flows are far more sensitive to friction than in deeper water.

When modelling volcanic tsunamis, as with other tsunamis, it is important to have sufficient resolution to fully resolve the tsunami waves throughout the modelling process. This may require high resolution, especially at the initialization and inundation phases where the tsunami waves may have steep gradients. A variety of different modelling techniques and grid types exist to ensure high enough resolution where it is required. One technique is the use of nesting (sometimes two-way nesting) of Cartesian grids (e.g., MOST (Titov et al., 2016), COMCOT (Liu et al., 2005; Wang & Power, 2011). This nested grid approach may need to be adapted for the near-field volcanic tsunami simulations, since high resolution is needed at both the inundation and source locations—not all nested grids models provide such capabilities. Another option is adaptive grids, which adapt the resolution as required spatially and temporally over the simulation. Examples of this are quad-tree grids [e.g., Basilisk (Popinet, 2011, 2012)] and block uniform grids [e.g. (Vacondio et al., 2017) or BG-Flood (Bosserelle et al., 2021)]. Yet another option is the use of an unstructured triangular or quad grid or a combination of these elements. In this case the grid is static, but it can be specifically designed with higher resolution at the source and inundation locations as desired (e.g., SELFE (Zhang & Baptista, 2008)).

Tsunami modelling is often computationally very expensive and so achieving faster, more efficient runtimes is very desirable in many situations. Faster run-times can often be achieved by models that can run in parallel (either OpenMP, or, especially for large domain, or high-resolution models MPI) or models that are able to run on General Purpose GPUs (Bosserelle et al., 2021; Qin et al., 2019).

4. *Volcanic Tsunami Hazard Assessment: Stromboli*

Stromboli volcano (southern Tyrrhenian Sea, Italy) is well-known for its moderate but persistent explosive activity, which has been occurring since the medieval age, one thousand years ago. The island of Stromboli rises 924 m above the sea level, but the volcano has deep roots around 2000 m below the sea surface (Fig. 4a). Thus the volcanic edifice is two-thirds underwater and almost 3000 m high, making Stromboli one of the largest volcanic edifices in Europe. The above-water volcano has grown over the last 100 ka as the result of a continuous sequence of eruptions together with a series of large-scale (up to 2 km^3) gravitational sector collapses (Pasquarè et al., 1993; Rosi, 1980; Tibaldi, 2001).

The last of these dramatic series of sector collapses (*NeoStromboli*) took place $\sim$ 5 ka ago on the NW facing flank, generating the 3 km long and 2 km wide Sciara del Fuoco depression (Fig. 4b) involving a total volume of approximately 1.2 km^3 (Kokelaar & Romagnoli, 1995; Tibaldi, 2010). The actual shape of the Sciara del Fuoco is linked to a collapse in Roman age $\sim$ 2 ka (*Pizzo*) with a volume of around 0.8 km^3 (Francalanci et al., 2013) that has generated a tsunami

with a run-up of around 50 m (Tinti et al., 2000). Recent work on paleo-events (Rosi et al., 2019) has identified three well-preserved *Medieval* (1300–1400 CE) tsunami deposits linked to a collapse of $\sim 180 \times 10^6$ m^3 of the Sciara del Fuoco, which seems to have destroyed the ports of Naples, Amalfi and Pozzuoli and caused fatalities in the Neapolitan Gulf in 1343 (Rosi et al., 2019).

The Sciara del Fuoco is now a 35° (on average) steep scar that extends $\sim$ 700 m below the sea surface. It represents the preferential runway of the volcanic products generated by the eruptive phenomena. Most of this eruptive material accumulates at a mean rate of $\sim 10^5$–10^6 m^3/year over the Sciara del Fuoco scarp providing the overloading condition for landslides and/or debris slides with volumes ranging between 10^5 and 10^7 m^3. This makes Stromboli one of the main sites in the Southern Tyrrhenian Sea where non-earthquake-induced tsunamis can be generated.

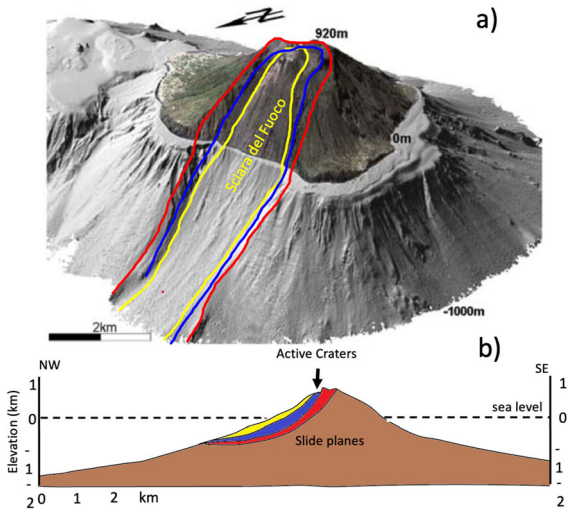

Figure 4
a 3D map of Stromboli volcano showing the Sciara del Fuoco slope above and below the sea surface (Chiocci et al., 2008). The lines indicate the position of the 3 main collapses in the NW flank occurred $\sim$ 13 ka (Vancori in red), $\sim$ 5 ka (NeoStromboli in blue) and $\sim$ 2 ka (Pizzo in yellow) in Roman age which have originated the present-day Sciara del Fuoco slope. **b** Section along the NW–SE profile of Stromboli volcano (dashed line in Fig. 4a) with the position of the sliding planes of the 3 main collapses (Redrawn from Tibaldi, 2001) of Vancori (in red), NeoStromboli (in blue) and Pizzo (in yellow).

4.1. Tsunami Hazard Scenarios

Gravitational mass-flow of the Sciara del Fuoco scarp have been generated during periods of intense volcanic activity (Fig. 5) and are responsible for a large number of tsunamis with an average of one event every 15 years from the beginning of the twentieth century (Fig. 5). The 1930 tsunami, for example, was associated with one of the most violent explosive eruptions of the last century. Hot avalanches overflowed the Sciara del Fuoco scarp and impacted the village of Stromboli and Ginostra. It also generated a tsunami observed along the Calabrian coast inundating up to 200 m and with a run-up of 2–3 m at Stromboli (Maramai et al., 2005).

Besides large sector collapses with volumes in the order of 10^9 m^3 (last one 2 ka ago), the historical record suggests that gravitational instabilities of the Sciara del Fuoco are triggered by violent explosive or effusive eruptions (Tinti et al., 2008), both associated with a strong deviation from the "normal" and moderate explosive activity (Fig. 5).

Effusive eruptions are generally linked to magma intrusion and to the opening of lateral effusive vents which compromise the stability of the Sciara del Fuoco flank. They can cause collapses of volume 10^7–10^8 m^3. The opening of an effusive vent is generally associated with the increase of the magma input rate, which leads to a transition from the explosive to the effusive regime. This process can last several days and should give enough time to warn the population of the imminent possibility of a tsunami. The last pyroclastic density current (PDC) triggered by lava effusion occurred on 4 December 2022 and triggered a tsunami recorded by the Early Warning System with a height of 1.5 m at $\sim$ 1100 m from the splash zone. This tsunami was large enough to trigger the automatic alert system of the Italian Department of Civil Defense (see Appendix for details). In this case, the sudden occurrence of the PDC only allowed a 4-min warning (Fornaciai et al., 2019), compatible with the modeled wave travel time from the coast of the Sciara del Fuoco to Stromboli village (Fig. 6).

Explosive eruptions (paroxysms) can occur suddenly and without clear precursors, representing a considerable threat to the population and a challenge in managing the risk. Since 1900, Stromboli has

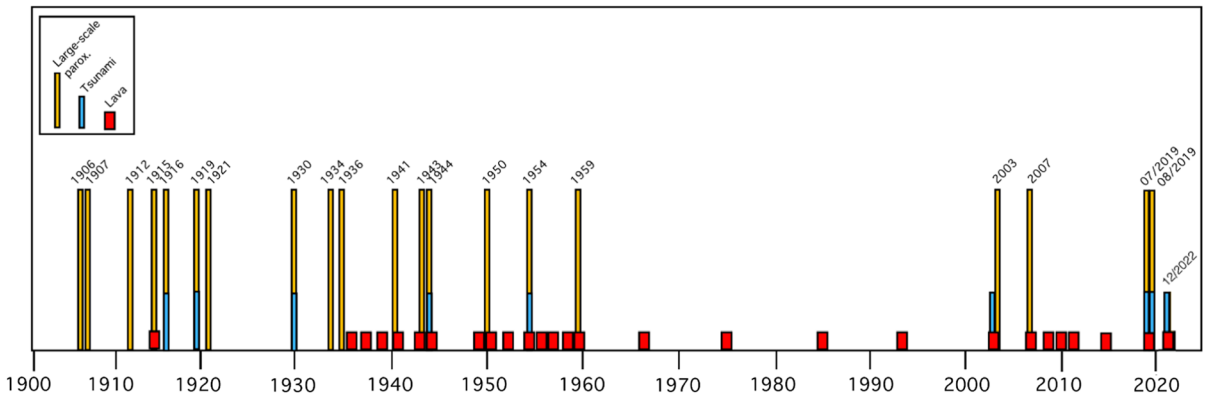

Figure 5

Relationship between volcanic activity and tsunami at Stromboli (from Rosi et al., 2019). Number of explosive paroxysms (yellow), effusive eruptions (red) and tsunami (blue) occurred since 1900. The 1960–2003 is a period of relatively low activity, mainly characterized by the typical moderate explosive strombolian activity. Most of the tsunami (7) are associated to explosive paroxysms. The largest ones occurred in 1930 and 1944 with marine ingression up to 300 m and a run-up of 3–4 m. The last tsunami was instead generated on 4 December 2022 by the partial collapse of the north-east crater sector as consequence of intense lava effusion

experienced 20 large paroxysms, approximately one every 6 years (Bevilacqua et al., 2020), with the last ones in July and August 2019. These violent explosive eruptions are always associated with PDC (volumes around 10^5–10^6 m^3) triggered either by the collapse of the volcanic plume or by the partial collapse of the crater rim. The July and August 2019 events generated tsunamis of ∼ 1–2 m height (Ripepe & Lacanna, 2024). A warning system is operating at Stromboli based on the automatic detection of inflation of the ground associated with the explosive paroxysm (Ripepe et al., 2021). This will detect a likely event 4–5 min before the tsunami generation, increasing to 8–9 min the tsunami warning time.

4.2. *Tsunami Hazard Assessment*

At Stromboli tsunami hazard was estimated considering the scenario associated with two landslides that occurred on 30 December 2002, at the beginning of a 9-month long effusive eruption. This was the largest tsunami recorded at Stromboli over the last century and it has been particularly well-studied in terms of generation and dynamics (Chiocci et al., 2008). The total landslide volume was greater than 17–20 × 10^6 m^3 (Chiocci et al., 2008) and generated a wave with a run-up of up to 11 m (Tinti et al., 2003) with a maximum inland inundation extent of around 200 m on both the Stromboli coast and the nearby (∼ 20 km) island of Panarea. The tsunami was also observed in several places along the coast of Italy, from the Campanian in the north-east to the western part of Sicily southward (Tinti et al., 2006).

The tsunami hazard was evaluated by modelling the propagation of tsunami waves triggered during this 2002 event and considering different landslide scenarios (Esposti Ongaro et al., 2021; Fornaciai et al., 2019). Rigid and deformable (granular) submarine landslide models were considered (Esposti Ongaro et al., 2021) to estimate their impact on Stromboli. They showed that solid slides cause larger waves and runup and that subaerial landslides generate tsunamis with larger amplitudes than submarine landslides (Fornaciai et al., 2019).

Additionally, the model predicts that the largest amplitude wave hit the populated Stromboli shore in less than 3–4 min from generation (Fig. 6). Within 20–30 min the whole Aeolian Arc and the coast of Calabria and Sicily (at ∼ 50 km) is impacted. Waves travel across the southern Tyrrhenian Sea and enter the Neapolitan Gulf after 1 h and 20 min (Fornaciai et al., 2019).

Recently, a consortium has formed to develop probabilistic volcanic tsunami hazard maps (Selva

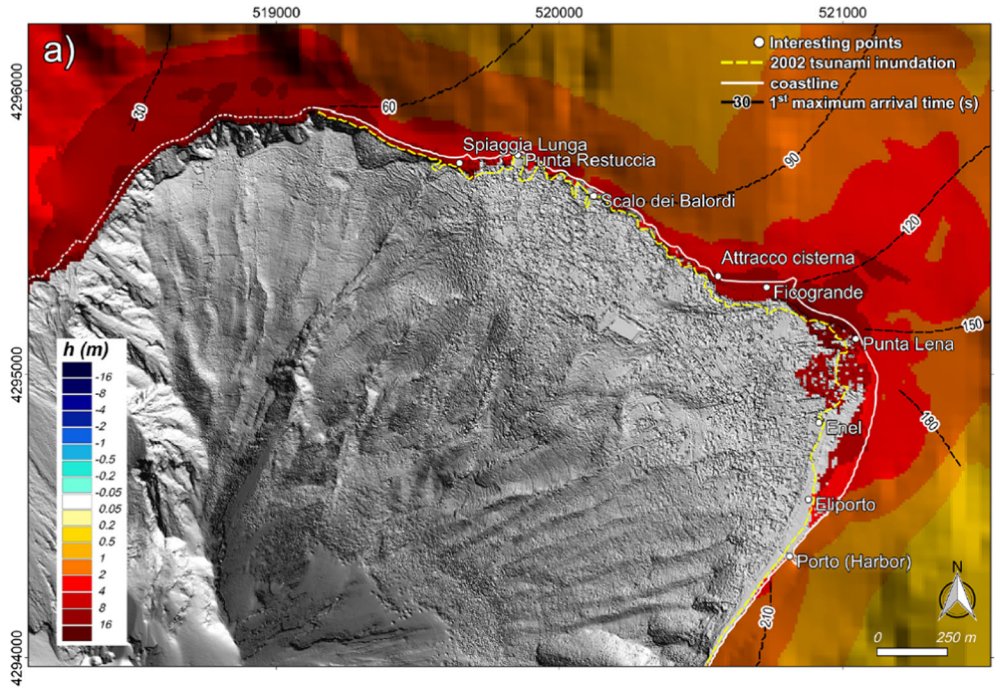

Figure 6
Comparison between observed (dashed line) and simulated tsunami effects at Stromboli. Stromboli map representing the maximum simulated inundation and wave height for a tsunami caused by a submarine slide along the Sciara del Fuoco of 17.6 × 10^6 m^3. the wave with the largest amplitude will hit the Stromboli coast between 2 and 2.5 (at Spiaggia Lunga) and 5–7 (at the Harbor) minutes (Fornaciai et al., 2019)

et al., 2021) for different scenarios and different probability level. This fits in the framework of the operational monitoring activities for the Italian Department of Civil Protection (DPC), under an agreement between with the National Institute of Geophysics and Volcanology (INGV) and the Universities of Pisa and Firenze, in cooperation with the University of Clermont-Ferrand, the Norwegian Geotechnical Institute (NGI) of Oslo, the University of Malaga, and Consejo Superior de Investigaciones Científicas (CSIC) of Barcelona.. These hazard maps will be used to evaluate inundation maps and will serve as a basis to define protocols for the mitigation of the risk associated with volcanic tsunamis.

5. *Volcano Monitoring Requirements for Tsunami Warning*

Current tsunami warning systems are not designed to deal with landslide or volcanic sources, (see Sect. 2) nor with tsunamis triggered by atmospheric anomalies as occurred during the recent Hunga eruption (e.g., Kubota et al., 2022). Most of the actual warning systems are built to handle earthquake-generated tsunamis, and only after the source and the magnitude of the earthquake have been estimated. Tsunami warnings are then issued based on the expected arrival time predicted by numerical simulations of wave propagation. These earthquake-generated tsunami warning systems are ineffective when a tsunami is generated by an unconventional source such as a volcanic eruption. Tsunamis generated by volcanoes are the consequence of magma dynamics which in most cases is a slower process than the brittle fracture dynamics associated to earthquakes and, on some occasions, can give rise to geophysical and geochemical evidence from minutes to months before the eruptive onset.

The input of new magma from a deep reservoir to the shallower part of the volcanic edifice generally triggers an increase in the geophysical and

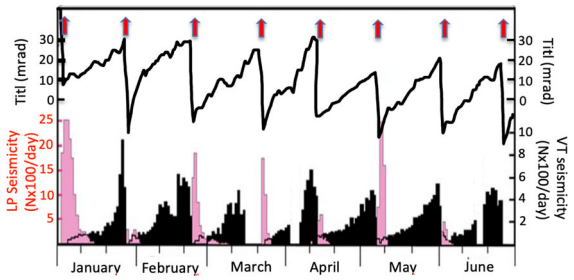

Figure 7
Ground deformation (tilt) compared to Volcano Tectonic (VT) earthquakes (black bars) and Long Period (LP) volcano (pink bars) seismicity (earthquake counts × 100) on Kilauea Volcano between January and June 1986. Each eruption (marked by arrows) is preceded by gradual inflation and terminated by abrupt deflation deformation of the ground measured by summit tiltmeter (from Tilling, 2008)

geochemical parameters, which can anticipate volcanic instability from several days to months. Monitoring networks can often detect this volcanic unrest and, unlike seismic tsunamis, could give enough time to prepare and warn the population of the possibility of a tsunami if it were properly identified. Although the possibility of a false alarm exists if the unrest does not lead to an eruption.

Monitoring systems are specifically designed to provide timely information on the transition between different volcano activity regimes which are detected as a deviation from the background level. Scenarios described in Sect. 2 can have however different preparation time and require different monitoring techniques. Magma migration towards the surface can last several days, or months, and the trigger mechanisms could have incubation time from few to tens of days. Explosive eruption, instead, can be generated by a fast magma dynamics which allow only short-term (hours, minutes) warnings. From a risk management point of view, while the magma intrusion can be responsible for collapsing volumes of 10^7–10^9 m^3, explosive eruptions involve smaller volumes of 10^5–10^6 m^3 (see Table 1).

The most common monitoring techniques used today by volcano observatories aim to define changes in the volcanic activity and could be used in some cases to anticipate the occurrence of possible tsunamigenic phenomena such as in the case of Stromboli volcano (Bertolaso et al., 2009).

5.1. *Volcano Seismicity*

Seismicity is the most common parameter used to monitor volcanoes around the globe (e.g., McNutt et al., 2015). Migration of the magma in the crust generates brittle fractures in the embedded rocks which is the source of volcano tectonic (VT) seismicity (e.g. earthquakes). While magma migrates into fissures seismicity propagates along and/or away from the volcano tracking the position of the magma in the crust (Duputel et al., 2019; Sigmundsson et al., 2022). Approaching the surface, rates of seismicity increase and earthquake locations become shallower. This seismicity can precede an eruption from 1 day to 3 months (Einarsson & Brandsdottir, 2021) and it is generally associated with ground deformation (e.g., Peltier et al., 2018; Sigmundsson et al., 2022). Caldera unrest, for example, is generally associated with inflation of the ground and seismicity (Fig. 7) contained within the ring faults delimiting the volcano structure (Galetto et al. 2022; Newhall & Dzurisin, 1988).

However, seismicity on volcanoes is also produced by the fluido-dynamics of the magmatic column which has different signature with respect to the brittle-fracture signature. This seismicity originates by the movement of magma or gas in the volcanic conduit and is generally characterized by long-period (LP), or very long period (VLP), events and tremors which have frequency content below 5 Hz, lower than seismicity generated by brittle fracture (Kawakatsu & Yamamoto, 2007).

Volcano seismicity is routinely processed automatically and in near real time by all volcano observatories (i.e., real-time seismic amplitude; Pallister & McNutt, 2015), providing updated information on earthquake location, type of seismicity, and/or volcano dynamics (Fig. 7). Many observatories use volcano seismicity as a reliable precursor of volcanic eruptions (Chouet et al., 1994). At Piton De La Fournaise (La Réunion Island),

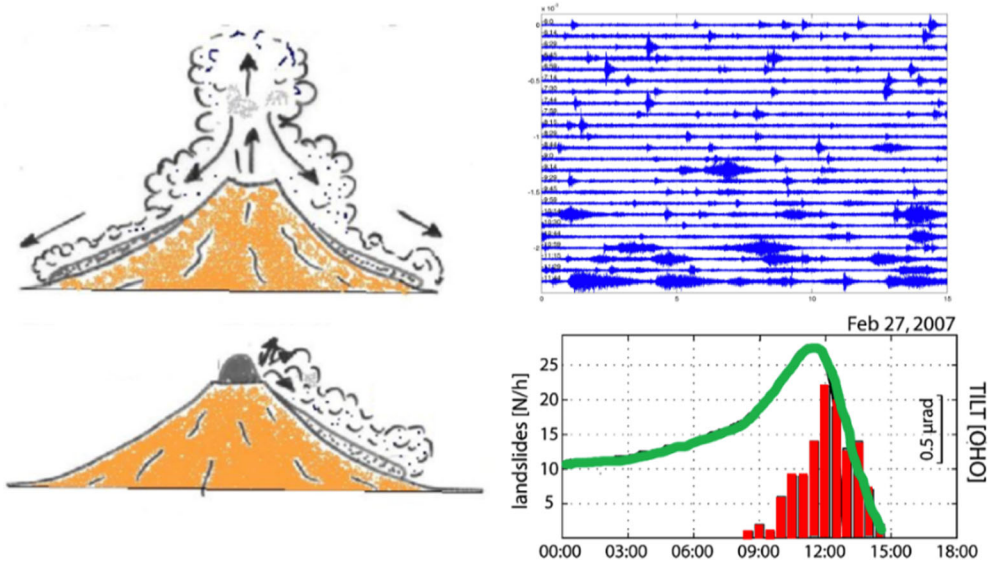

Figure 8
Collapse of the eruptive plume and/or crater rim/dome generates pyroclastic flows and rock avalanches along the steep volcano slope (from Francis, 1993). Magma intrusion inflates the volcano edifice (green line in D) which makes the flank unstable generating rockflows and pyroclastic flows which have the characteristic cigar-shaped seismic transients, Tilt amplitude recorded by the radial component of tiltmeter (green line) and number of rockfalls per hour as recorded by seismic station (from Marchetti et al., 2009)

volcanic seismicity has been used to generate successful real-time early warning alerts for 22 eruptions with a lead time of a few minutes to hours (Roult et al., 2014). Volcano seismic signals are also easy to recognize using new machine learning techniques (Falcin et al., 2021) and, in general, an increase of volcano seismicity is the most common signal for anticipating volcanic unrest (McNutt et al., 2015).

Large mass flow moving downhill the volcano slopes (Kanamori & Given, 1982) such as rockfalls (or rock avalanches), landslide or pyroclastic flows (Calder et al., 2002) are also an efficient source of seismic signals. Assuming that a proportional law exists between destabilization forces and failure mass, or volume, the occurrence of frequent smaller-scale rockfalls can be considered as a potential precursor of larger flank failures (Allstadt et al., 2018) that might evolve into flank collapses (Fig. 8). From this perspective, rockfall monitoring could allow us to anticipate major flank instabilities (Hibert et al., 2014) or track the occurrence of pyroclastic flow (De Angelis et al., 2007; Uhira et al., 1994).

5.2. *Ground Deformation*

When magma is intruded into the volcanic structure the surrounding rock will deform in order to accommodate the new material (Dzurisin, 2003). Ground deformation can be detected by several monitoring techniques using Global Navigation Satellite System (GNSS) receivers, tiltmeters (Dzurisin et al., 1983), strain meters (Linde et al. 1993) and by radar interferometry using ground-based Synthetic Radar Aperture (GB-InSAR) instruments (Schaefer et al., 2019). The inflation of a magma reservoir is often anticipating many eruptions (Biggs & Pritchard, 2017; Dzurisin, 2003; Segall, 2013) and it may be followed by a rapid deflation as magma is erupted (Fig. 7).

Magma can be forced towards the surface also by the rapid exsolution of gas and this may cause also deformation of the ground. Gas exsolution is leading

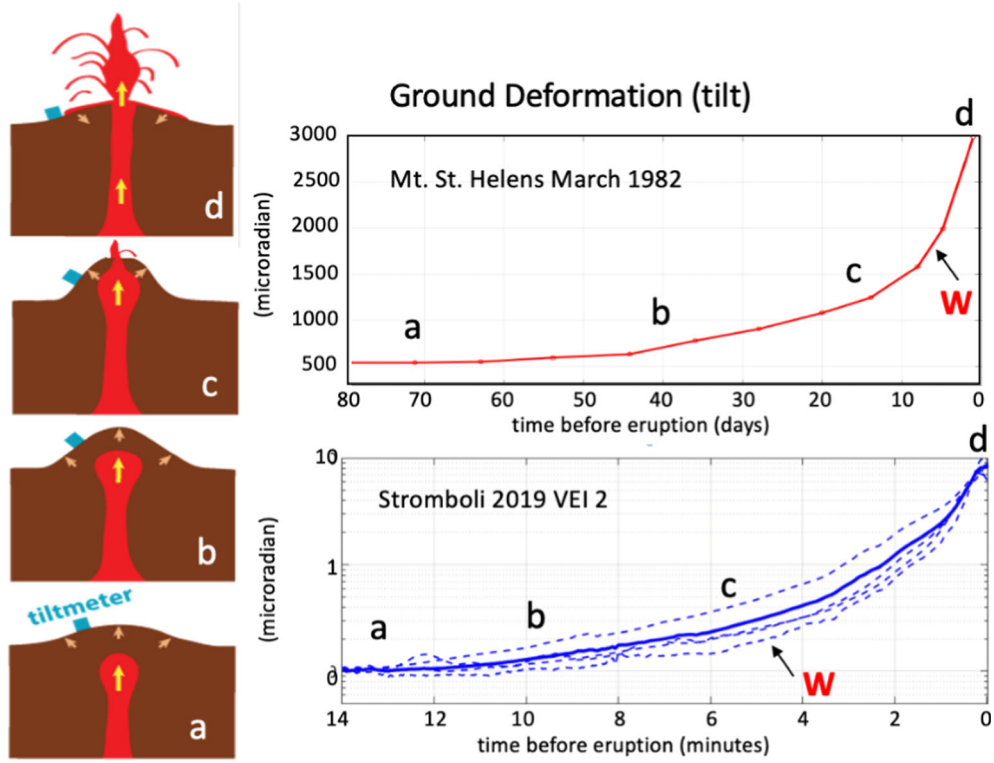

Figure 9
Before explosive eruptions upward magma migration is progressively inflating the ground. This inflation can be used to deliver a warning days or minutes before eruption. Inflation at Mt. St. Helen (upper panel) started several days before the 19 March 1982 eruption and allowed to give a warning (indicated with the letter W) few days before the explosion (from USGS report). At Stromboli (lower panel) ground inflation is smaller than St. Helen but is following a regular patter which is used to automatically issue alerts 4–5 min before violent explosive events (Ripepe et al., 2021)

to intense periods of magmatic degassing (Girona et al., 2015) and to the volumetric expansion of magma in the feeding system. This process increases the net pressure in the magmatic system and induces the inflation of the ground (Nishimura, 2009). Improving our ability to detect the inflation of volcano edifice could allow us to anticipate from days to minutes the eruptions on many basaltic as well andesitic volcanoes (Bonaccorso et al., 2012; Iguchi et al., 2008; Peltier et al., 2011; Ripepe et al., 2021).

In the'80 ground deformation was already used to forecast most ($\sim$ 70%) of the vulcanian explosion at Sakurajima volcano (Kamo, 1989) and made possible to forecast days before the eruptive activity at Mount St. Helens in 1980 (Swanson et al., 1983). More recently, the ground tilt recorded at Stromboli during violent explosions (paroxysms) shows a systematic pattern in the way the volcano edifice inflates several minutes (10 min) before the explosions (Fig. 9). This pattern was used to develop an Early Warning Alert System which automatically detected the occurrence of a violent explosive eruption 4–5 min before its onset (Ripepe et al., 2021). In August 2019, this strategy provided a warning almost 7 min before a tsunami was generated by the collapse of volcanic plume (see Sect. 6).

5.3. *Acoustic Pressure to Monitor Explosive Processes*

Among the monitoring techniques, infrasound is probably the one that more closely reflects the explosive process. Infrasound is, in fact, generated

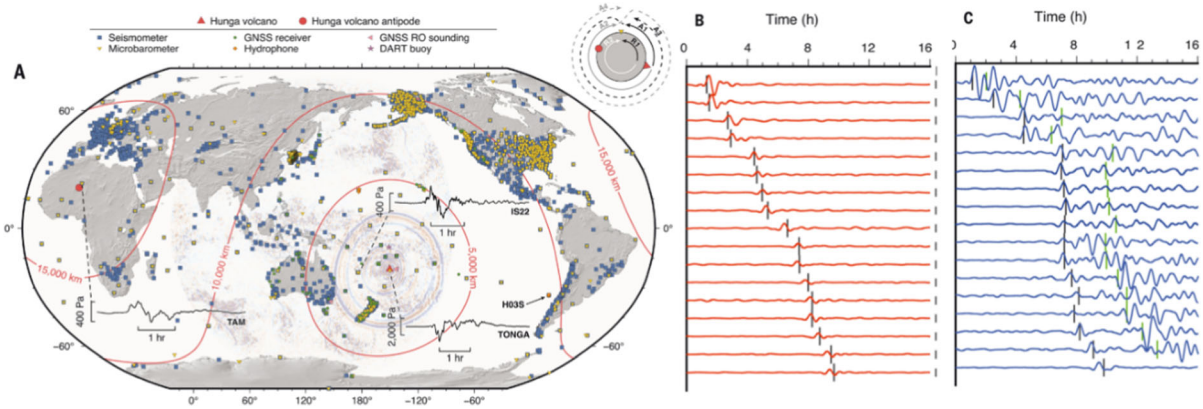

Figure 10

A Global distribution of recording geophysical sensors Background image is brightness temperature difference (Himawari-8) at 0710 UTC on 15 January 2022. Selected 4-h pressure waveforms are filtered from 10,000 to 100 s. Upper-right inset shows Hunga wave paths around Earth. **B** Observed barograms. **C** Observed ocean bottom pressure gauge waveform (Kubota et al., 2022; Matoza et al., 2022).

only when the volcano dynamics become coupled with the atmosphere, which mainly occurs during an explosive eruption. In addition, the limited attenuation in atmospheric waveguides makes infrasound travelling long distances (Drob et al., 2003), providing evidence of ongoing eruptions even at long source-to-receiver distances (e.g., Campus, 2006; Dabrowa et al., 2011). During the last decade, pilot experiments on the automatic detection and notification of volcanic eruptions with infrasound arrays were performed in South America (Garcés et al., 2008) and in Italy (Ulivieri et al., 2013). Notifications were automatically delivered to the Volcanic Ash Advisory Centers (VAAC) at the onset and the end of large explosive eruptions at Tungurahua Volcano (Fee et al., 2010). At Mt. Etna, a fully automated and operational warning system based on local (< 6 km) infrasound array data has detected in the last 10 years more than 150 explosive eruptions with a reliability rate of 96.5% and without negative false alerts (Ripepe et al., 2018).

Acoustic waves can be also generated by a source moving along the volcanic flank at the ground-atmosphere interface, such as potentially tsunamigenic pyroclastic flows (Yamasato 1997; Ripepe et al., 2009). While seismic waves are driven by the friction of the sliding source with the ground, infrasound is associated to the displacement of the atmosphere during the movement (Allstadt et al., 2018). In these cases, the record of acoustic waves is more effective than seismic in tracking the flow in real time, improving the efficiency of the response of Volcano Observatory (Marchetti et al., 2019a).

Recently, the atmospheric perturbation (Lamb wave) associated to the January 2022 violent eruption of Hunga volcano (Matoza et al., 2022) triggered tsunami waves worldwide (Fig. 10), with a leading wave that surprisingly propagated faster than expected for long waves in the deep ocean (Kubota et al., 2022). The results highlight the capability of infrasound for near-real-time volcano monitoring at a regional and global scale and demonstrate how it could supplement other monitoring techniques in remote areas poorly instrumented. In favorable propagation conditions, global arrays are capable of identifying explosive activity, and infrasound monitoring on a global scale can provide timely input even when a latency of $\sim$ 1 h is expected due to propagation time (Marchetti et al., 2019b; Matoza et al., 2017).

5.4. *Satellite Monitoring*

Ground-based measurements have a large sensitivity, but they are limited to few points located on the Earth's surface. Therefore, in recent years, there has been a dramatic increase in the number and capabilities of satellites to monitor volcanoes (Poland

Volcano Observatory Notice for Aviation (VONA)

ICAO Colour code		Status of activity of volcano
GREEN		Volcano is in normal, non-eruptive state. *or, after a change from a higher alert level*: Volcanic activity considered to have ceased, and volcano reverted to its normal, non-eruptive state.
YELLOW		Volcano is experiencing signs of elevated unrest above known background levels. *or, after a change from higher alert level*: Volcanic activity has decreased significantly but continues to be closely monitored for possible renewed increase.
ORANGE		Volcano is exhibiting heightened unrest with increased likelihood of eruption. *or,* Volcanic eruption is underway with no or minor ash emission *[specify ash-plume height if possible]*.
RED		Eruption is forecasted to be imminent with significant emission of ash into the atmosphere likely. *or,* Eruption is underway with significant emission of ash into the atmosphere *[specify ash-plume height if possible]*.

Figure 11
Color code representing the Volcano Observatory Notice for Aviation (VONA) alert levels used by Volcano Observatory to issue alerts of ash dispersal in atmosphere to aviation, which could be integrated in the Tsunami Warning Systems to actuate pre-warning procedures

& Anderson, 2020; Pavolonis et al. 2018). Data from satellite instruments have proven to be useful in volcano monitoring by detecting and tracking unrest and ongoing eruptions (Coppola et al., 2016) as well as for eruption forecasting (Biggs et al., 2014; Dean et al., 2015; Dehn & Harris, 2015; Hooper et al., 2012; Pritchard et al., 2022). Ultraviolet, optical, infrared, and microwave (synthetic aperture radar) measurements can provide information on the volcanic thermal, gas emissions, ground displacement, and topographic change before, during and after a volcanic eruption (e.g., Valade et al., 2019). As with ground-based data, parameters measured by satellite (for example, thermal emissions, outgassing, and deformation) can record changes which can precede eruptions, in some cases by months to years, and sometimes they were used to issue alerts (see examples in Schneider et al., 2000; Pallister et al., 2013; Pritchard et al., 2018). About 50% of satellite deformation detections preceded an eruption, whereas most thermal emission ($\sim$ 80%) and SO_2 outgassing ($\sim$ 95%) detections are instead co-eruptive (Furtney et al., 2018). From 2000 to 2010, deformation, thermal anomaly and SO_2 outgassing were detected with a mean ranging from 36 to 1001 days before an eruption (Phillipson et al., 2013). However, satellite data will never replace terrestrial monitoring; rather, they provide a critical complement to ground monitoring.

5.5. *Volcano Alert Levels*

Only around 10% of the historically active volcanoes (approximately 1500 according to the database of the Global Volcanism Program of the Smithsonian Institution) are monitored in real time (Pallister & McNutt, 2015). Volcanic hazard based on monitoring data remains still empirical, although forecasts are becoming more quantitatively-based on an improved understanding of the physics of magmatic processes (Sparks, 2003), and on the use of probabilistic methods (e.g., Newhall & Hoblitt, 2002; Marzocchi & Bebbington, 2012; Poland et al., 2020).

Volcano Alert Levels (VAL) represent today the most worldwide way to communicate the state of activity of a volcano (e.g., Potter et al., 2014), and provide also a short-term forecasts (Winson et al., 2014). Alert levels include a scale of four levels associated with different colors (Fig. 11). They are largely used to communicate a change in the activity level or basic information on the state of unrest or ongoing eruption (Papale, 2017). Alert levels are usually defined by volcano observatories, and represent the "official" communication of volcano status by scientists to civil protection authorities (Tilling, 2008). However, there is no international standard to define the volcano alert levels. Volcano observatories have developed protocols that are variable and can differ significantly in detail. Quite often VAL is often reflecting a local, rather than a general, impact and

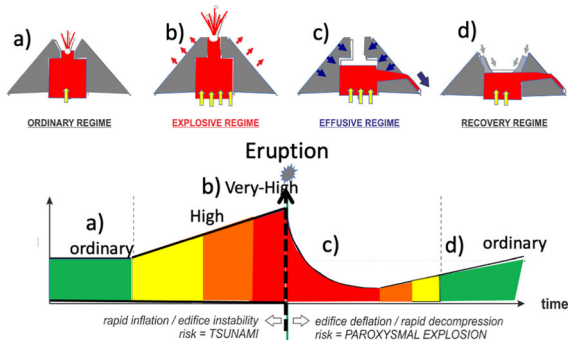

Figure 12
Conceptual model of the proposed VONA color change as function of significant variations in the monitoring parameters, and implications for associated Tsunami hazards (redrawn from Valade et al., 2016)

this makes the use of VAL for the definition of the tsunami hazard quite complicated.

A similar four-level color scale named VONA (Volcano Observatory Notice for Aviation) is used by Volcano Observatory to inform civil aviation authorities through the Volcanic Ash Advisory Centers (VAAC) on the potential presence of ash clouds in the atmosphere (Pallister & McNutt, 2015) and is following instead a structure of information which represents an international standard.

We foresee an alert level similar to VONA notification to mitigate the possible risk of tsunami generated by volcanic unrest (Fig. 12). Similar to the strategy followed by ICAO (International Civil Aviation Organization) for ash dispersal in the atmosphere, the Alert notification for Tsunami warning should be transmitted in near real-time to National Tsunami Warning Centres (NTWC) or designated authorities to help them issue more timely public alerts to minimizing the tsunami risk. Where a local Volcano observatory is present, notification should indicate:

a) pre-eruption volcanic activity (YELLOW) indicating an unusual and/or small increasing volcanic activity.
b) pre-eruption volcanic activity (ORANGE) indicating a significant unusual and/or increasing volcanic activity which could presage a volcanic eruption; preliminary tsunamis (usually of small magnitude) might be observed.
c) ongoing volcanic eruption (RED); description of the eruption including phenomena that could generate tsunamis at any moment (e.g., large pyroclastic flows, eruptive column collapse to the sea).
d) volcanic eruption cessation (GREEN); no more tsunami hazard.

For volcanoes in remote areas that are poorly instrumented, global monitoring network such as the International Monitoring System (IMS) of the Comprehensive Nuclear-Test-Ban Treaty Organization's (CTBTO), designed to detect nuclear explosions anywhere on Earth, could provide efficient information on seismic, infrasonic and hydroacoustic (for submarine activity) activity related to volcanic unrest (Matoza et al., 2017; Mialle et al., 2019)) which could cause a tsunami. The CTBTO global network is in fact already involved both in Tsunami Warning Agreements with 19 countries, and collaborates with VAAC for the testing of the volcanic information system (VIS), to establish a real-time operational system of Warning Volcanic eruptions (Ceranna et al., 2019).

The use of CTBTO's data in case of both tsunami generated by earthquakes and volcanic eruptions has

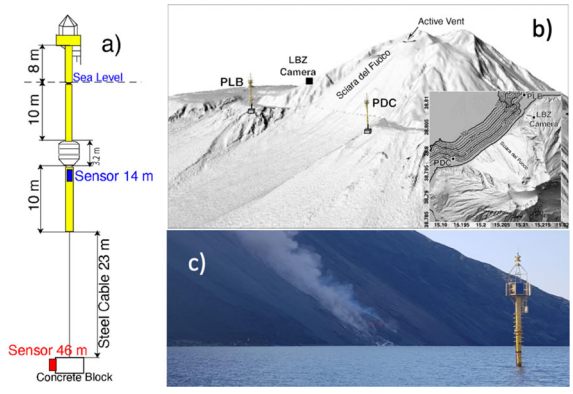

Figure 13
a Schematic technical illustration of the main components of the elastic beacon. Pressure sensors used to detect the tsunami are at 14 (blue) and 46 m (red) Position of the two elastic beacons (PLB and PDC) on 3D (**b**) and 2D (inlet) map of Stromboli volcano showing the Sciara del Fuoco slope above and below the sea surface. **c** Photo of PLB elastic beacon at ~ 300 m in front of the Sciara del Fuoco during the 9 October 2022 effusive eruption. The structure stands ~ 9 m above the sea surface.

proven to be more reliable and speedier than data from some other sources.

6. Volcanic Tsunami Warning Systems

6.1. Stromboli Volcanic Tsunami Warning System (Italy)

The short propagation time (3–4 min) to the populated coast of Stromboli volcano and the densely inhabited nearby (< 60 km) coast of Italy, which could be impacted in only 15–20 min (Fornaciai et al., 2019; Tinti et al., 2003), required the development of a fully automatic warning system, able to detect tsunamis as rapidly as possible.

In response to the tsunami generated by a partial flank collapse that occurred in 30 December 2002, in 2007, the Laboratory of Geophysics of University of Florence (LGS) has developed a system based on two elastic beacons (Fig. 13a) deployed in 2008 and 2017 (Lacanna & Ripepe, 2020) offshore the Sciara del Fuoco, at 260 m and at 350 m distance from Punta dei Corvi (PDC) and Punta Labronzo (PLB) capes (Fig. 13b), respectively. The system consists of two parts (see Appendix): (I) the detection of the tsunami wave (by LGS) and (II) the activation of an acoustic alert system of sirens by the Italian DPC deployed at Stromboli and in the Aeolian islands and in Sicily (Milazzo).

6.1.1 The Elastic Beacons Tsunami Gauge System

The Tsunami Early Warning System (TEWS) operating at Stromboli is based on the sea level measurements at four pressure sensors installed along the two elastic beacons at ∼ 14 and ∼ 48 m below the sea surface (Fig. 13). Both elastic beacons are equipped with two IDROMAR pressure sensors, sampled at 125 Hz. The depth of the pressure sensor on the seabed is optimal to reduce the effect of the sea wave at periods < 13 s and guarantee the best signal-to-noise ratio in the range of period (50–120 s) typical of the tsunami generated by landslides (Fig. 14).

6.1.2 Tsunami Detection Algorithms

The tsunami early-warning system algorithm is grounded on the short-term average (STA) long-term average (LTA) ratio. Whereas STA is sensitive to rapid fluctuations in the sea level, the LTA provides information on the background noise. The algorithm was calibrated considering synthetic tsunami waves modelled for the reference scenario of 30 December 2002 (Fornaciai et al., 2019) and assuming periods ranging between 30 and 165 s, larger than those expected for the tsunami occurred at Stromboli in 2002 and at Anak Krakatau volcano in 2018 (Grilli et al., 2019). The detection algorithm operates on five consecutive steps: (I) spike removal, (II) detrending signal for tide removal, (III) low-pass filtering, (IV) data decimation and finally (V) the STA/LTA ratio (see Appendix for details). The automatic alert is issued only when the STA/LTA ratio is larger than the detection threshold (STA/LTA > 20) at both tsunami gauges for at least 120 s (Fig. 27). This threshold ratio provides the best performance in rough sea conditions (Fig. 29) and it guarantees to automatically alert if a tsunami as large as 40 cm will occur in the worst sea conditions and with no false alert. The short alert time (< 4 min) gives no time to run models to estimate the possible inundation effects on the nearby coast. Therefore, in spite of the amplitude of the tsunami wave, the TEWS will send the alert before tsunami wave have been fully

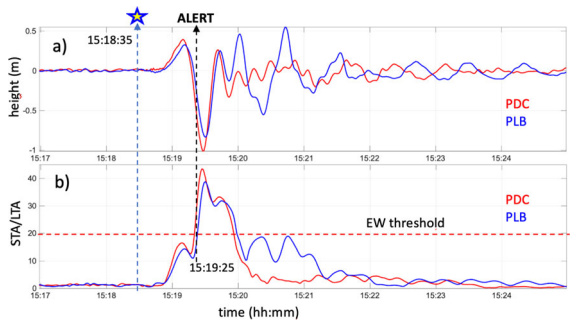

Figure 14
a The small tsunami generated by the impact of the pyroclastic density current occurred at Stromboli on December 4, 2022 and recorded at the two elastic beacons (PDC and PLB) at a distance of ∼ 1300 m from the splash zone. **b** The STA/LTA ratio increased above the fixed warning threshold of 20 at 15:19:25, triggering the alert system 9 s before the maximum height and 50 s after the PDC onset.

developed (generally within the first 20 s from the onset). Future development of the present system will consider pre-calculated tsunami scenarios to relate the amplitude at the gauges to that on the nearby coasts.

6.1.3 TEWS Performance

On August 28, 2019 the tsunami early warning alert was still being under test using only one gauge, but it allowed Civil defence authorities to activate the acoustic alert manually only 11 s after the tsunami onset and 3–4 min before the tsunami reached the populated coast of Stromboli (Ripepe & Lacanna, 2024). Since 9 September 2019, the early-warning system is fully operative and automatically linked to the acoustic alert system of the Italian Civil Defence. On December 4, 2022, a pyroclastic flow generated by a small ($\sim 10^5$ m^3) collapse of the summit crater triggered a 1.4 m (peak-to-peak) height tsunami which was automatically detected by the TEWS $\sim$ 20 s after the onset and 9 s before the maximum negative amplitude of 1 m was reached (Fig. 14). The detection has automatically activated the acoustic alert system of Italian DPC deployed in the Aeolian islands and in Sicily, triggering the emergency procedure along Sicily and Calabrian coasts.

6.2. Hawaii Island (USA) Tsunami Inundation Detection System (TIDS)

The largest and southernmost island of the Hawaiian Islands archipelago, Hawaii Island, has a history of coastal inundation from distant earthquakes around the Pacific as well as local earthquakes associated with the island's active volcanism. To help monitor Hawaii Island's coasts for tsunami inundation, the Pacific Tsunami Warning Center (PTWC) uses on-land, specially-designed, inexpensive, easy-to-deploy, remotely-reporting sensors (Coastal Runup Detectors, CRD) that rapidly send a signal to PTWC if they become wet from coastal flooding. This system is known as the Tsunami Inundation Detection System (TIDS, Figs. 15, 16a). The sensors are based on commercial home and business security alarm technology. PTWC acts, in effect, like the company providing alarm services to the home or business owner. When a sensor gets flooded, a signal is sent to the control centre of the security company that provided the sensors to PTWC and then the signal is relayed to PTWC within seconds over the public internet. The sensors are flood sensors that normally would be used in a basement to detect basement flooding, but in this case they are used to detect flooding along a coast. In their normal application, power and communication would be through the electric and telephone utilities of the building, but within the TIDS network the power is supplied by solar panels and a battery and the mobile phone network is used for communication .

The flood sensors are mounted inside a box that is attached to a tree, building or some other sturdy permanent structure. The bottom of the box is open and situated 10–20 cm above the ground permitting floodwater to enter and fill the box from below. When the floodwater reaches the sensor, then it triggers. The location of the sensor, including its elevation and distance from shore, is decided through a combination of idealised tsunami modelling and practical considerations such as landowner permissions and a suitable and secure mounting location. The sensor should be sited so it does not get triggered by tidal fluctuations, high surf, or heavy rain. Once a day, each sensor sends a test message through the control centre to PTWC to indicate it is still working. Once or twice a year, a field test is conducted where the sensor is manually wetted using a bucket of water slipped under the box to ensure that the system is still

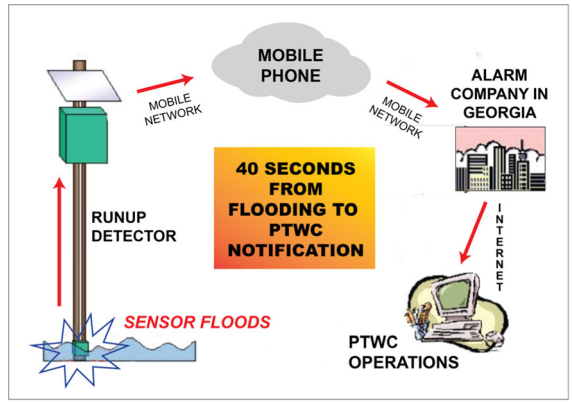

Figure 15
Schematic diagram of the communications links for the PTWC Tsunami Inundation Detection System (TIDS). (Source: PTWC)

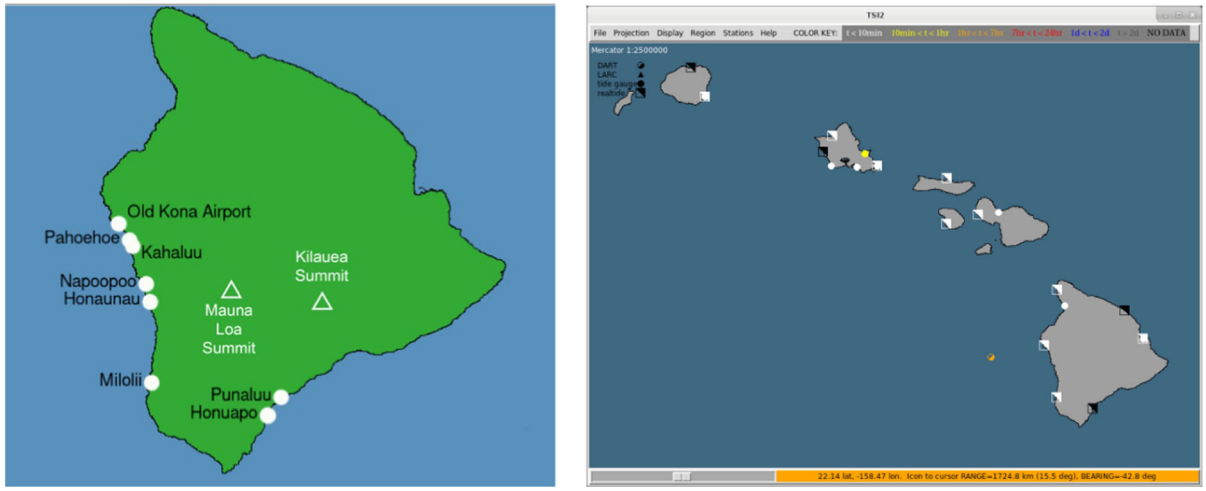

Figure 16
PTWC Hawaii sea-level network: **a** (left) TIDS coastal runup stations (white circles). **b** (Right) Coastal sea level stations (near real-time (triangle, filled circle), real-time (square)) and Deep-ocean Assessment and Reporting of Tsunamis (DART, half circle) system. (source: PTWC)

working end-to-end. The solar panel, battery, mobile telephone, and other electronics are usually mounted above the box in a location high enough to not be flooded and destroyed by a big tsunami before it has time to send a signal, and secure enough to not be vandalized. The TIDS signal alerts the PTWC duty officer who assesses the threat according to criteria outlined below (see Fig. 17). The total delay time is less than one minute between the sensor getting wet and the alarm sounding at PTWC.

TIDS sensors do not provide as much information as normal sea level gauges (Fig. 16b), but they are much less expensive and much easier to install and maintain. They can be used to fill gaps along coasts where it is not possible or is too expensive to install a normal sea level gauge. They have proven to be reliable—PTWC has been using eight of them on Hawaii Island for nearly 20 years with minimal down time and maintenance (Fig. 16a). Over the entire time of operation there has been only a single real TIDS trigger (from the 2011 tsunami from Japan) and only a couple of false triggers. In the case of a locally generated tsunami, TIDS triggers as well as tsunami signals on coastal sea-level gauges (Fig. 16b) can be used to evaluate if a warning needs to be issued or expanded to other islands in the State of Hawaii following procedures developed using numerical modelling of local tsunami scenarios.

6.2.1 Local Tsunami Warnings for Hawaii Island

Hawaiian volcanoes are not the type that erupt with massive explosions or pyroclastic flows that can generate tsunamis. However, changing internal stresses associated with active volcanism, such as from

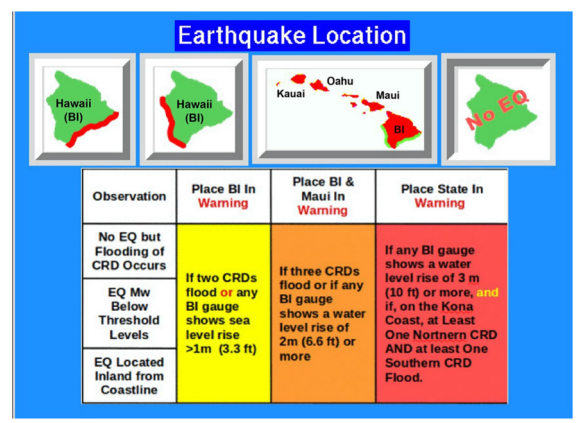

Figure 17
Hawaii Tsunami Warning Criteria and Standard Operating Procedures for a local tsunami from earthquake (red lines on BI maps, and green lines on State map) and non-seismic source. TIDS system of Coastal Runup Detectors (CRD) provides critical information. (Source: PTWC)

Kilauea Volcano or Mauna Loa Volcano can sometimes produce tsunamigenic earthquakes when flank displacements push against the sea. In addition, there is bathymetric evidence of past significant underwater landslides that could have generated tsunamis.

If a shallow near-shore or undersea earthquake equal to or larger than the magnitude M_w6.9 threshold, then a Local Tsunami Warning is issued based on the earthquake parameters (Fig. 17). The Warning extent (only Hawaii island (BI), BI and Maui, entire State of Hawaii), depends on the earthquake epicenter (SE or western BI) and its magnitude). The TIDS network and real-time sea-level networks (Fig. 16) are subsequently monitored to help detect and characterize the tsunami and provide further warning information if necessary.

If an earthquake is recorded that is less than M_w6.9 magnitude threshold, or is located inland, or no earthquake occurs, but more than one TIDS sensor (Coastal Runup Detector, CRD) floods, or a nearby coastal sea level gauge measures fluctuations over one meter in amplitude, then a Local Tsunami Warning is also issued (extent depends on earthquake epicenter, number of CRDs that trigger, and amplitude of waves on coastal sea level stations), as this could be evidence for a landslide-generated, or volcano-generated tsunami. However, if a single TIDS sensor triggers with no additional supporting data indicative of a tsunami, then it is assumed the trigger was a malfunction.

6.3. *Hunga Interim Volcanic Tsunami Warning System (UNESCO/IOC)*

The Hunga volcano erupted violently on 15 January 2022. The eruption began around 0347 UTC (4:47 pm local time) with the eruptive plume first being observed on satellite imagery shortly after 0400 UTC and violent volcanic explosions occurring at 0415 and 0426 UTC. Tsunami waves were first observed at the Kanokupolu Peninsula on the northwest side of Tongatapu around 0415 with the first wave arrival at the Nuku'alofa, Tongatapu sea level gauge occurring at 0427 UTC (Borrero et al., 2022). This volcanic eruption came from an existing largely submerged volcanic edifice represented at the surface by two small islands (Hunga Tonga and Hunga Ha'apai). This activity is part of a broader eruption episode that started in 2009 and continued in 2014, 2015, December 2021 and January 2022 (Cronin et al., 2017). One day before the large explosion, on 14 January 2022, an eruption occurred that also generated small tsunami waves recorded at Nuku'alofa (Borrero et al., 2022).

On January 15, the eruption plume ascended very quickly, punctured the stratosphere (Fig. 18) and produced a massive acoustic pressure wave that travelled in the atmosphere several times around the globe (Matoza et al., 2022; Wright et al., 2022). Processes associated with the volcanic eruption generated a series of tsunami waves that caused land threats (> 1 m amplitude) at local, regional, and distant coastlines (Fig. 19, Kong et al., 2022) and caused fatalities in Tonga and Peru (Lynett et al., 2022; Omira et al., 2022).

Figure 18
15 January 2022 Hunga Tonga Hunga Ha'apai explosion as observed at 0407 UTC by the Himarawi-8 satellite

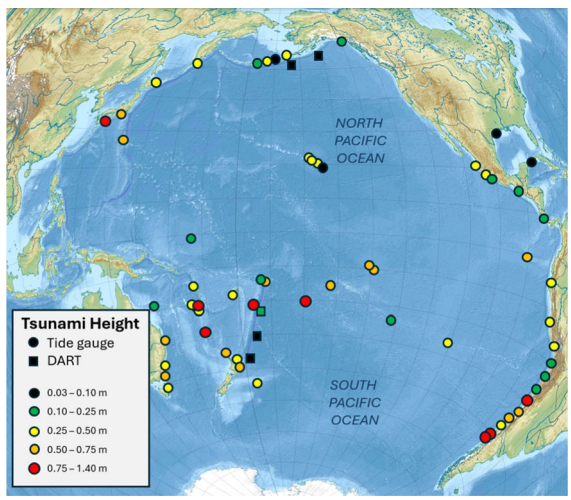

Figure 19
Maximum tsunami amplitudes reported by PTWC on 15 January 2022 recorded on coastal sea level gauges (circle) and DARTs (square)

In response to the HTHH volcanic explosion and tsunami, the Intergovernmental Coordination Group (ICG) for the Pacific Tsunami Warning and Mitigation System (PTWS) established a Task Team on Hunga Tonga-Hunga Ha'apai Tsunami Hazard Response to develop an implementation plan for responding to future tsunamis originating from volcanic eruptions or processes similar to the HTHH event. This plan has been disseminated in the IOC Circular Letter 2882. https://oceanexpert.org/downloadFile/50389. It includes Interim Standard Operating Procedures (SOPs) for responding to these events. Effective from 15 March 2022, the SOPs are implemented by the PTWC acting as a Tsunami Service Provider (TSP) in the PTWS. These SOPs are included in the document "PTWC Interim Procedures and PTWS Products User's Guide" disseminated in the IOC Circular Letter 2902 (https://oceanexpert.org/document/30759). A summary is presented below.

6.3.1 Interim Standard Operating Procedures

The PTWC will use the first available information that a tsunami has been generated to underpin PTWC Threat Messages for any future HTHH events. Specifically, PTWC will:

- Use observed tsunami amplitudes from the 15 January 2022 event as the basis for a forecast. These include amplitudes measured at the Nuku'alofa sea level gauge and the deep ocean NZG DART gauge (the nearest DART to the HTHH volcano). Tsunamis generated at the HTHH volcano will arrive at these stations within approximately 20–30 min. Observations at these stations will likely constitute the first evidence of a tsunami threat.
- Estimate the time of the HTHH event from the tsunami arrival times at Nuku'alofa (nkfa) and/or DART NZG (dnzg) and/or other gauges depending on the information available at the time.
- Create the forecast for the future HTHH event by scaling observed maximum amplitudes across the Pacific from the 15 January 2022 event with observed amplitudes of the future HTHH event, starting with the observed amplitudes at Nukuàlofa, the NZG DART, or other nearby sea level stations. Forecast values will therefore only be available for specific sea level locations (see Fig. 20).
- Calculate estimated tsunami arrival (ETA) times according to tsunami propagation generated by a sea level disturbance at HTHH (Fig. 20). While the meteo-tsunami caused small far-field arrivals before this time, the majority of the tsunami energy still took around the standard tsunami propagation time to reach locations around the Pacific Ocean (Kubota et al., 2022).

Should there be future activity at HTHH resulting in another tsunami, PTWC may not become aware of it until the tsunami waves reach either the closest coastal sea level gauge at Nuku'alofa (nkfa), the closest deep-ocean gauge (DART 01003—dnzg) or some other nearby sea level gauge. These signals will cause PTWC alarms to sound and PTWC Duty Scientists to respond. Other early alerts, such as observations of an ash cloud or explosive eruption in Tonga, satellite observations through the Volcanic Ash Advisory Centers, or detection of an atmospheric pressure wave could also be used to activate the PTWC.

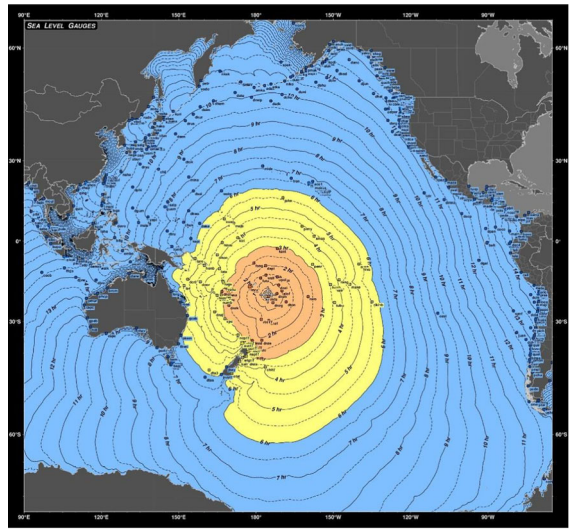

Figure 20
Estimated tsunami travel times from HTHH across the Pacific. On this map are noted the coastal and deep-ocean (DART) gauge locations where maximum amplitudes will be forecast (source: PTWC)

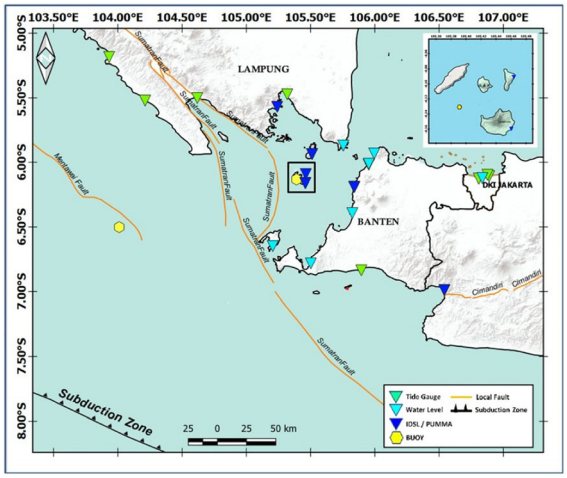

Figure 21
Sea level network along the Sunda Strait used to monitor tsunamis from the Anak Krakatau volcano (source: BMKG)

Based on the amplitude of the tsunami waves at the closest stations, PTWC will issue either:

1. Tsunami Information Statement reporting the activity but indicating there is no tsunami threat (unique message), or
2. Tsunami Threat Message indicating that there is a tsunami threat.

A Tsunami Threat Message will be followed by additional Threat Messages at least once an hour until the threat has passed and a Final Threat Message will be issued.

6.4. *Anak Krakatau Volcanic Tsunami Warning System (Indonesia)*

Following the flank collapse of Anak Krakatau volcano and the ensuing tsunami along the Sunda Strait on 22 December 2018, an Indonesian Presidential Decree (no 93/2019) was issued ordering the strengthening and further development of the earthquake and tsunami early warning information system in Indonesia to include the monitoring of and tsunami warning for non-seismic generated tsunamis. Many agencies and ministries were involved in enacting the decree, including the following: Badan Informasi Geospasial (BIG)/Geospatial Information Agency; Badan Meteorologi, Klimatologi, dan Geofisika (BMKG)/Meteorological, Climatological, and Geophysical Agency; Badan Pengkajian dan Penerapan Teknologi (BPPT)/Agency for the Assessment and Application of Technology; Badan Riset dan Inovasi Nasional (BRIN)/National Research and Innovation Agency; Energi dan Sumber Daya Mineral (ESDM)/Ministry of Energy and Mineral Resources; Kementerian Kelautan dan Perikanan (KKP)/Marine and Fisheries Ministry; Lembaga Ilmu Pengetahuan Indonesia (LIPI)/Indonesia Institute of Science; Pusat Vulkanologi dan Mitigasi Bencana Geologi (PVMBG)/Center for Volcanology and Geological Hazard Mitigation.

In Indonesia, the BMKG serves as the Tsunami Early Warning System (TEWS) authority and was the lead for implementing the non-seismic tsunami warning system (InaTNT), specifically focusing on landslide and volcanic tsunami sources. For the InaTNT, in addition to the BMKG, government stakeholders involved are BIG, PVMBG, and BRIN. The standard operating procedures (SOP) for tsunamis generated by an Anak Krakatau volcanic eruption and/or landslide, were collaboratively developed and signed by BMKG and ESDM. These SOP are general and could be applied to other volcanoes.

6.4.1 *Anak Krakatau Sea Level Monitoring Network*

The local tsunami early warning system for Anak Krakatau was established from 2019. Several types of sea water level sensors are deployed (Fig. 21), including seven *Automatic weather station water level* (AWS-WL), six *inexpensive devices for sea level measurement* (IDSL), eight tide gauges and two buoys. Stations on Sebesi Island, Rakata Island, and Panjang Island are located about 5-min tsunami travel time from the volcano, or within 3-km radius. This should enable BMKG to detect and then disseminate warnings to the local communities quickly after a wave is observed. The IDSL stations are a collaboration between KKP and the Joint Research Center (JRC) of the European Commission. The AWS-WL and IDSL instruments are co-located and powered by solar panels. Additionally, the closed-circuit television CCTV provides visual imagery of the ocean and a barometer detects air pressure that can be used to detect meteotsunamis.

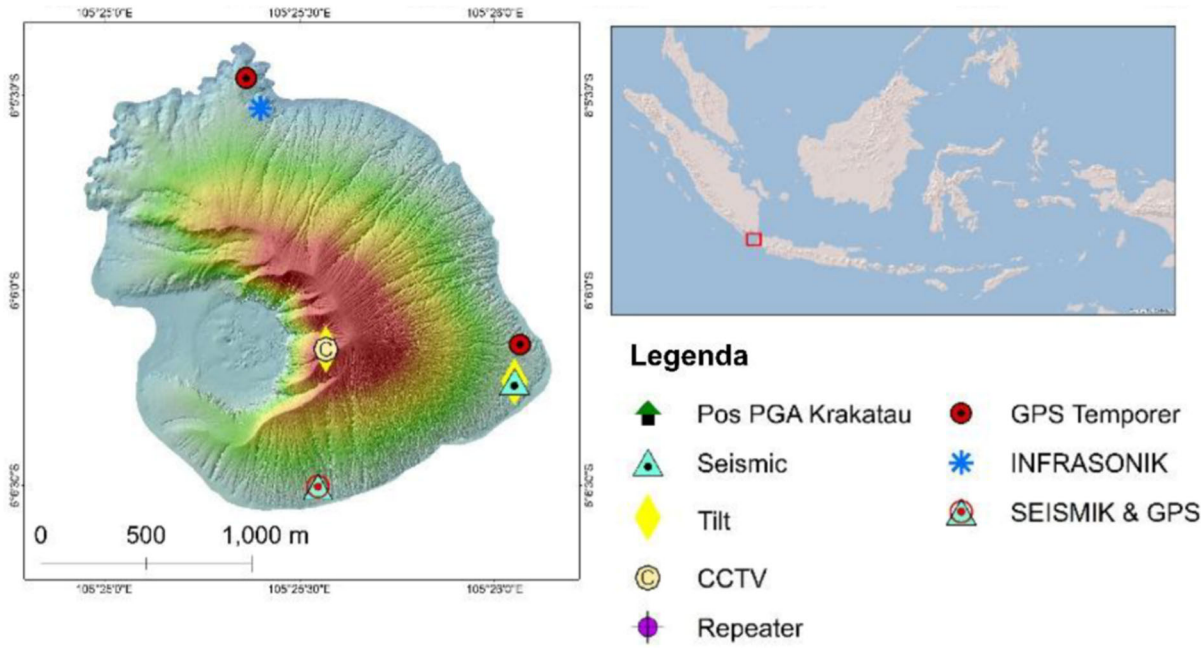

Figure 22
Monitoring equipment installed on Anak Krakatau volcano (source: PVMBG)

A dedicated satellite system (BAKTI), installed by the Ministry of Communication and Information, provides real-time, high-frequency data transfer from the IDSL stations to a remote server at the JRC for processing and display. BMKG monitors the stations and can issue at part Indonesian Tsunami Early Warning System (InaTEWS) alerts before the waves reach the coasts of Java and Sumatra (typically, tsunami travel time of 20–40 min).

Local communities are involved in the installation and maintenance of the stations, thus promoting community-based preparedness. In a major German government funded collaboration (Tsunami Risk Project), German scientists and engineers are working with their Indonesian counterparts to further develop the InaTEWS to also monitor and warn for tsunamis generated by non-seismic and complex sources, such as volcanoes and submarine landslides.

Since the 2018 disaster, PVMBG (ESDM) has installed new equipment on the volcano itself (2 seismic stations, 3 GNSS receivers, an infrasound station, 2 tiltmeters, and one webcam), on nearby islands (seismic stations on Rakata and Sertung Islands), and an infrasound station on the eastern coast of Sumatra (Fig. 22).

These data streams and tools support the decision-making process of the InaTEWS duty operator. When there is a report of a volcanic eruption, the duty operator can quickly scan the InaTNT website that displays all the sea level stations in near real time to see if a tsunami was generated. The site uses a local IP, but can be accessed publicly using public networks.

6.4.2 Standard Operating Procedures

When there is increased volcanic activity, the PVMBG informs BMKG on the eruption status, the volcano characteristics, and the landslide potential. BMKG then monitors sea level stations through the InaTNT website and CCTV, and uses local community reports. If a seal level anomaly is detected, the operator checks other sensors in the surrounding areas and confirms the wave observations to PVMBG. BMKG issues a Tsunami Warning 3 which includes the height, location, and arrival time of the tsunami waves. The status is continuously updated,

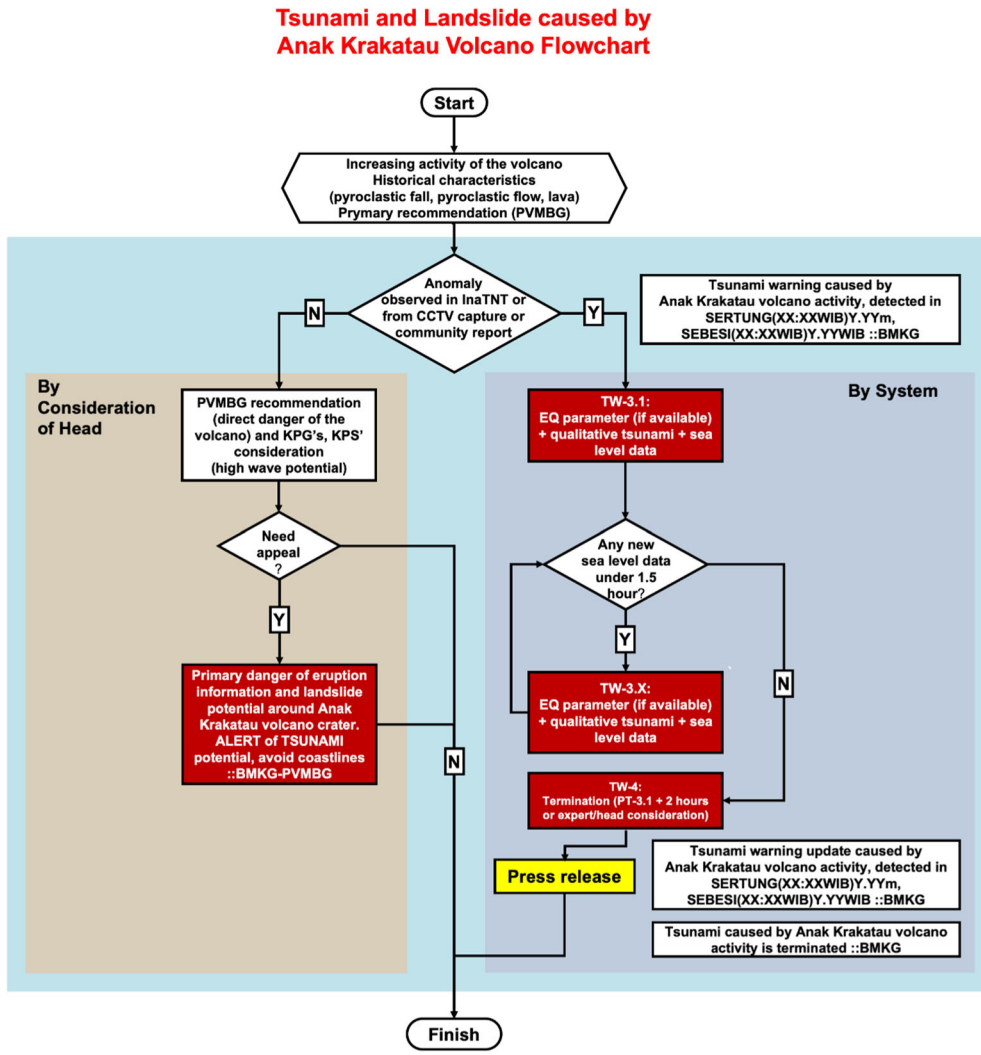

Figure 23
Anak Krakatau volcanic and landslide tsunami standard operating procedures (SOP) (source: BMKG). Tsunami Warning (PT, Peringatan Tsunami) decisions are decided by the Head of Earthquake and Tsunami Centre (KPG, Kepala Pusat Gempabumi dan Tsunami BMKG), and Head of Engineering Seismology, Potential Geophysics, and Time Mark Centre (KPS, Kepala Pusat Seismologi Teknik, Geofisika Potensial dan Tanda Waktu BMKG, and/or by the System. Sertung and Sebesi are islands in the surrounding Sunda Strait, which may detect the tsunami at the time XX:XX (Western Indonesia Time) with a height of YY meters, as reported by the BMKG. Island maps: Sebesi (https://maps.app.goo.gl/1QGR8VMktQdPkS9T6), Sertung (https://maps.app.goo.gl/rR4ik1wF4FP7tcCR6

including with new wave observations. If there are no more tsunami waves arriving 1.5 h after the last arrival, BMKG issues a termination (Tsunami Warning 4) and follows this with a Press Release. All warning information is disseminated via a WhatsApp Group to the nearest BMKG regional office and later forwarded to the local stakeholders (Fig. 23).

6.5. *Caribbean Tsunami Warning Procedures Using Volcano Notice of Tsunami Threat (VONUT)(UNESCO/IOC)*

In the Caribbean, 27% (16 of 59) of the tsunamis reported as "probable" or "definite" in the NCEI/WDS database were generated by volcanoes (Dunbar et al. 2008; NOAA, NCEI/WDS 2023), Recent eruptions of Kick'em Jenny (2015, 1965, 1939),

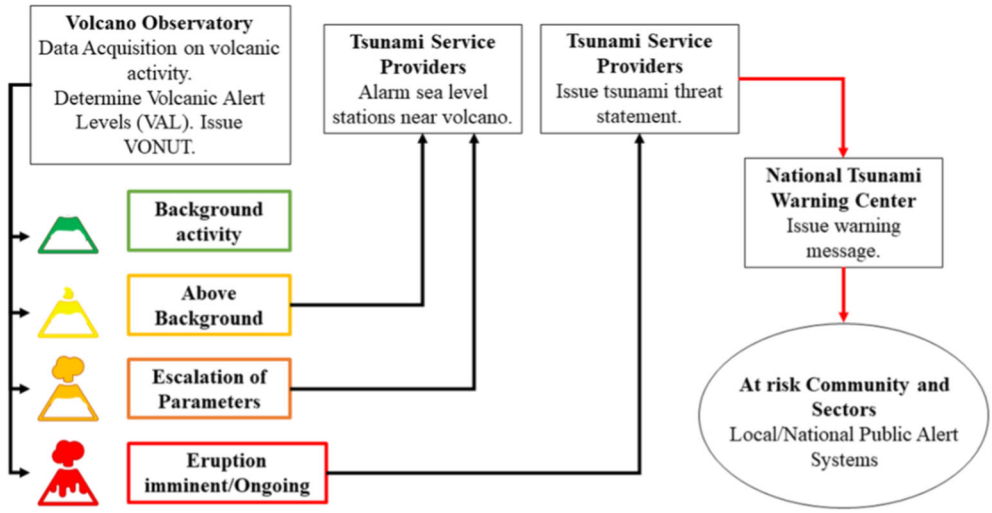

Figure 24
CARIBE-EWS proposed system for issuing alerts about tsunamis generated by volcanoes. The color codes of the volcano pictograms are the same as those in the VONA

Soufriere volcano on Saint Vincent (2021, 2020, 1902) and Mount Pelée on Martinique (1902), and Soufriere Hills in Montserrat (2006, 2003, 1999) have raised awareness on the potential tsunami hazard.

In 2023 as part of the CARIBEWAVE tsunami exercise (UNESCO/IOC 2023, www.caribewave.info), the UNESCO/IOC Intergovernmental Coordination Group for the Tsunami and other Coastal Hazards Warning Systems tested the use of a Volcano Observatory Notice for tsUnami Threat (VONUT) message (Clouard et al., 2024). The VONUT is derived from the Volcano Observatory Notice for Aviation (VONA) bulletin. Volcano observatories issue the initial VONUT to the CARIBE-EWS Tsunami Service Providers (Pacific Tsunami Warning Center, and starting in 2024 Central American Tsunami Advisory Center) to advise them of heightened volcanic activity indicative of an impending eruption and the potential for tsunami generation (Fig. 24). This alerts the TSPs, who can then monitor the sea-level gauges nearest the volcano, and pre-compute tsunami travel times from the volcano to nearby coasts. The second VONUT is issued if the eruption occurs. If tsunami waves are observed on the nearest sea-level gauges, then the TSP will issue a tsunami threat message to Member State NTWCs. The threat message will advise on the eruption and tsunami, and give computed estimated times of arrival (ETA) at nearby locations. Subsequent TSP messages would report on the location, time and amplitude of observed tsunami waves. This continues until the threat has passed. Currently there is no capability to provide a tsunami forecasts in the VONUT threat messages.

7. *Conclusions*

Volcanic tsunamis have a range of different source mechanisms, as identified by Paris et al., (2014a, 2014b) and enumerated in Sect. 2 above. The different mechanisms involved in volcanic tsunami generation are characterized by different energies or mass fluxes, and they can act over a range of different timescales. This is why these sources are called complex (Paris, 2015). Furthermore, a single volcanic eruption could generate tsunami waves through a range of different mechanisms and these mechanisms could reinforce each other (especially in the case of atmospheric pressure anomalies).

There are a range of different methods that exist to initialize volcanic tsunami sources. These span from models that attempt to replicate aspects of the physics of the eruption to understand the generation

process but may simplify the geometry and bathymetry through to very simplified 'order of magnitude' initialization that may use realistic bathymetry. Which method is best to use very much depends on what the intended purpose of the modelling is and the time and computational resources available for the modeling. Very different methods may be appropriate depending on whether the intent is to understand the generation mechanism, initialize modelling for a scenario-based hazard assessment, initialize modelling for a probabilistic hazard assessment or model in forecasting mode for tsunami warning. Section 3 gives an overview of the types of methods available and what situations they are appropriate for. Many of these methods are suitable for hazard assessments. In most situations, however, they would not be suitable for use in forecasting mode to support tsunami warning centers. Future forecasting efforts could rely on hybrid models or GPGPU-enabled models.

Very few volcanoes have been included in tsunami hazard assessments, which usually just cover seismic tsunamis and occasionally have included landslide tsunami hazard. The case of Stromboli is almost unique in this situation. Other volcanoes are, however, being studied to expand the number of locations where volcanic tsunami hazard assessments exist, such as Krakatau.

A variety of different volcano monitoring methods already exist, in particular based on volcano seismicity monitoring, ground deformation measurement, and satellite monitoring. Many of these can indicate heightened levels of volcanic activity that could precede a tsunamigenic eruption. Some techniques can even indicate that an eruption is taking place. Most of this monitoring is focused on a single volcano, though, so relies on being deployed to that volcano. Even when an eruption is identified, there is still a big research-level step to quantify the size of the eruption and its tsunamigenic potential rapidly enough to activate specific warnings. We recommend further research to develop and implement techniques for monitoring and alerting for volcanic tsunamis.

Currently, only a few volcanic tsunami warning systems are in place around the world. These rely on measurements and signal detection from sea level measurement stations, Anak Krakatau, Hunga Tonga, and Stromboli, and on humidity sensors (Hawaii). Some systems are organized at the local level (Stromboli, Hawaii, Anak Krakatau). At the international level, only the Hunga Tonga system has been coordinated and implemented, within the framework of the PTWS, and with contributions from the PTWC and several countries. The Hunga system is based on scaling the global tsunami that occurred due to the 15 January 2022 eruption. In the CARIBE-EWS, there is a proposal to use a VONUT, derived from the VONA, and issued by the Volcano Observatory to the IOC Tsunami Service Providers to alert them of heightened volcanic activity.

Because of the raised awareness of volcanic tsunamis due to the recent events at Anak Krakatau 2018 and Hunga 2022, other systems are under development. Many national volcanic observatories are aware that some of the volcanoes they monitor could produce tsunamis during eruptions. The current publication is not able to identify all the specifics of different monitoring techniques that these observatories might currently be using or developing for deployment. It does give an overview of some of the methods known and used to date. Due to the events of 2018 and 2022, we expect that other countries and volcano warning centers will be setting up new monitoring, methods, and warning systems on potentially tsunamigenic volcanoes (see Appendix).

We hope that tsunami generated by volcano hazard and risk assessments will be undertaken to identify the most vulnerable communities, and that multi-stakeholder meetings that include scientists, warning and response agencies and the public will meet to discuss the worst-case and credible scenarios, what to do to prepare, how the alert warning will be issued, and where to evacuate to be safe from both the volcano and the tsunami.

We hope that this paper provides impetus for future research and action, and that this publication provides a strong foundation to that research and for mitigation and preparedness actions that implement

volcano tsunami warning systems that can reliably warn communities at risk.

Acknowledgements

Acknowledgement to Pacific Tsunami Warning Center to provide information for Chapter 6.2 and figures 15–17 and 20. Acknowledgement to BMKG to provide figures 21 and 23. Acknowledgement to PVMBG to provide figure 22.

Author contributions F.S. and E.L. wrote the Abstract, Introduction. F.S. wrote chapter 6.3, prepared the table of content, figures 2 and 19, and validated the manuscript. R.P wrote section 2 , prepared figure 1, and Tables 1 - 3. V. T. and E.L. wrote section 3. M.R. wrote section 4, section 5, chapter 6.1 and prepared figures 4, 5, 6, 7, 8, 8, 11, 12, 13, 14, 26, 27, 28, 29, 30, 31. L.K wrote chapters 6.2 and 6.4 and prepared figures 15 and 17. F.S., E.L. and L.K. wrote Conclusions. E.L. wrote second version text of sections 2 and 3. F.S. and R.B. coordinated the work of the ad-hoc team. R.P. and F.S. wrote the point-by-point response to reviewers and editors. All authors reviewed the manuscript.

Funding

No outside funding or grants directly related to the research presented in this manuscript.

Data Availability

No datasets were generated or analysed during the current study.

Declarations

Conflict of interest The authors declare no competing interests.

Appendix

List of Potentially Tsunamigenic Volcanoes in the World

Most of these volcanoes have been active during the XXth or XXIst centuries. Modified and updated from Paris et al., (2014a, 2014b) for South-East Asia, and the National Geophysical Data Center / World Data Service (NCEI/WDS Global Historical Tsunami Database. NOAA National Centers for Environmental Information). As proposed by Paris et al., (2014a, 2014b), an active or dormant volcano is considered to be potentially tsunamigenic if it belongs to one of the following types of volcanoes:

A. It is a steep-flanked stratovolcano whose main eruptive centre is located less than 6 km from the coast (sea or lake). In such cases the main tsunamigenic mechanisms are pyroclastic flows and flank instability, from rock falls (106 m^3) to debris avalanches (108–109 m^3). The typical example is Stromboli volcano (Aeolian Islands, Italy), whose activity and recurrent flank instability generated 7 tsunamis since the year 1900 (Maramai et al., 2005). Another example case-study was provided by the 1995–2010 eruption of Soufrière Hills, during which 4 tsunamis were generated by the entrance of pyroclastic flows into the sea (Pelinovsky et al., 2004).
B. The volcano belongs to a complex of eruptive centres in a partly submerged caldera. A distinction can be made between caldera lakes (e.g. Taal, Philippines, 5 tsunamis since AD 1700: Paris & Ulvrova, 2019), calderas opened to the sea (e.g. Rabaul, Papua-New Guinea, tsunamis in 1878, 1937 and 1994: Blong & McKee, 1995) and submerged calderas with emerged eruptive centres (e.g. Krakatau, Indonesia, tsunamis associated with the major 1883 eruption, and more recently the 2018 Anak Krakatau flank collapse: Simkin & Fiske, 1983; Paris et al., 2019). Potential tsunami sources in such volcanic systems include pyroclastic flows, underwater explosions, atmospheric shock wave, rapid ground subsidence (e.g. caldera collapse), and small-scale flank instability.
C. It is a submarine volcano, whose activity (e.g. underwater explosions at shallow depth) and

NAME	COUNTRY	REGION	VOLCANO TYPE	DISTANCE / COAST (km)	LAST ERUPTION
Mount Pelee	FRANCE	WEST INDIES	A	5,6	1932
Soufriere	FRANCE	WEST INDIES	A	8,7	1976
Fani Maore	FRANCE	COMORES	C	0	2022
Piton de la Fournaise	FRANCE	REUNION ISLAND	D	9	2021
Kolumbo	GREECE	AEGEAN SEA	C	0	1650
Santorini	GREECE	AEGEAN SEA	B	0,8	1950
Kick em Jenny	GRENADA	WEST INDIES	C	0	2017
Katla	ICELAND	ICELAND	A	23,4	1918
Vestmannnaeyjar	ICELAND	ICELAND	C	0	1973
Snaefellsjokull	ICELAND	ICELAND	A	7,8	
Barren Island	INDIA	ANDAMA ISLANDS	A	1,5	2020
Anak Krakatau	INDONESIA	JAVA-SUMATRA	B	0,5	2022
Banda Api	INDONESIA	BANDA SEA	A	1,5	1988
Teon	INDONESIA	BANDA SEA	A	1,5	1904
Batu Tara	INDONESIA	FLORES SEA	A	1	2022
Rokatenda	INDONESIA	FLORES SEA	A	2,3	2013
Sangeang Api	INDONESIA	FLORES SEA	A	5,2	2022
Gamalama	INDONESIA	MALUKU	A	4,3	2018
Gamkonora	INDONESIA	MALUKU	A	4,8	2007
Iliwerung	INDONESIA	NUSA TENGGARA EAST	A	1,5	2021
Lewotolo	INDONESIA	NUSA TENGGARA EAST	A	4	2012
Awu	INDONESIA	SULAWESI	A	5,5	2004
Karangetang	INDONESIA	SULAWESI	A	4	2020
Ruang	INDONESIA	SULAWESI	A	1,6	2002
Stromboli	ITALY	AEOLIAN ISLANDS	A	1,6	2022
Vulcano	ITALY	AEOLIAN ISLANDS	B	0,9	1890
Campi Flegrei	ITALY	CAMPANIA	B	0	1538
Vesuvius	ITALY	CAMPANIA	A	6,4	1944
Etna	ITALY	SICILIA	A	17	2023
Fukutoku-Okanoba	JAPAN	IZU ISLANDS	C	0	2021
Miyake-jima	JAPAN	IZU ISLANDS	A	3	2010
Myojinsho	JAPAN	IZU ISLANDS	C	0	1970
Nishino-jima	JAPAN	IZU ISLANDS	B	0,2	2021
Sumisu	JAPAN	IZU ISLANDS	C	0	1916
Tori-jima	JAPAN	IZU ISLANDS	A	1,1	2002
Oshima-Oshima	JAPAN	JAPAN SEA	A	1	1790
Kikai	JAPAN	RYUKYU ISLANDS	B	1	2020
Suwanose-jima	JAPAN	RYUKYU ISLANDS	A	2,2	2020
Soufriere Hills	MONTSERRAT	WEST INDIES	A	3,2	2013
Saba	NETHERLANDS	WEST INDIES	A	1,3	1640
The Quill	NETHERLANDS	WEST INDIES	A	1,2	
White Island	NEW ZEALAND	BAY OF PLENTY	A	0,8	2019
Raoul Island	NEW ZEALAND	KERMADEC	A	1,6	2006
Okataina	NEW ZEALAND	NORTH ISLAND	B	0	1981
Taupo	NEW ZEALAND	NORTH ISLAND	B	0	260
Momotombo	NICARAGUA	LAKE MANAGUA	A	3,5	2016
Cosiguina	NICARAGUA	PACIFIC COAST	A	6,1	1859
Bam	PAPUA - NEW GUINEA	BISMARCK SEA	A	1,1	1960
Kadovar	PAPUA - NEW GUINEA	BISMARCK SEA	A	0,5	2020
Long Island	PAPUA - NEW GUINEA	BISMARCK SEA	A	7	1993
Manam	PAPUA - NEW GUINEA	BISMARCK SEA	A	5	2020
Ritter Island	PAPUA - NEW GUINEA	BISMARCK SEA	C	0	2007
Dakataua	PAPUA - NEW GUINEA	NEW BRITAIN	B	5,5	1895
Rabaul	PAPUA - NEW GUINEA	NEW BRITAIN	B	0,6	2014
Tuluman	PAPUA - NEW GUINEA	NEW BRITAIN	C	0	1957
Ulawun	PAPUA - NEW GUINEA	NEW BRITAIN	A	10,5	2022
Didicas	PHILIPPINES	BABUYAN ISLANDS	B	0,2	1978
Camiguin	PHILIPPINES	BOHOL SEA	B	4	1953
Taal	PHILIPPINES	LUZON	B	2,2	2021
Sao Jorge	PORTUGAL	AZORES ISLANDS	D	1,5	1902
Raikoke	RUSSIA	KURIL ISLANDS	A	0,7	2019
Sarychev	RUSSIA	KURIL ISLANDS	A	2,8	2021
Tinakula	SOLOMON ISLANDS	EAST SOLOMON	A	1,1	2020
Kavachi	SOLOMON ISLANDS	WEST SOLOMON	C	0	2021
Savo	SOLOMON ISLANDS	WEST SOLOMON	A	2,3	1847?
Cumbre Vieja	SPAIN	CANARY ISLANDS	D	1,2	2021
Liamuiga	ST KITTS & NEVIS	WEST INDIES	A	4,4	1843?
Soufriere	ST VINCENT	WEST INDIES	A	3,5	2020
Home Reef	TONGA	TONGA	C	0	2006
Hunga Ha apai	TONGA	TONGA	B	0,1	2022
Lateiki - Metis Shoal	TONGA	TONGA	C	0	2019
Tofua	TONGA	TONGA	A	3	2014
Unnamed	TONGA	TONGA	C	0	2017
Augustine	USA	ALASKA	A	4	2006
Bogoslof	USA	ALEUTIAN ISLANDS	A	0,2	2017
Kasatochi	USA	ALEUTIAN ISLANDS	A	0,4	2008
Mono Lake	USA	CALIFORNIA	B	0,6	1790
Kilauea	USA	HAWAII	D	14	2022
Loihi	USA	HAWAII	D	0	1996
Anatahan	USA	MARIANA ISLANDS	A	1,5	2008
NW-Rota 1	USA	MARIANA ISLANDS	C	0	2010
Ruby	USA	MARIANA ISLANDS	C	0	1995
South Sarigan	USA	MARIANA ISLANDS	C	0	2010
Edgecumbe	USA	ALASKA	A	5,1	2080 BCE
East Epi	VANUATU	VANUATU	C	0	2023
Eastern Gemini	VANUATU	VANUATU	C	0	1996
Kuwae	VANUATU	VANUATU	C	0	1974
Lopevi	VANUATU	VANUATU	A	2,2	2007
Yasur	VANUATU	VANUATU	B	2,2	2020

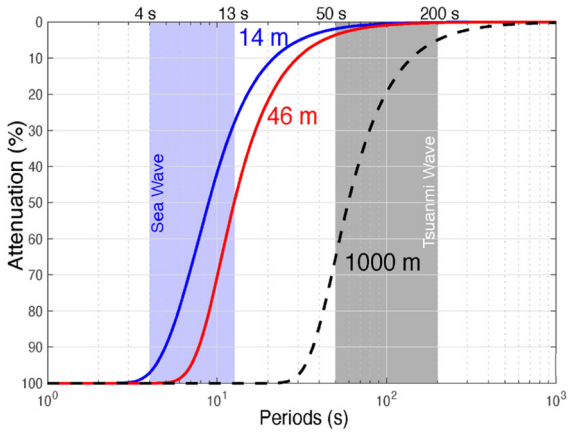

Figure 25
Wave dispersion calculated for the 14 and 46 m sensors show how this depth is optimal to reduce by 40 and 80%, respectively, the contamination of the sea waves. Depth around 50 m below the sea level are optimal to maintain the best signal-to-noise ratio in the period range (50–200 s) typical of tsunami generated by landslide. For this period range, the amplitude of tsunami will be reduced of 5 to 65%, when recorded by a sensor placed at 1000 m below the sea surface

instability (e.g. submarine landslide, collapse of newly formed lava bench) are clearly potential sources of tsunamis, as demonstrated by the Hunga Ha'apai eruption in 2022.

D. It is a shield volcano (ocean island) showing evidence of flank deformation, such as Kilauea volcano in Hawaii (e.g. Kalapana earthquake and tsunami in 1975: Ma et al., 1999), and Piton de la Fournaise in Reunion Island (e.g. large-scale flank deformation observed during the 2007 eruption: Froger et al., 2015).

Stromboli Tsunami Warning System

The Elastic beacons The elastic beacon is a semi-rigid structure with a 35 m long metallic pipe anchored with a concrete block (sinker) of ∼ 24 tons on the seabed through an anti-torsion steel cable (Fig. 13a). Instruments are located on a small tower which stands ∼ 8–10 m above the sea level, where the digitizer (Guralp – DM24S6EAMU), radio transmission system (5 GHz 10/100 Mbits and UMTS) and power supply (solar panels and batteries) are

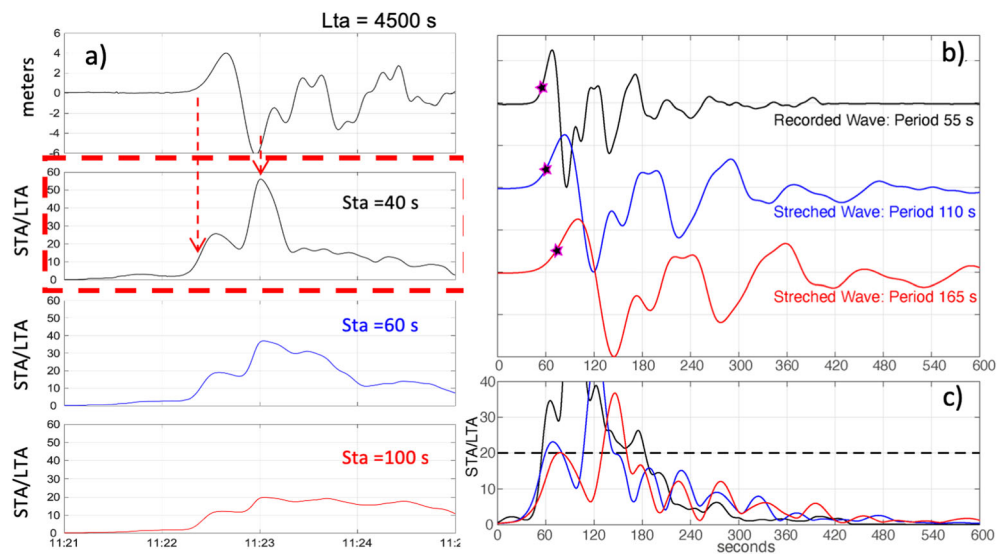

Figure 26
a STA/LTA ratio calculated for LTA = 4500 s and different STA time window shows the best performance with STA = 40 s to detect the onset of the tsunami. Signal used to test the algorithm is the tsunami wave modeled for the December 2002 landslide (Fornaciai et al., 2019). The 40 s large time window for the STA is also giving the best performance when **b** different period of the tsunami ranging from 50 to 165 s are considered. **c** Larger the period of the tsunami larger the STA time window or smaller the STA/LTA ratio should be for the most rapid detection of the tsunami onset.

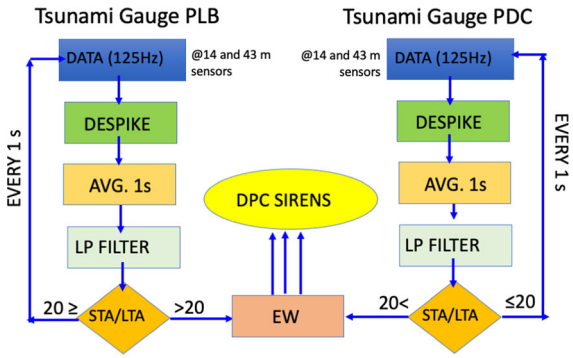

Figure 27
Chart flow of the automatic tsunami detection algorithm operating at Stromboli

placed. Sea level is measured by pressure sensors located at ∼ 14 and ∼ 48 m (at the seabed) below the sea surface (Fig. 13a). Both elastic beacons are equipped with IDROMAR pressure sensors (sampled 125 Hz), one at 14 m below the sea level and the second on the concrete block. Depth of the pressure sensor is optimal to reduce the effect of the sea wave at periods < 13 s and to guarantee the best signal-to-noise ratio in the range of period (50–120 s) typical of the tsunami generated by landslides and/or pyroclastic flows (Fig. 25).

Tsunami Detection Algorithm The automatic detection of the tsunami waves is based on a five-steps algorithm: (I) spike removal, (II) detrending signal for tide removal, (III) low-pass filtering, (IV) data decimation and finally (V) the STA/LTA ratio.

I. Spikes or sudden high frequency signal are usually the result of transmission error in the telemetry, disturbance from short electronic glitches or in the case of Stromboli also by fishing activities around the elastic beacons. Spikes can contaminate the record resulting in the sudden increase of the STA and thus possible false detection.
II. Linear detrend removes the tidal and/or barometric oscillations from the signal.
III. The sea waves component is filtered using a FIR low-pass filter with a cut-off frequency f_c = 0.067 Hz and a bandwidth of 0.04 Hz to increase the signal-to-noise ratio.
IV. Data are decimated from 125 sampling rate down to 1 sample per second.

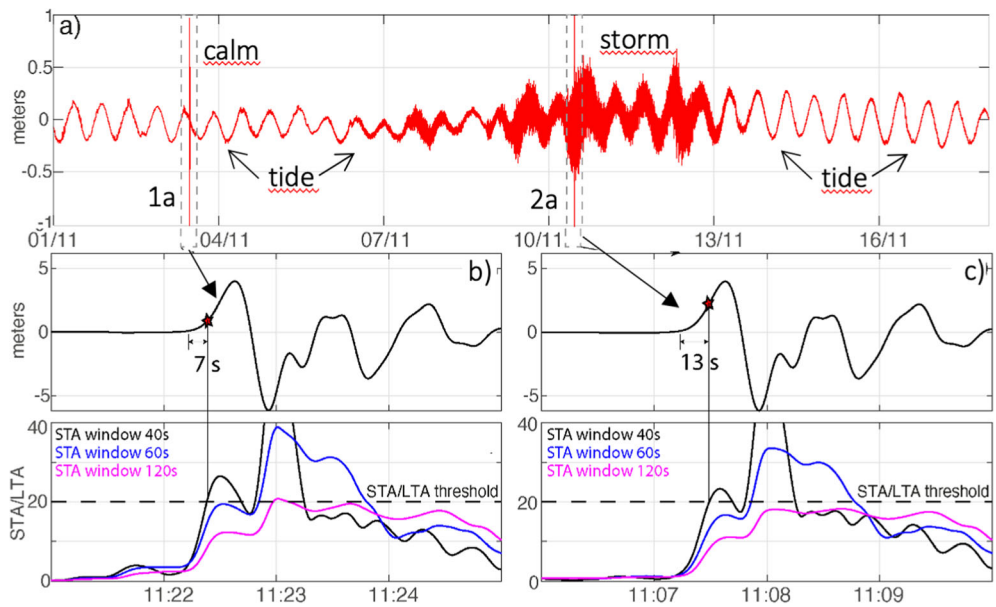

Figure 28
Sensitivity of the STA/LTA ratio to the sea condition has been tested by superimposing the theoretical waveform modeled for the December 2002 tsunami **a** to calm (1a) and stormy (2a) sea conditions with waves up to 9 m. Onset of the tsunami is detected **b** 7 s after the onset (STA = 40s) but with a delay **c** of only 6 s during the sea storm

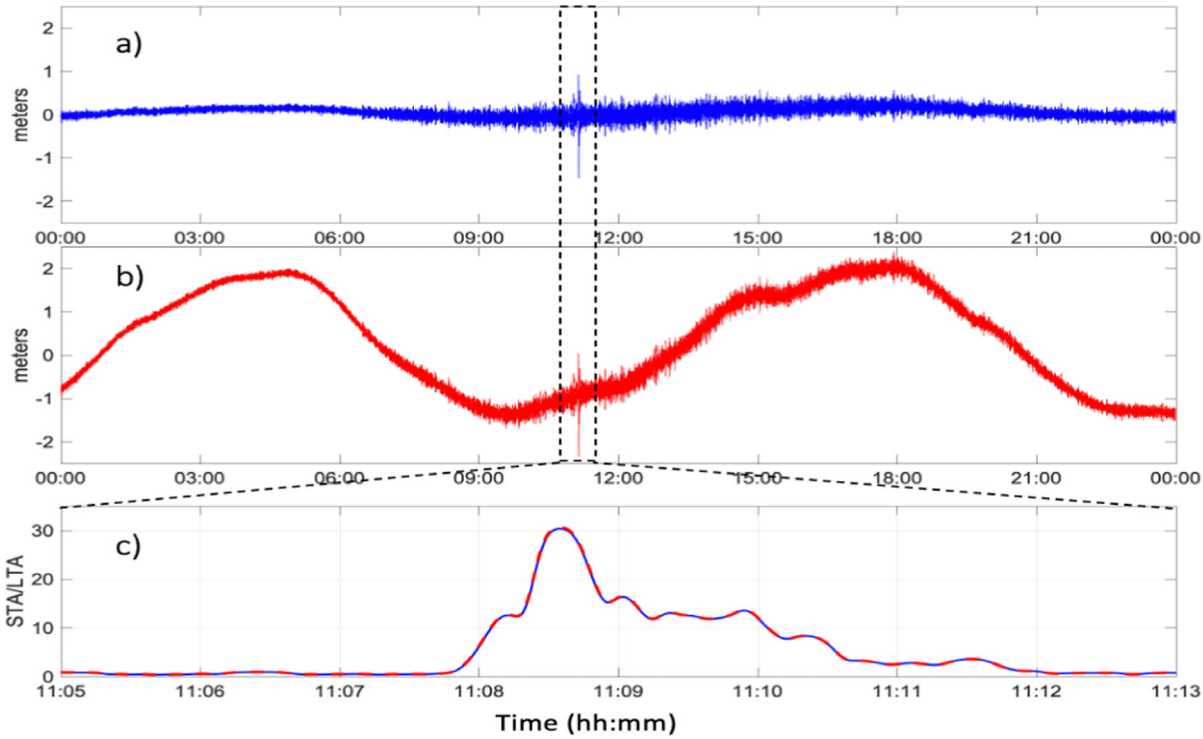

Figure 29
The TEW algorithm **a** developed at Stromboli with tide of $\sim$ 40 cm and sea waves of $<$ 15 s period was tested **b** also for sea basins different than Mediterranean using larger tide ($\sim$ 2 m) and longer wave period and it shows **c** how marine contaminations are removed and the STA/LTA ratio remains the same

V. Finally, the STA/LTA ratio is calculated on the resampled data. To assure the correct description of the sea state and to reduce the statistical scatter, the LTA window should contain at least 300 times the larger sea wave period of 15 s (typical of rough sea state in the southern Mediterranean sea) which gives a LTA window of 4500 s. The STA window length depends instead strictly on the period of the tsunami wave to be detected and it was fixed to 40 s which gives the larger value of the STA/LTA ratio at the onset of tsunami for periods ranging between 50 and 200 s (Fig. 26).

The algorithm issues the alert only when the STA/LTA ratio is larger than the pre-defined threshold of 20 at both elastic beacons (tsunami gauges) within a time interval no longer than 120 s (Fig. 27). This threshold would also depend on the sea state typical of the area where the elastic beacons are installed and on the depth of the sensors.

Calibrating Algorithm Sensitivity The efficiency of the TEWS depends on the STA/LTA threshold used to automatically detect the tsunami keeping the false alert to zero. This threshold was calibrated by contaminating the tsunami wave modelled for the 2002 Stromboli eruption with the noise relative to the most energetic sea storm recorded at Stromboli in the last 15 years (significative wave of 8 m) that generated waves of $\sim$ 1 m with periods of $\sim$ 12 s at 46 m depth below sea level (Fig. 29). In this case, the STA/LTA ratio was never above 12 and thus threshold was fixed to 20 considering also that the period of the tsunami could range between 50 and 165 s (Fig. 28). Threshold represents than a compromise between reducing the false alert and detecting the tsunami as early as possible. The sea storm is not affecting the algorithm efficiency but is producing a

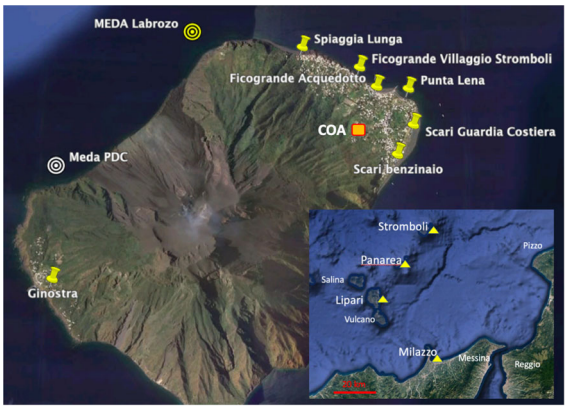

Figure 30
Position of the Advanced Operations Center (COA) and the Acoustic Alert (siren) system used to warn population on the possible occurrence of a tsunami

delay of only 6 s on the detection of the tsunami. Tide as large as 2 m do not have any effect on the detection capability of the TEWS (Fig. 29).

Non-SOP procedure In case of a tsunami detection by the TEWS (Fig. 27) the Italian DPC has defined national PROCEDURE for non-conventional tsunami, in cooperation with the Sicily Regional Civil Protection, the Lipari Municipality and the monitoring centers of INGV and University of Florence (LGS). Once received the notification from the TEWS, the DPC will automatically activate for three minutes the acoustic alert (sirens) at Stromboli and Ginostra villages, Panarea and Lipari island, and in the control room of the Harbour Office of Milazzo (see Fig. 30) with a continuous monotone sound. In parallel, emails and SMS messages will be automatically sent to a list of previously selected Authorities with the following text: "Tsunami wave in progress at Stromboli".

The early-warning message is thus automatically delivered to control room for the Emergency of (1) the National Civil Protection, (2) the Sicily Regional Civil Protection, (3) the Lipary Municipality, (4) the Prefecture of Messina and (5) the National Institute of Geophysics and Volcanology (INGV).

SOP Procedure The TEWS implemented at Stromboli is the first early warning system developed to automatically deliver an alert in case of a tsunami generated by volcanic activity (Lacanna & Ripepe, 2020) and is then at the moment operating outside the standard procedure developed for earthquake-generated tsunami. However, on August 2022 the University of Florence (LGS) and the National Institute of Geophysics and Volcanology, in the framework of the operational monitoring activities for the Italian Department of Civil Protection, signed a Cooperation Agreement to integrate the TEWS of Stromboli within the activities the national Tsunami Alert Center (CAT) of the INGV. The CAT-INGV operates as a Tsunami Service Provider accredited by the ICG/NEAMTWS (Intergovernmental Coordination Group for the Tsunami Early Warning and Mitigation System in the North-Eastern Atlantic, the Mediterranean and connected seas) which is an integral part of the global tsunami risk warning and mitigation system, established and coordinated by the Intergovernmental Oceanographic Commission (IOC) of UNESCO.

At the moment, the signals recorded by the tsunami systems at Stromboli are transmitted in real time in a standard format to the CAT-INGV in Rome. A feasibility study for integrating the Stromboli TEWS within the NEAMTWS procedures is currently ongoing. The purpose is to integrate the information received by the local TEWS within the SOPs of the NEAMTWS, both at the local, national as well as at international level.

References

Abadie, S. M., Harris, J. C., Grilli, S. T., & Fabre, R. (2012). Numerical modelling of tsunami waves generated by the flank collapse of the Cumbre Vieja Volcano (La Palma, Canary Islands): Tsunami source and near field effects. *Journal of Geophysical Research-Oceans*. https://doi.org/10.1029/2011jc007646

Allstadt, K. E., Matoza, R. S., Lockhart, A. B., Moran, S. C., Caplan-Auerbach, J., Haney, M. M., et al. (2018). Seismic and acoustic signatures of surficial mass movements at volcanoes. *Journal of Volcanology and Geothermal Research, 364*, 76–106. https://doi.org/10.1016/j.jvolgeores.2018.09.007

Ando, M. (1979). The Hawaii earthquake November 29, 1975: Low dip angle faulting due to forceful injection of magma. *Journal of Geophysical Research, 84*(B13), 7616–7626.

Astafyeva, E., Maletckii, B., Mikesell, T. D., Munaibari, E., Ravanelli, M., Coisson, P., et al. (2022). The 15 January 2022 Hunga Tonga eruption history as inferred from ionospheric observations. *Geophysical Research Letters, 49*, e2022GL098827.

Battershill, L., Whittaker, C. N., Lane, E. M., Popinet, S., White, J. D. L., Power, W. L., & Nomikou, P. (2021). Numerical simulations of a fluidized granular flow entry into water: Insights into modelling tsunami generation by pyroclastic density currents. *Journal of Geophysical Research: Solid Earth*. https://doi.org/10.1029/2021JB022855

Belousov, A., Voight, B., Belousova, M., & Muravyev, Y. (2000). Tsunamis generated by underwater volcanic explosions: Unique data from 1996 eruption in Karymskoye Lake, Kamchatka, Russia. *Pure and Applied Geophysics, 157*, 1135–1143.

Bertolaso, G., De Bernardinis, B., Bosi, V., et al. (2009). Civil protection preparedness and response to the 2007 eruptive crisis of Stromboli volcano, Italy. *Journal of Volcanology and Geothermal Research, 182*(3–4), 269–277. https://doi.org/10.1016/j.jvolgeores.2009.01.022

Bevilacqua, A., Bertagnini, A., Pompilio, M., Landi, P., Del Carlo, P., Di Roberto, A., et al. (2020). Major explosions and paroxysms at Stromboli (Italy): A new historical catalog and temporal models of occurrence with uncertainty quantification. *Scientific Reports, 10*(1), 1–18.

Biggs, J., Ebmeier, S. K., Aspinall, W. P., Lu, Z., Pritchard, M. E., Sparks, R. S. J., & Mather, T. A. (2014). Global link between deformation and volcanic eruption quantified by satellite imagery. *Nature Communications, 5*, 3471. https://doi.org/10.1038/ncomms4471

Biggs, J., & Pritchard, M. E. (2017). Global volcano monitoring: What does it mean when volcanoes deform? *Elements, 13*(1), 17–22.

Blong, R. J., & McKee, C. O. (1995). *The Rabaul eruption 1994: Destruction of a town* (p. 52). Macquarie University.

Bonaccorso, A., Calvari, S., Garfì, L., Lodato, L., & Patanè, D. (2003). Dynamics of the December 2002 flank failure and tsunami at Stromboli volcano inferred by volcanological and geophysical observations. *Geophysical Research Letters, 30*, 1941.

Bonaccorso, A., Calvari, S., Linde, A., Sacks, S., & Boschi, E. (2012). Dynamics of the shallow plumbing system investigated from borehole strainmeters and cameras during the 15 March 2007 Vulcanian paroxysm at Stromboli volcano. *Earth and Planetary Science Letters, 357–358*, 249–256.

Borrero, J. C., Cronin, J. C., Helina Latu'ila, F., Tukuafu, P., Heni, N., Maea Tupou, A., et al. (2022). Tsunami Runup and inundation in Tonga from the January 2022 Eruption of the Hunga Volcano. *Pure and Applied Geophysics, 180*, 1–22. https://doi.org/10.1007/s00024-022-03215-5

Borrero, J. C., Solihuddin, T., Fritz, H. M., Lynett, P. J., Prasetya, G. S., Skanavis, V., et al. (2020). Field survey and numerical modelling of the December 22, 2018, Anak Krakatau Tsunami. *Pure Applied Geophysics, 177*, 2457–2475. https://doi.org/10.1007/s00024-020-02515-y

Bosserelle, C. D., Lane, E. M., & Harang, A. (2021). BG-Flood: A GPU adaptive, open-source, general inundation hazard model. *Proceedings of the Australasian Coasts and Ports Conference* 2021. 30 November - 3 December 2021. https://www.coastsandports.org/papers/2021/150_bosserelle_finalpaper.pdf

Bougouin, A., Paris, R., & Roche, O. (2020). Impact of fluidized granular flows into water: Implications for tsunamis generated by pyroclastic flows. *Journal of Geophysical Research Solid Earth, 125*, e2019JB018954.

Bougouin, A., Paris, R., Roche, O., Siavelis, M., & Courdavault, A. P. (2024). Tsunamis generated by pyroclastic flows: experimental insights into the effect of the bulk flow density. *Bulletin of Volcanology*. https://doi.org/10.1007/s00445-024-01704-0

Bougouin, A., Roche, O., Paris, R., & Huppert, H. E. (2021). Experimental insights on the propagation of fine-grained geophysical flows entering water. *Journal of Geophysical Research-Oceans*. https://doi.org/10.1029/2020JC016838

Calder, E. S., et al. (2002). Mechanisms of lava dome instability and generation of rockfalls and pyroclastic flows at Soufriere Hills Volcano, Montserrat. *Geological Society, London, Memoirs, 21*(1), 173–190.

Campus, P. (2006). Monitoring volcanic eruptions with the IMS infrasound network. *Inframatics, 15*, 6–12.

Carazzo, G., Kaminski, E., & Tait, S. (2015). The timing and intensity of column collapse during explosive volcanic eruptions. *Earth and Planetary Science Letters, 411*, 208–217.

Carey, S., Sigurdsson, H., Mandeville, C., & Bronto, S. (2000). Volcanic hazards from pyroclastic flow discharge into the sea: Examples from the 1883 eruption of Krakatau, Indonesia. *Geological Society of America Special Publication, 345*, 1–14.

Carvajal, M., Sepúlveda, I., Gubler, A., & Garreaud, R. (2022). Worldwide signature of the 2022 Tonga volcanic tsunami. *Geophysical Research Letters*. https://doi.org/10.1029/2022GL098153

Ceranna, L., Matoza, R., Hupe, P., Le Pichon, A., & Landès, M. (2019). Systematic array processing of a decade of global IMS infrasound data. In A. Le Pichon, E. Blanc, & A. Hauchecorne (Eds.), *Infrasound monitoring for atmospheric studies—challenges in middle-atmosphere dynamics and societal benefits*. Berlin: Springer. https://doi.org/10.1007/978-3-319-75140-5_13

Chacón-Barrantes, S., Rivera-Cerdas, F., & Murillo-Gutiérrez, A. (2023). Impact of the tsunami caused by the Hunga Tonga-Hunga Ha'apai eruption in Costa Rica on 15 January 2022. *Bulletin of Volcanology, 85*, 36. https://doi.org/10.1007/s00445-023-01648-x

Chang, C. H., & Wang, K. H. (2015). Numerical study on three-dimensional waves produced by a bottom jet. *Applied Ocean Research, 50*, 141–154.

Chiocci, F. L., Romagnoli, C., Tommasi, P., & Bosman, A. (2008). The Stromboli 2002 tsunamigenic submarine slide: characteristics and possible failure mechanisms. *Journal of Geophysical Research: Solid Earth, 113*(B10). https://doi.org/10.1029/2007JB005172

Chouet, B. A., Page, R. A., Stephens, C. D., Lahr, J. C., & Power, J. A. (1994). Precursory swarms of long-period events at Redoubt Volcano (1989–1990), Alaska: Their origin and use as a forecasting tool. *Journal of Volcanology and Geothermal Research, 62*, 95–135.

Clouard, V., von Hillebrandt-Andrade, C., McCreery, C., & Sostre Cortés, J. J. (2024). Implementation of tsunami warning procedures in the Caribbean in case of a volcano crisis: Use of a Volcano Notice for tsunami Threat (VONUT). *Bulletin of Volcanology*. https://doi.org/10.1007/s00445-023-01702-8

Coppola, D., Laiolo, M., Cigolini, C., Donne, D. D., & Ripepe, M. (2016). Enhanced volcanic hot-spot detection using MODIS IR data: Results from the MIROVA system. *Geological Society London, Special Publications, 426*, 181–205. https://doi.org/10.1144/SP426.5

Cronin, S. J., Brenna, M., Smith, I. E. M., Barker, S. J., Tost, M., Ford, M., et al. (2017). New volcanic island unveils explosive past. *Eos Transactions of the American Geophysical Union*. https://doi.org/10.1029/2017EO076589

Dabrowa, A. L., Green, D. N., Rust, A. C., & Phillips, J. C. (2011). A global study of volcanic infrasound characteristics and the potential for long-range monitoring. *Earth and Planetary Science Letters, 310*, 369–379. https://doi.org/10.1016/j.epsl.2011.08.027

Day, S. J. (2015). Volcanic tsunamis. In J. Sigurdson (Ed.), *Encyclopedia of volcanoes* (pp. 993–1009). New York: Academic Press, Elsevier.

Day, S. J., Watts, P., Grilli, S. T., & Kirby, J. T. (2005). Mechanical models of the 1975 Kalapana, Hawaii earthquake and tsunami. *Marine Geology, 215*, 59–92.

De Angelis, S., Bass, V., Hards, V., & Ryan, G. (2007). Seismic Characterization of pyroclastic flow activity at Soufrière Hills Volcano, Montserrat, 8 January 2007. *Natural Hazards and Earth System Sciences, 7*(4), 467–472. https://doi.org/10.5194/nhess-7-467-2007

De Lange, W. P., Prasetya, G. S., & Healy, T. R. (2001). Modelling of tsunamis generated by pyroclastic flows (Ignimbrites). *Natural Hazards, 24*(3), 251–266.

Dean, K. G., Osiensky, J., Gordeev, E., Senyukov, S., Rybin, A. V., Karagusov, Y. V., et al. (2015). An overview of satellite monitoring of volcanoes. In K. G. Dean & J. Dehn (Eds.), *Monitoring volcanoes in the North Pacific—observations from space* (pp. 261–302). Springer.

Dehn, J., & Harris, A. J. L. (2015). Thermal anomalies at volcanoes. In K. G. Dean & J. Dehn (Eds.), *Monitoring volcanoes in the North Pacific* (pp. 49–78). Springer.

Dietz, R. S., & Sheehy, M. J. (1954). Transpacific detection of Myojin volcanic explosions by underwater sound. *Bulletin of the Geological Society of America, 65*, 941–965.

Drob, D. P., Picone, J. M., & Garcés, M. (2003). Global morphology of infrasound propagation. *Journal of Geophysical Research, 108*(D21), 4680. https://doi.org/10.1029/2002JD003307

Duffy, D. G. (1992). On the generation of oceanic surface waves by underwater volcanic explosions. *Journal of Volcanology and Geothermal Research, 50*, 323–344.

Duputel, Z., Lengliné, O., & Ferrazzini, V. (2019). Constraining spatiotemporal characteristics of magma migration at Piton de la Fournaise volcano from pre-eruptive seismicity. *Geophysical Research Letters, 46*(1), 119–127.

Dzurisin, D. (2003). A comprehensive approach to monitoring volcano deformation as a window on the eruption cycle. *Reviews of Geophysics, 41*(1), 1001. https://doi.org/10.1029/2001RG000107

Dzurisin, D., Westphal, J. A., & Johnson, D. J. (1983). Eruption prediction aided by electronic tiltmeter data at Mount St. Helens. *Science, 221*, 1381–1383.

Egorov, Y. (2007). Tsunami wave generation by the eruption of underwater volcano. *Natural Hazards and Earth System Sciences, 7*, 65–69.

Einarsson, P., & Brandsdottir, B. (2021). Seismicity of the Northern Volcanic Zone of Iceland. *Frontiers Earth Science*. https://doi.org/10.3389/feart.2021.628967

Esposti Ongaro, T., de'Micheli Vitturi, M., Ceraminara, M., Fornaciai, A., Nanniperi, L., Favalli, M., et al. (2021). Modelling tsunamis generated by submarine landslides at Stromboli Volcano (Aeolian Islands, Italy): A numerical benchmark study. *Frontiers Earth Science, 9*, 1–21.

Falcin, A., Métaxian, J. P., Mars, J., Stutzmann, É., Komorowski, J. C., Moretti, R., et al. (2021). A machine-learning approach for automatic classification of volcanic seismicity at La Soufrière Volcano, Guadeloupe. *Journal of Volcanology and Geothermal Research, 411*, 107151.

Falvard, S., Paris, R., Belousova, M., Belousov, A., Giachetti, T., & Cuven, S. (2018). Scenario of the 1996 volcanic tsunamis in Karymskoye Lake, Kamchatka, inferred from X-ray tomography of heavy minerals in tsunami deposits. *Marine Geology, 396*, 160–170.

Fee, D., Garcés, M., & Steffke, A. (2010). Infrasound from Tungurahua volcano 2006–2008: Strombolian to plinian eruptive activity. *Journal of Volcanology and Geothermal Research, 193*(1–2), 67–81. https://doi.org/10.1016/j.jvolgeores.2010.03.006

Firdaus, K., Matin, M. A., Nurisman, N., & Magdalena, I. (2022). Numerical study for Sunda Strait Tsunami wave propagation and its mitigation by mangroves in Lampung, Indonesia. *Results in Engineering, 16*, 100605. https://doi.org/10.1016/j.rineng.2022.100605

Fornaciai, A., Favalli, M., & Nanniperi, L. (2019). Numerical simulation of the tsunamis generated by the Sciara del Fuoco landslides (Stromboli Island, Italy). *Science and Reports, 9*, 18542. https://doi.org/10.1038/s41598-019-54949-7

Francalanci, L., Lucchi, F., Keller, J., De Astis, G., & Tranne, C. A. (2013). Eruptive, volcano-tectonic and magmatic history of the Stromboli volcano (north-eastern Aeolian archipelago). *Geological Society, London, Memoirs, 37*(1), 397–471.

Francis, P. (1993). *Volcanoes. A planetary perspective*.

Freundt, A. (2003). Entrance of hot pyroclastic flows into the sea: Experimental observations. *Bulletin of Volcanology, 65*, 144–164.

Fritz, H., Hager, W., & Minor, H. (2004). Near field characteristics of landslide generated impulse waves. *Journal of Waterway Port Coastal and Ocean Engineering, 130*, 287–302.

Froger, J. L., Famin, V., Cayol, V., Augier, A., Michon, L., & Lénat, J. F. (2015). Time-dependent displacements during and after the April 2007 eruption of Piton de la Fournaise, revealed by interferometric data. *Journal of Volcanology and Geothermal Research, 296*, 55–68. https://doi.org/10.1016/j.jvolgeores.2015.02.014

Furtney, M. A., Pritchard, M. E., Biggs, J., Carn, S. A., Ebmeier, S. K., Jay, J. A., et al. (2018). Synthesizing multi-sensor, multi-satellite, multi-decadal data sets for global volcano monitoring. *Journal of Volcanology and Geothermal Research, 365*, 38–56. https://doi.org/10.1016/j.jvolgeores.2018.10.002

Galetto, F., Acocella, V., Hooper, A., & Bagnardi, M. (2022). Eruption at basaltic calderas forecast by magma flow rate. *Nature Geocience*. https://doi.org/10.1038/s41561-022-00960-z

Garcés, M., Fee, D., Steffke, A., McCormack, D. P., Servranckx, R., Bass, H., et al. (2008). Capturing the acoustic fingerprint of stratospheric ash injection. *EOS Transactions, 89*(40), 377–378. https://doi.org/10.1029/2008EO400001

Gauer, P., Kvalstad, T. K., Forsberg, C. F., Bryn, P., & Berg, K. (2005). The last phase of the Storegga Slide: Simulation of retrogressive slide dynamics and comparison with slide-scar morphology. *Marine Petroleum Geology, 22*, 171–178. https://doi.org/10.1016/j.marpetgeo.2004.10.004

Girona, T., Costa, F., & Schubert, G. (2015). Degassing during Quiescence as a Trigger of Magma Ascent and Volcanic Eruptions. *Science and Reports, 5*, 1–7. https://doi.org/10.1038/srep18212

Gisler, G., Weaver, R., & Gittings, M. L. (2006). Two-dimensional simulations of explosive eruptions of Kick-Em Jenny and other submarine volcanoes. *Science of Tsunami Hazards, 25*(1), 34–41.

Glimsdal, S., Pedersen, G. K., Harbitz, C. B., & Løvholt, F. (2013). Dispersion of tsunamis: Does it really matter? *Natural Hazards and Earth Systems Sciences, 13*, 1507–1526.

Gray, J. P., & Monaghan, J. J. (2003). Caldera collapse and the generation of waves. *Geochemistry, Geophysics, Geosystems, 4*, 1015.

Grilli, S. T., Tappin, D. R., Carey, S., Watt, S. F., Ward, S. N., Grilli, A. R., et al. (2019). Modelling of the tsunami from the December 22, 2018 lateral collapse of Anak Krakatau volcano in the Sunda straits, Indonesia. *Scientific Reports, 9*(1), 1–13. https://doi.org/10.1038/s41598-019-48327-6

Grilli, S. T., & Watts, P. (2005). Tsunami generation by submarine mass failure. Modelling, experimental validation, and sensitivity analyses. *Journal of Waterway, Port, Coastal, and Ocean Engineering, 131*, 283–297.

Gusman, A. R., Kaneko, Y., Power, W., & Burbidge, D. (2020). Source process for two enigmatic repeating vertical-T CLVD tsunami earthquakes in the Kermadec ridge. *Geophysical Research Letters, 47*(16), 78. https://doi.org/10.1029/2020gl087805

Harbitz, C. B., Løvholt, F., Pedersen, G., & Masson, D. G. (2006). Mechanisms of tsunami generation by submarine landslides: A short review. *Norwegian Journal of Geology, 86*, 255–264.

Harkrider, D. G., & Press, F. (1967). The Krakatoa air-sea waves: An example of pulse propagation in coupled systems. *Geophysical Journal of the Royal Astronomical Society, 13*, 149–159.

Hayward, M. W., Whittaker, C. N., Lane, E. M., Power, W. L., Popinet, S., & White, J. D. L. (2022). Multilayer modelling of waves generated by explosive subaqueous volcanism. *Natural Hazards and Earth System Sciences, 22*(2), 617–637. https://doi.org/10.5194/nhess-22-617-2022

Hébert, H., Piatanesi, A., Heinrich, P., Schindelé, F., & Okal, E. A. (2002). Numerical modeling of the September 13, 1999 landslide and tsunami on Fatu Hiva Island (French Polynesia). *Geophysical Research Letters, 29*, 1484. https://doi.org/10.1029/2001GL013774

Heidarzadeh, M., Ishibe, T., Sandanbata, O., Muhari, A., & Wijanarto, A. (2020). Numerical modelling of the subaerial landslide source of the 22 December 2018 Anak Krakatoa volcanic tsunami. *Indonesia Ocean Engineering*. https://doi.org/10.1016/j.oceaneng.2019.106733

Herd, R. A., Edmonds, M., & Bass, V. A. (2005). Catastrophic lava dome failure at Soufriere Hills Volcano, Montserrat, 12–13 July 2003. *Journal of Volcanology and Geothermal Research, 148*, 234–252.

Hibert, C., et al. (2014). Automated identification, location, and volume estimation of rockfalls at Piton de la Fournaise volcano. *Journal of Geophysical Research: Earth Surface, 119*(5), 1082–1105.

Hooper, A., Prata, F., & Sigmundsson, F. (2012). Remote sensing of volcanic hazards and their precursors. *Proceedings of the Institute of Electrical and Electronics Engineers (IEEE), 100*(10), 2908–2930. https://doi.org/10.1109/JPROC.2012.2199269

Hunt, J. E., Tappin, D. R., Watt, S. F. L., Susilohadi, S., Novellino, A., Ebmeier, S. K., et al. (2021). Submarine landslide megablocks show half of Anak Krakatau island failed on December 22nd, 2018. *Nature Communications, 12*, 2827.

Iguchi, M., Yakiwara, H., Tameguri, T., Hendrasto, H., & Hirabayashi, J. (2008). Mechanism of explosive eruption revealed by geophysical observations at the Sakurajima, Suwanosejima and Semeru volcanoes. *Journal of Volcanology and Geothermal Research, 178*, 1–9.

Inoue, K. (2000). Shimabara-Shigatusaku earthquake and topographic change by Shimabara Catastrophe in 1792. *Geographical Reports of Tokyo Metropolitan University, 35*, 59–69.

Johnson, R. W. (1987). Large-scale volcanic cone collapse; the 1888 slope failure of Ritter volcano. *Bulletin of Volcanology, 49*, 669–679.

Karstens, J., Berndt, C., Urlaub, M., Watt, S. F. L., Micallef, A., Ray, M., et al. (2019). From gradual spreading to catastrophic collapse – reconstruction of the 1888 Ritter Island volcanic sector collapse from high-resolution 3D seismic data. *Earth and Planetary Science Letters, 517*, 1–13. https://doi.org/10.1016/j.epsl.2019.04.009.

Kamo, K. A. (1989). In Latter J. H. (ed) *Volcanic hazards: Assessment methods and monitoring*. Springer, Berlin, pp 585–598

Kanamori, H., & Given, J. W. (1982). Analysis of long-period seismic waves excited by the May 18, 1980, eruption of Mount St. Helens—a terrestrial monopole? *Journal of Geophysical Research Solid Earth, 87*(B7), 5422–5432.

Kawakatsu, H., & Yamamoto, M. (2007). Volcano seismology. *Earthquake Seismology*. https://doi.org/10.1016/B978-0-444-53802-4.00081-6

Kelfoun, K. (2011). Suitability of simple rheological laws for the numerical simulation of dense pyroclastic flows and long-runout volcanic avalanches. *Journal of Geophysical Research-Solid Earth*. https://doi.org/10.1029/2010JB007622

Kokelaar, P. (1986). Magma-water interactions in subaqueous and emergent basaltic volcanism. *Bulletin of Volcanology, 48*, 275–289.

Kokelaar, P., & Romagnoli, C. (1995). Sector collapse, sedimentation, and clast population evolution at an active island-arc volcano: Stromboli, Italy. *Bulletin of Volcanology, 57*(4), 240–262.

Kong, L., Aliaga, B., Korovulavula, J., Fa'anunu, 'O., Gusman, A., & Kula, T., et al. (2022). Hunga-Tonga Hunga Ha'apai Eruption and Tsunami: Importance of real-time sea level data for tsunami warning decision. International Ocean Data Conference 2022, 14–16 February 2022. http://itic.ioc-unesco.org/images/stories/list_of_tsunamis/2022/15Jan2022_Hunga-Tonga/HTHH_SLTsunamiWarning_IntlOceanData_LauraKong_feb22_4_A4.pdf

Kubota, T., Saito, T., & Nishida, K. (2022). Global fast-traveling tsunamis driven by atmospheric Lamb waves on the 2022 Tonga eruption. *Science, 377*(6601), 91–94. https://doi.org/10.1126/science.abo4364

Lacanna, G., & Ripepe, M. (2020). Genesis of tsunami waves generated by pyroclastic flows and the early-warning system. In *Rittmann Conference 2020, Session S13. The Summer 2019 Stromboli Paroxysms: A Precious Opportunity to Expand the Knowledge on the Volcano* (Catania).

Lander, J. F., Whiteside, L. S., & Lockridge, P. A. (2002). A brief history of tsunami in the Caribbean Sea. *Science of Tsunami Hazards, 20*, 57–94.

Lane, E. M., Mountjoy, J. M., Power, W. L., & Popinet, S. (2016). Initialising landslide-generated tsunamis for probabilistic tsunami hazard assessment in Cook Strait. *International Journal of Ocean and Climate Systems*. https://doi.org/10.1177/1759313115623162

Lassa, J. (2009). The forgotten disaster? Remembering the Larantuka and Lembata disaster 1979–2009. *Journal of NTT Studies, 1*, 159–184. In Indonesian.

Le Méhauté, B. L. (1971). Theory of explosion-generated water waves. In V. T. Chow (Ed.), *Advances in hydroscience* (Vol. 7, pp. 1–79). Academic Press.

Le Méhauté, B. L., & Wang, S. (1996). *Water waves generated by underwater explosion. Advanced series on ocean engineering* (Vol. 10). World Scientific Publishing.

Lee, C. H., & Huang, Z. (2020). Multi-phase flow simulation of impulsive waves generated by a sub-aerial granular landslide on an erodible slope. *Landslides, 18*, 881–895.

Linde, A. T., Agustsson, K., Sacks, I. S., & Stefansson, R. (1993). Mechanism of the 1991 eruption of Hekla from continuous borehole strain monitoring. *Nature*, *365*, 737–740. https://doi.org/10.1038/365737a0

Lipiejko, N., Whittaker, C. N., Lane, E. M., & Power, W. L. (2023). Wave generation by fluidized granular flows: experimental insights into the maximum near-field wave amplitude. *Journal of Geophysical Research-Oceans*. https://doi.org/10.1029/2022JC019583

Lipiejko, N., Whittaker, C. N., Lane, E. M., White, J. D. L., & Power, W. L. (2021). Tsunami generation by underwater volcanic explosions: Application to the 1952 explosions of Myojinsho volcano. *Pure and Applied Geophysics, 178*, 4743–4761.

Lipiejko, N., Whittaker, C. N., Lane, E. M., White, J. D. L., & Power, W. L. (2022). Experimental modeling of tsunamis generated by pyroclastic density currents: The effects of particle size distribution on wave generation. *Journal of Geophysical Research-Solid Earth*. https://doi.org/10.1029/2022JB024847

Liu, P.L.-F., Wu, T.-R., Raichlen, F., Synolakis, C. E., & Borrero, J. C. (2005). Runup and rundown generated by three-dimensional sliding masses. *Journal of Fluid Mechanics, 536*, 107–144.

Løvholt, F., Pedersen, G., Harbitz, C. B., Glimsdal, S., & Kim, J. (2015). On the characteristics of landslide tsunamis. *Philosophical Transactions of the Royal Society A, 373*, 20140376. https://doi.org/10.1098/rsta.2014.0376

Lynett, P. J., Gately, K., Wilson, R., Montoya, L., Arcas, D., Aytore, B. Y., et al. (2017). Inter-model analysis of tsunami-induced coastal currents. *Ocean Modelling, 114*, 14–32. https://doi.org/10.1016/j.ocemod.2017.04.003

Lynett, P., McCann, M., Zhou, Z., Renteria, W., Borrero, J., Greer, D., et al. (2022). Diverse tsunamigenesis triggered by the Hunga Tonga-Hunga Ha'apai eruption. *Nature, 609*(7928), 728–733. https://doi.org/10.1038/s41586-022-05170-6

Ma, G., Shi, F., & Kirby, J. T. (2012). Shock-capturing non-hydrostatic model for fully dispersive surface wave processes. *Ocean Modelling, 43*, 22–35.

Ma, K. F., Kanamori, H., & Satake, K. (1999). Mechanism of the 1975 Kalapana, Hawaii, earthquake inferred from tsunami data. *Journal of Geophysical Research, 104*(B6), 13153–13167.

Mader, C. L., & Gittings, M. L. (2006). Numerical model for the Krakatoa hydrovolcanic explosion and tsunami. *Science of Tsunami Hazards, 24*(3), 174.

Maeno, F., & Imamura, F. (2011). Tsunami generation by a rapid entrance of pyroclastic flow into the sea during the 1883 Krakatau eruption, Indonesia. *Journal of Geophysical Research, 116*, B09205.

Maeno, F., Imamura, F., & Taniguchi, H. (2006). Numerical simulations of tsunamis generated by caldera collapse during the 7.3 ka Kikai eruption, Kyushu, Japan. *Earth, Planets and Space, 58*, 1013–1024.

Maramai, A., Graziani, L., Alessio, G., Burrato, P., Colini, L., Cucci, L., et al. (2005). Near- and far-field survey report of the 30 December 2002 Stromboli Southern Italy tsunami. *Marine Geology, 215*, 93–106.

Marchetti, E., Genco, R., & Ripepe, M. (2009). Ground deformation and seismicity related to the propagation and drainage of the dyke feeding system during the 2007 effusive eruption at Stromboli volcano (Italy). *Journal of Volcanology and Geothermal Research, 182*(3–4), 155–161.

Marchetti, E., Ripepe, M., Campus, P., Le Pichon, A., Vergoz, J., Lacanna, G., et al. (2019). Long range infrasound monitoring of Etna volcano. *Scientific Reports UK, 9*, 18015. https://doi.org/10.1038/s41598-019-54468-5

Marchetti, E., Walter, F., Barfucci, G., Genco, R., Wenner, M., Ripepe, M., et al. (2019). Infrasound array analysis of debris flow activity and implication for early warning. *Journal of Geophysical Research: Earth Surface, 124*, 567–587. https://doi.org/10.1029/2018JF004785

Marzocchi, W., & Bebbington, M. S. (2012). Probabilistic eruption forecasting at short and long time scales. *Bulletin of Volcanology, 74*, 1777–1805.

Matoza, R. S., Fee, D., Assink, J. D., Iezzi, A. M., Green, D. N., Kim, K., et al. (2022). Atmospheric waves and global seismoacoustic observations of the January 2022 Hunga eruption, Tonga. *Science, 377*, 95–100. https://doi.org/10.1126/science.abo7063

Matoza, R. S., Green, D. N., Le Pichon, A., Shearer, M., Fee, D., Mialle, P., & Ceranna, L. (2017). Automated detection and cataloging of global explosive volcanism using the International Monitoring System infrasound network. *Journal of Geophysical Research: Solid Earth, 122*, 2946–2971. https://doi.org/10.1002/2016JB013356

Mattox, T. N., & Mangan, M. T. (1997). Littoral hydrovolcanic explosions: A case-study of lava-seawater interaction at Kilauea volcano. *Journal of Volcanology and Geothermal Research, 75*, 1–17.

McNutt, S. R., Thompson, G., Johnson, J. B., De Angelis, S., & Fee, D. (2015). Seismic and infrasonic monitoring. In *The encyclopedia of volcanoes*, (2nd ed., pp. 1071–1099). Academic Press. https://doi.org/10.1016/B978-0-12-385938-9.00063-8

Mialle, P., Brown, D., Arora, N., Colleagues from IDC. (2019). Advances in operational processing at the International Data Centre. In A. Le Pichon, E. Blanc, & A. Hauchecorne (Eds.), *Infrasound monitoring for atmospheric studies*. Cham: Springer. https://doi.org/10.1007/978-3-319-75140-5_6

Mirchina, N. R., & Pelinovsky, E. N. (1988). Estimation of underwater eruption energy based on tsunami wave data. *Natural Hazards, 1*, 277–283.

Morrissey, M., Gisler, G., Weaver, R., & Gittings, M. (2010). Numerical model of crater lake eruptions. *Bulletin of Volcanology, 72*, 1169–1178.

Muhari, A., Heidarzadeh, M., Susmoro, H., Nugroho, H. D., Kriswati, E., Supartoyo, S., et al. (2019). The December 2018 Anak Krakatau volcano tsunami as inferred from post-tsunami field surveys and spectral analysis. *Pure Applied Geophysics, 176*, 5219–5233.

Nakano, M., Unoki, S., Hanzawa, M., Marumo, R., & Fukuoka, J. (1954). Oceanographic features of a submarine eruption that destroyed the Kaiyo-Maru No. 5. Sears foundation. *Journal of Marine Research, 13*, 48–66.

Newhall, C. G., & Dzurisin, D. (1988). Historical unrest at large calderas of the world: U.S. Geological Survey Bulletin 1855.

Newhall, C. G., & Hoblitt, R. (2002). Constructing event trees for volcanic crises. *Bulletin of Volcanology, 64*, 3–20. https://doi.org/10.1007/s004450100173

Nishimura, T. (2009). Ground deformation caused by magma ascent in an open conduit. *Journal of Volcanology and Geothermal Research, 187*, 178–192.

Nishimura, Y., Nakagawa, M., Kuduon, J., & Wukawa, J. (2005). Timing and scale of tsunamis caused by the 1994 Rabaul eruption, East New Britain, Papua New Guinea. In K. Satake (Ed.), *Tsunamis: case studies and recent developments* (pp. 43–56). Springer.

Omira, R., Ramalho, R. S., Kim, J., González, P. J., Kadri, U., Miranda, J. M., et al. (2022). Global Tonga tsunami explained by a fast-moving atmospheric source. *Nature, 609*, 734–740. https://doi.org/10.1038/s41586-022-04926-4

Pakoksung, K., Suppasri, A., & Imamura, F. (2021). Probabilistic tsunami hazard analysis of inundated buildings following a subaqueous volcanic explosion based on the 1716 tsunami scenario in Taal Lake, Philippines. *Geosciences, 11*, 92. https://doi.org/10.3390/geosciences11020092

Pallister, J., & McNutt, S. (2015). Synthesis of volcano monitoring. In *The encyclopedia of volcanoes,* (2nd ed., pp. 1151–1171). Academic Press. https://doi.org/10.1016/B978-0-12-385938-9.00066-3

Pallister, J., Schneider, D., Griswold, J. P., Keeler, R. H., Burton, W. C., Noyles, C., et al. (2013). Merapi 2010 eruption—chronology and extrusion rates monitored with satellite radar and used in eruption forecasting. *Journal of Volcanology and Geothermal Research, 261*, 144–152.

Papale, P. (2017). Rational volcanic hazard forecasts and the use of volcanic alert levels. *Journal of Applied Volcanology*. https://doi.org/10.1186/s13617-017-0064-7

Paris, R. (2015). Source mechanisms of volcanic tsunamis. *Philosophical Transactions of the Royal Society A, 373*, 20140380. https://doi.org/10.1098/rsta.2014.0380

Paris, R., Switzer, A. D., Belousova, M., Belousov, A., Ontowirjo, B., Whelley, P. L., et al. (2014a). Volcanic tsunami: A review of source mechanisms, past events, and hazards in Southeast Asia (Indonesia, Philippines, Papua New Guinea). *Natural Hazards, 70*(1), 447–470.

Paris, R., & Ulvrova, M. (2019). Tsunamis generated by subaqueous volcanic explosions in Taal Caldera Lake, Philippines. *Bulletin of Volcanology, 81*, 14. https://doi.org/10.1007/s00445-019-1272-2.

Paris, R., Ulvrová, M., Selva, J., Brizuela, B., Costa, A., Grezio, A., et al. (2019). Probabilistic hazard analysis for tsunamis generated by subaqueous volcanic explosions in the Campi Flegrei caldera, Italy. *Journal of Volcanology and Geothermal Research, 379*, 106–116. https://doi.org/10.1016/j.jvolgeores.2019.05.010

Paris, R., Wassmer, P., Lavigne, F., Belousov, A., Belousova, M., Iskandarsyah, Y., et al. (2014b). Coupling eruption and tsunami records: The Krakatau 1883 case-study, Indonesia. *Bulletin of Volcanology, 76*, 814.

Pasquarè, G., Francalanci, L., Garduño, V. H., & Tibaldi, A. (1993). Structure and geologic evolution of the Stromboli volcano, Aeolian Islands, Italy. *Acta Vulcanologica, 3*, 79–89.

Pavolonis, M. J., Sieglaff, J., & Cintineo, J. (2018). Automated detection of explosive volcanic eruptions using satellite-derived cloud vertical growth rates. *Earth Space Science, 5*, 903–928. https://doi.org/10.1029/2018EA000410

Pelinovsky, E., Choi, B. H., Stromkov, A., Didenkulova, I., & Kim, H. S. (2005). Analysis of tide-gauge records of the 1883 Krakatau tsunami. In K. Satake (Ed.), *Tsunamis: case studies and recent developments* (pp. 57–78). Springer.

Pelinovsky, E., Zahibo, N., Dunkley, P., Edmonds, M., Herd, R., Talipova, T., et al. (2004). Tsunamis generated by the volcano eruption on July 12–13, 2003, at Montserrat, Lesser Antilles. *Science of Tsunami Hazards, 22*, 44–57.

Peltier, A., Bachèlery, P., & Staudacher, T. (2011). Early detection of large eruptions at Piton de la Fournaise volcano (La Réunion Island): Contribution of a distant tiltmeter station. *Journal of Volcanology and Geothermal Research, 199*(1–2), 96–104. https://doi.org/10.1016/j.jvolgeores.2010.11.006

Peltier, A., Villeneuve, N., Ferrazzini, V., Testud, S., Hassen Ali, T., Boissier, P., et al. (2018). Changes in the Long-Term Geophysical Eruptive Precursors at Piton de la Fournaise: Implications for the Response Management. *Frontiers in Earth Science, 6*, 104. https://doi.org/10.3389/feart.2018.00104

Perttu, A., Caudron, C., Assink, J. D., Metz, D., Tailpied, D., Perttu, B., et al. (2020). Reconstruction of the 2018 tsunamigenic flank collapse and eruptive activity at Anak Krakatau based on eyewitness reports, seismo-acoustic and satellite observations. *Earth and Planetary Science Letters, 541*, 116268.

Phillipson, G., Sobradelo, R., & Gottsmann, J. (2013). Global volcanic unrest in the 21st century—An analysis of the first decade. *Journal of Volcanology and Geothermal Research, 264*, 183–196.

Poland, M. P., & Anderson, K. R. (2020). Partly cloudy with a chance of lava flows—Forecasting volcanic eruptions in the twenty-first century. *Journal of Geophysical Research Solid Earth, 125*(1), 32. https://doi.org/10.1029/2018JB016974

Poland, M. P., Lopez, T., Wright, R., & Pavolonis, M. J. (2020). Forecasting, detecting, and tracking volcanic eruptions from space. *Remote Sensing in Earth Systems Sciences, 3*(1), 55–94. https://doi.org/10.1007/s41976-020-00034-x

Popinet, S. (2011). Quadtree-adaptive tsunami modelling. *Ocean Dynamics, 61*(9), 1261–1285. https://doi.org/10.1007/s10236-011-0438-z

Popinet, S. (2012). Adaptive modelling of long-distance wave propagation and fine-scale flooding during the Tohoku tsunami. *Natural Hazards and Earth System Sciences, 12*(4), 1213–1227.

Popinet, S. (2015). A quadtree-adaptive multigrid solver for the Serre–Green–Naghdi equations. *Journal of Computational Physics, 302*(1), 336–358. https://doi.org/10.1016/j.jcp.2015.09.009

Potter, S. H., Jolly, G. E., Neall, V. E., Johnston, D. M., & Scott, B. J. (2014). Communicating the status of volcanic activity: Revising New Zealand's volcanic alert level system. *Journal of Applied Volcanology, 3*, 13.

Pritchard, M. E., Biggs, J., Wauthier, C., Sansosti, E., Arnold, D. W. D., Delgado, F., et al. (2018). Towards coordinated regional multi-satellite InSAR volcano observations—Results from the Latin America pilot project. *Journal of Applied Volcanology, 7*, 5. https://doi.org/10.1186/s13617-018-0074-0

Pritchard, M. E., Poland, M., Reath, K., Andrews, B., Bagnardi, M., & Biggs, J., et al. (2022). Optimizing satellite resources for the global assessment and mitigation of volcanic hazards—Suggestions from the USGS Powell Center Volcano Remote Sensing Working Group. U.S. Geological Survey Scientific Investigations Report 2022–5116. https://doi.org/10.3133/sir20225116

Proudman, J. (1929). The effects on the sea of changes in atmospheric pressure. *Geophysical Supplements to the Monthly Notices of the Royal Astronomical Society, 2*, 197–209.

Putra, P. S., Aswan, A., Maryunani, K. A., Yulianto, E., Nugroho, S. H., & Setiawan, V. (2020). Post-event field survey of the 22 December 2018 Anak Krakatau Tsunami. *Pure Applied. Geophysics, 177*, 2477–2492.

Qin, X., LeVeque, R. J., & Motley, M. R. (2019). Accelerating an adaptive mesh refinement code for depth-averaged flows using GPUs. *Journal of Advances in Modelling Earth Systems, 11*, 2606–2628. https://doi.org/10.1029/2019MS001635

Range, M. M., Arbic, B. K., Johnson, B. C., Moore, T. C., Titov, V., Adcroft, A. J., et al. (2022). The Chicxulub Impact Produced a Powerful Global Tsunami. *Agu Advances, 3*(5), e2021AV000627. https://doi.org/10.1029/2021av000627.

Ren, Z., Wang, Y., Wang, P., et al. (2020). Numerical study of the triggering mechanism of the 2018 Anak Krakatau tsunami: Eruption or collapsed landslide? *Natural Hazards, 102*, 1–13. https://doi.org/10.1007/s11069-020-03907-y

Ripepe, M., De Angelis, S., Lacanna, G., Poggi, P., Williams, C., Marchetti, E., et al. (2009). Tracking pyroclastic flows at Soufrière Hills Volcano. *Eos, Transactions of the American Geophysical Union, 90*(27), 229–230. https://doi.org/10.1029/2009EO270001

Ripepe, M., & Lacanna, G. (2024). Volcano generated tsunami recorded in the near source. *Nature Communication*. https://doi.org/10.1038/s41467-024-45937-1

Ripepe, M., Lacanna, G., Pistolesi, M., Silengo, M. C., Aiuppa, A., Laiolo, M., et al. (2021). Ground deformation reveals the scale-invariant conduit dynamics driving explosive basaltic eruptions. *Nature Communications, 12*(1), 1–8.

Ripepe, M., Marchetti, E., Delle Donne, D., Genco, R., Innocenti, L., Lacanna, G., et al. (2018). Infrasonic early-warning for explosive eruption. *Journal Geophysics Research Solid Earth, 123*(11), 9570–9585. https://doi.org/10.1029/2018JB015561

Roche, O., Druitt, T. H., & Merle, O. (2000). Experimental study of caldera formation. *Journal of Geophysical Research, 105*, 395–416.

Rosi, M. (1980). The island if Stromboli. *Rend Society Italian Mineralogy Petroleum, 36*, 345–368.

Rosi, M., Levi, S. T., Pistolesi, M., Bertagnini, A., Brunelli, D., Cannavò, V., et al. (2019). Geoarchaeological evidence of middle-age tsunamis at Stromboli and consequences for the tsunami hazard in the Southern Tyrrhenian Sea. *Scientific Reports, 9*(1), 1–10.

Roult, G. C., Beauducel, F., Ferrazzini, V., Boissier, P., & Villeneuve, N. (2014). The" Jerk" Method for Predicting Intrusions and Eruptions of Piton De La Fournaise (La Réunion Island) from the Analysis of the Broadband Seismological Rer Station. *AGU Fall Meeting Abstracts* (Vol. 2014, pp. V43A-4844).

Sandanbata, O., Watada, S., Satake, K., Kanamori, H., & Rivera, L. (2023). Two volcanic tsunami events caused by trapdoor faulting at a submerged caldera near Curtis and Cheeseman Islands in the Kermadec Arc. *Geophysical Research Letters, 50*, e2022GL101086. https://doi.org/10.1029/2022GL101086

Sandanbata, O., Watada, S., Satake, K., Kanamori, H., Rivera, L., & Zhan, Z. (2022). Sub-decadal volcanic tsunamis due to submarine trapdoor faulting at Sumisu caldera in the Izu-Bonin Arc. *Journal of Geophysical Research: Solid Earth, 127*, e2022JB024213.

Satake, K. (2007). Volcanic origin of the 1741 Oshima-Oshima tsunami in Japan Sea. *Earth, Planets and Space, 59*, 381–390. https://doi.org/10.1186/BF03352698

Satake, K., & Kato, Y. (2001). The 1741 Oshima-Oshima eruption: Extent and volume of submarine debris avalanche. *Geophysical Research Letters, 28*, 427–430. https://doi.org/10.1029/2000GL012175

Sato, H., & Taniguchi, H. (1997). Relationship between crater size and ejecta volume of recent magmatic and phreato-magmatic eruptions: Implications for energy partitioning. *Geophysical Research Letters, 24*, 205–208. https://doi.org/10.1029/96gl04004

Savage, S. B., & Hutter, K. (1989). The motion of a finite mass down a rough incline. *Journal of Fluid Mechanics, 199*, 177–215. https://doi.org/10.1017/S0022112089000340

Schaefer, L. N., Di Traglia, F., Chaussard, E., Lu, Z., Nolesini, T., & Casagli, N. (2019). Monitoring volcano slope instability with Synthetic Aperture Radar: A review and new data from Pacaya (Guatemala) and Stromboli (Italy) volcanoes. *Earth-Science Reviews, 192*, 236–257.

Schneider, D. J., Dean, K. G., Dehn, J., Miller, T. P., & Kirianov, V. Y. (2000). Monitoring and analyses of volcanic activity using remote sensing data at the Alaska Volcano Observatory—Case study for Kamchatka, Russia, December 1997. In: Mouginis-Mark, P. J., Crisp, J. A., and Fink, J. H., (Eds)., *Remote sensing of active volcanism. American Geophysical Union, Geophysical Monograph Series* (Vol. 116, pp. 65–85)

Seabrook, S., Mackay, K., Watson, S. J., Clare, M. A., Hunt, J. E., Yeo, I. A., et al. (2023). Volcaniclastic density currents explain widespread and diverse seafloor impacts of the 2022 Hunga Volcano eruption. *Nature Communications, 14*(1), 7881. https://doi.org/10.1038/s41467-023-43607-2

Segall, P. (2013). Volcano deformation and eruption forecasting. *Geological Society, London, Special Publications, 380*, 22. https://doi.org/10.1144/SP380.4

Selva, J., Lorito, S., Volpe, M., Romano, F., Tonini, R., Perfetti, P., et al. (2021). Probabilistic tsunami forecasting for early warning. *Nature Communications, 12*(1), 1–14.

Shen, Y., Whittaker, C. N., Lane, E. M., White, J. D. L., Power, W., & Nomikou, P. (2021). Laboratory experiments on tsunamigenic discrete subaqueous volcanic eruptions. Part 1: Free surface disturbances. *Journal of Geophysical Research, Oceans, 126*, e2020JC016588.

Shen, Y., Whittaker, C. N., Lane, E. M., White, J. D. L., Power, W., & Nomikou, P. (2021). Laboratory experiments on tsunamigenic discrete subaqueous volcanic eruptions. Part 2: Properties of

generated waves. *Journal of Geophysical Research, Oceans, 126*, e2020JC016587.

Sigmundsson, F., Parks, M., Hooper, A., Geirsson, H., Vogfjörd, K. S., Drouin, V., et al. (2022). Deformation and seismicity decline before the 2021 Fagradalsfjall eruption. *Nature, 609*, 523–528.

Simkin, T., & Fiske, R. S. (1983). *Krakatau 1883: The volcanic eruption and its effects* (p. 464). Smithsonian Institution Press.

Sparks, R. S. J. (2003). Forecasting volcanic eruptions. *Earth and Planetary Science Letters, 10*, 1–15. https://doi.org/10.1016/S0012-821X(03)00124-9

Stehn, C. E. (1929). The geology and volcanism of the Krakatau group. *Proceedings of the Fourth Pacific Science Congress*, Batavia (pp. 1–55).

Stix, J., & Kobayashi, T. (2008). Magma dynamics and collapse mechanisms during four historic caldera-forming events. *Journal of Geophysical Research, 113*, B09205.

Sue, L. P., Nokes, R. I., & Davidson, M. J. (2011). Tsunami generation by submarine landslides: Comparison of physical and numerical models. *Environmental Fluid Mechanics, 11*(2), 133–165.

Swanson, D. A., Casadevall, T. J., Dzurisin, D., Malone, S. D., Newhall, C. G., & Weaver, C. S. (1983). Predicting eruptions at Mount St. Helens, June 1980 through December 1982. *Science, 221*(4618), 1369–1376. https://doi.org/10.1126/science.221.4618.1369

Synolakis, C. E., Bernard, E. N., Titov, V. V., Kânoğlu, U., & González, F. I. (2008). Validation and verification of tsunami numerical models. *Pure and Applied Geophysics, 165*(11–12), 2197–2228.

Themens, D. R., Watson, C., Žagar, N., Vasylkevych, S., Elvidge, S., McCaffrey, A., et al. (2022). Global propagation of ionospheric disturbances associated with the 2022 Tonga volcanic eruption. *Geophysical Research Letters, 49*, e2022GL098158. https://doi.org/10.1029/2022GL098158

Tibaldi, A. (2001). Multiple sector collapses at Stromboli volcano, Italy: How they work. *Bulletin of Volcanology, 63*(2), 112–125.

Tibaldi, A. (2010). A new geological map of Stromboli volcano (Tyrrhenian Sea, Italy) based on application of lithostratigraphic and unconformity-bounded stratigraphic (UBS) units. *GSA Specical Papers, 464*, 33–49.

Tilling, R. I. (2008). The critical role of volcano monitoring in risk reduction. *Advances in Geosciences, 14*, 3–11.

Tinti, S., Bortolucci, E., & Romagnoli, C. (2000). Computer simulations of tsunamis due to sector collapse at Stromboli, Italy. *Journal of Volcanology and Geothermal Research, 96*, 103–128. https://doi.org/10.1016/S0377-0273(99)00138-9

Tinti, S., Pagnoni, G., & Zaniboni, F. (2006). The landslides and tsunamis of the 30th of December 2002 in Stromboli analysed through numerical simulations. *Bulletin of Volcanology, 68*, 462–479. https://doi.org/10.1007/s00445-005-0022-9

Tinti, S., Pagnoni, G., Zaniboni, F., & Bortolucci, E. (2003). Tsunami generation in Stromboli Island and impact on the south-east Tyrrhenian coasts. *Natural Hazards and Earth System Sciences, 3*(5), 299–309.

Tinti, S., Zaniboni, F., Pagnoni, G., & Manucci, A. (2008). Stromboli Island (Italy): Scenarios of tsunamis generated by submarine landslides. *Pure and Applied Geophysics, 165*(11), 2143–2167.

Titov, V. V., Kânoğlu, U., & Synolakis, C. (2016). Development of MOST for real-time tsunami forecasting. *Journal of Waterway, Port, Coastal and Ocean Engineering. American Society of Civil Engineers, 142*(6), 03116004. https://doi.org/10.1061/(ASCE)WW.1943-5460.0000357

Torsvik, T., Paris, R., Didenkulova, I., Pelinovsky, E., Belousov, A., & Belousova, M. (2010). Numerical simulation of explosive tsunami wave generation and propagation in Karymskoye Lake, Russia. *Natural Hazards and Earth System Sciences, 10*, 2359–2369.

Tsuji, Y., & Hino, T. (1993). Damage and inundation height of the 1792 Shimabara landslide tsunami along the coast of Kumamoto prefecture. *Bulletin of the Earthquake Research Institute, University of Tokyo, 682*, 91–176.

Uhira, K., Yamasato, H., & Takeo, M. (1994). Source mechanism of seismic waves excited by pyroclastic flows observed at Unzen volcano, Japan. *Journal of Geophysical Research: Solid Earth, 99*(B9), 17757–17773.

Ulivieri, G., Ripepe, M., & Marchetti, E. (2013). Infrasound reveals transition to oscillatory discharge regime during lava fountaining: Implication for early-warning. *Geophysical Research Letters, 40*, 3008–3013. https://doi.org/10.1002/grl.50592

Ulvrova, M., Paris, P., Kelfoun, K., & Nomikou, P. (2014). Numerical simulations of tsunamis generated by underwater volcanic explosions at Karymskoye lake (Kamchatka, Russia) and Kolumbo volcano (Aegean Sea, Greece). *Natural Hazards and Earth System Sciences, 14*(2), 401–412.

Ulvrova, M., Paris, R., Nomikou, P., Kelfoun, K., Leibrandt, S., Tappin, D. R., et al. (2016). Source of the tsunami generated by the 1650 AD eruption of Kolumbo submarine volcano (Aegean Sea, Greece). *Journal of Volcanology and Geothermal Research, 321*, 125–139.

UNESCO/IOC. (2023). Exercise CARIBE WAVE 23. A Caribbean and Adjacent Region Tsunami Warning Exercise, 23 March 2023 (Gulf of Honduras and Mount Pelée Scenarios). Volume 1: Participant Handbook. IOC Technical Series No. 178, Vol. 1. Paris: UNESCO (English only).

US NOAA. (2023). National Centers for Environmental Information and International Tsunami Information Center, Tsunami Sources 1610 B.C. to A.D. 2023, From Earthquakes, Volcanic Eruptions, Landslides, and Other Causes (2023). http://itic.ioc-unesco.org/images/stories/awareness_and_education/map_posters/2023_tsu_poster_20231003_a2.pdf.

Vacondio, R., Dal Palu, A., Ferrari, A., Mignosa, P., et al. (2017). A non-uniform efficient grid type for GPU parallel shallow water equations models. *Environmental Modelling & Software, 88*(4), 119–137. https://doi.org/10.1016/j.envsoft.2016.11.012

Valade, S., Lacanna, G., Coppola, D., Laiolo, M., Pistolesi, M., & Delle Donne, D., et al. (2016). Tracking dynamics of magma migration in open-conduit systems. *Bulletin of Volcanology*, *78*, 1–12.

Valade, S., Ley, A., Massimetti, F., D'Hondt, O., Laiolo, M., Coppola, D., Loibl, D., et al. (2019). Towards global volcano monitoring using multisensor sentinel missions and artificial intelligence—The MOUNTS monitoring system. *Remote Sensing, 11*(113), 1528. https://doi.org/10.3390/rs11131528

Valentine, G. A., & White, J. D. L. (2012). Revised conceptual model for maar-diatremes: subsurface processes, energetics, and eruptive products. *Geology, 40*, 1111–1114.

Viroulet, S., Cébron, D., Kimmoun, O., & Kharif, C. (2013). Shallow water waves generated by subaerial solid landslides. *Geophysical Journal International, 193*, 747–762.

Voellmy, A. (1955). Über die zerstörungskraft von lawinen. *Schweiz. Bautzeiltung, 73*, 159–165.

Walter, T. R., Haghshenas Haghighi, M., Schneider, F. M., Coppola, D., Motagh, M., Saul, J., et al. (2019). Complex hazard cascade culminating in the Anak Krakatau sector collapse. *Nature Communications, 10*, 4339.

Wang, X., & Power, W. L. (2011). COMCOT: A tsunami generation, propagation, and run-up model. Lower Hutt (NZ): *GNS Science*. (GNS Science report; 2011/43).

Wang, Y., Wang, P., Kong, H., & Wong, C.-S. (2023). Tsunamis in Lingding Bay, China, caused by the 2022 Tonga volcanic eruption. *Geophysical Journal International, 232*(3), 2175–2185. https://doi.org/10.1093/gji/ggac291

Ward, S. N. (2001). Landslide tsunami. *Journal of Geophysical Research, 6*, 11201–11215.

Ward, S.N., & Day, S. (2003). Ritter Island—lateral collapse and the tsunami of 1888. *Geophysics Journal International, 154*, 891–902.

Watts, P., Grilli, S. T., Kirby, J. T., Fryer, G. J., & Tappin, D. R. (2003). Landslide tsunami case studies using a Boussinesq model and a fully nonlinear tsunami generation model. *Natural Hazards and Earth System Sciences, 3*(5), 391–402.

Watts, P., & Waythomas, C. F. (2003). Theoretical analysis of tsunami generation by pyroclastic flows. *Journal of Geophysical Research, 108*(B112), 2563. https://doi.org/10.1029/2002JB002265

Waythomas, C. F., & Watts, P. (2003). Numerical simulation of tsunami generation by pyroclastic flow at Aniakchak Volcano, Alaska. *Geophysical Research Letters, 30*(14), 1751. https://doi.org/10.1029/2003GL017220

Williams, D. A., Horsburgh, K. J., Schultz, D. M., et al. (2021). Proudman resonance with tides, bathymetry and variable atmospheric forcings. *Natural Hazards, 106*, 1169–1194. https://doi.org/10.1007/s11069-020-03896-y

Winson, A. E. G., Costa, F., Newhall, C. G., & Woo, G. (2014). An analysis of the issuance of volcanic alert levels during volcanic crises. *Journal of Applied Volcanology, 3*(1), 14. https://doi.org/10.1186/s13617-014-0014-6

Wohletz, K. H. (1986). Explosive magma-water interactions: Thermodynamics, explosion mechanisms, and field studies. *Bulletin of Volcanology, 48*, 245–2654.

Woods, A. W. (1988). The fluid dynamics and thermodynamics of eruption columns. *Bulletin of Volcanology, 50*, 169–193.

Wright, C. J., Hindley, N. P., Alexander, M. J., Barlow, M., Hoffmann, L., Mitchell, C. N., et al. (2022). Surface-to-space atmospheric waves from Hunga Tonga-Hunga Ha'apai eruption. *Nature, 609*, 741–746. https://doi.org/10.1038/s41586-022-05012-5

Yamasato, H. (1997). Quantitative analysis of pyroclastic flows using infrasonic and seismic data at Unzen volcano, Japan. *Journal of Physics of the Earth, 45*(6), 397–416.

Yavari-Ramshe, S., & Ataie-Ashtiani, B. (2016). Numerical modelling of subaerial and submarine landslide-generated tsunami waves - recent advances and future challenges. *Landslides, 13*(6), 1325–1368.

Yudhicara, Y., Bani, P., & Darmawan, A. (2015). Geothermal System as the Cause of the 1979 Landslide Tsunami in Lembata Island, Indonesia. *Indonesian Journal on Geoscience, 2*(2), 91–99.

Zengaffinen, T., Løvholt, F., Pedersen, G. K., & Muhari, A. (2020). Modelling 2018 Anak Krakatoa flank collapse and tsunami—Effect of landslide failure mechanism and dynamics on tsunami generation. *Pure and Applied Geophysics, 177*, 2493–2516.

Zhang, Y. J., & Baptista, A. M. (2008). An efficient and robust tsunami model on unstructured grids. Part I: Inundation benchmarks. *Pure and Applied Geophysics, 165*, 2229–2248. https://doi.org/10.1007/s00024-008-0424-7

(Received January 5, 2024, revised May 14, 2024, accepted May 22, 2024)